

*14/2 p.*

**ADVANCED  
TECHNOLOGY  
LABORATORIES**

OTS PRICE

XEROX

\$

11.00 ph.

MICROFILM

\$

4.61 inf.

**N63 18159**

*Code - 1*

**DESIGN CRITERIA FOR ZERO-LEAKAGE  
CONNECTORS FOR LAUNCH VEHICLES, VOL. 3,  
SEALING ACTION AT THE SEAL INTERFACE**

Edited by  
F.O. RATHBUN, JR.

CONTRACT NAS 8-4012

MARCH 15, 1963

**GENERAL  ELECTRIC**

U.S. DEPARTMENT OF COMMERCE  
National Technical Information Service

N63-18159

DESIGN CRITERIA FOR ZERO LEAKAGE CONNECTORS FOR  
LAUNCH VEHICLES

General Electric Company  
Schenectady, NY

Mar 63

FINAL REPORT FOR FIRST CONTRACT PERIOD

(March 1962 through February 1963)

DESIGN CRITERIA  
FOR ZERO LEAKAGE CONNECTORS  
FOR LAUNCH VEHICLES

Contract NAS 8-4012

VOLUME 3  
SEALING ACTION AT THE SEAL INTERFACE  
Edited by F.O. Rathbun, Jr.

March 15, 1963

PREPARED FOR: Propulsion and Vehicle Engineering Division  
George C. Marshall Space Flight Center  
National Aeronautics and Space Administration  
Huntsville, Alabama

PREPARED BY: Advanced Technology Laboratories  
General Electric Company  
Schenectady, New York

SPONSORED BY: Missile and Space Division  
General Electric Company  
Philadelphia, Pennsylvania

N.A.S.A. TECHNICAL MANAGER: C.C. Wood (M-P&VE-PT)

REPRODUCED BY  
NATIONAL TECHNICAL  
INFORMATION SERVICE  
U.S. DEPARTMENT OF COMMERCE  
SPRINGFIELD, VA. 22161

CP-50559

## CONTENTS

	<u>Page</u>
31. INTRODUCTION, CONCLUSIONS AND RECOMMENDATIONS	
31.1 Introduction	31-2
31.2 Conclusions and Recommendations	31-4
32. GASKET COMPRESSION PHENOMENON	
32.1 The Elastic-Plastic Compression Phenomenon	32-2
32.2 Characterizing Regimes of Deformation	32-5
32.3 References	32-6
33. STATISTICAL ANALYSIS OF INTERFACE EFFECTS	
33.1 Introduction	33-2
33.2 Distribution of Surface Asperities	33-3
33.3 Relation Between Deformation and Flow Area	33-5
33.4 Relation Between Load and Deformation	33-9
33.5 Relation of Load to Flow Passage	33-15
33.6 Effect of Surface Waviness	33-18
33.7 References	33-19
34. MECHANICAL PROPERTIES OF FLANGE AND GASKET MATERIALS	
34.1 Sealing-Surface Materials	34-2
34.2 Gasket Materials	34-5
34.3 Plastic Gasket Materials	34-11
34.4 Rubber Gasket Materials	34-14
34.5 References	34-20
35. EXPERIMENTAL PROGRAM	
35.1 Evaluation of Surface Finishes	35-2
35.2 Evaluation of Degree of Mating of Surfaces	35-5
35.3 Leakage Experiment	35-8
35.4 References	35-19
36. EXPERIMENTAL DATA AND RESULTS	
36.1 Experimental Results - Metal Gaskets	36-2
36.2 Experimental Results - Plastic Gaskets	36-30
36.3 Experimental Results - Rubber Gaskets	36-47
37. EXPERIMENTAL OBSERVATIONS AND CONCLUSIONS	
37.1 Experimental Observations for Metal Gaskets	37-2
37.2 Experimental Observations for Plastic Gaskets	37-18
37.3 Elastomer Gaskets	37-23
37.4 References	37-25



### 31. INTRODUCTION, CONCLUSIONS AND RECOMMENDATIONS

by

Forrest O. Rathbun, Jr.

#### 31.0 Summary

18159

Consideration has been given to the problem of leakage through passages at the interface of a gasket-sealing surface system. Both analytically and experimentally, predictions have been made relating leakage rates to strength properties of the connector materials, sealing stresses, and surface finishes employed. Experiments have been performed measuring leaks down to  $10^{-8}$  cc/sec. through several connector systems. The results of these experiments have been analyzed and compared with analytic predictions. Recommendations are presented based on this investigation.

All experiments conducted incorporated flat annular gaskets compressed normally between two flat sealing surfaces on which various surface finishes were machined or ground. The gasket materials included five metals (indium, lead, aluminum, copper, nickel), five plastics ("KEL-F81," "Saran," "Teflon-TFE," "Teflon FEP," "Duroid 5600") and four rubbers ("Viton-A," Neoprene, "Hypalon," Silicone). Leakage through these sealing systems has been measured as a function of the normal stress applied and the pressure differential across the seal. Results of these tests showed that large plastic deformations of the metal gaskets is necessary for reliable sealing. Excellent sealing was evidenced when rubbers were utilized; plastics seal under normal stresses less than their yield stresses.

### 31.1 Introduction

If the fluid connector problem is viewed as involving three areas of study, (1) the leakage of a fluid through passages at the interface between two sealing surfaces, (2) the design response of the supporting structure which positions the sealing surfaces, and (3) the environmental conditions which the system will encounter, it is seen that the basic leakage phenomenon is that of area (1). It is also noted that this area of study has received in the past less analytical and experimental consideration than the others. While some flange geometries and a few mechanical devices have been determined which will cause a gasket-flange system to respond in a certain manner under various environmental conditions, our knowledge to date of the interface phenomenon has been extremely limited. Hence the investigation described in this volume has been undertaken - that of both analytically and experimentally describing the leakage phenomenon in terms of a limited number of meaningful parameters.

Parameters which naturally suggest themselves are the gas (or liquid) pressure differential  $\Delta p$  existing across the seal, the stress applied to the gasket, and the rate of leakage through the connector. Under this report, the leakage  $L$  is measured as a volumetric rate - atmosphere cubic centimeters per second. The stress referred to as a parameter is applied normally to the surface of a flat annular gasket and is an average value over the surface; hence, a nominal normal stress  $\sigma$  is used.

The above three parameters are, of course, inadequate to completely describe the phenomenon. Some quantitative parameters must be used to describe the gasket and the "flanges". Rather than the consideration of "compatible" materials and the resultant conclusions for certain materials, it appears more basic to consider material properties as parameters rather than the sealing characteristics of particular materials. Thus, two material properties - yield strength and the strain hardening property - are referenced. Each material can be described in terms of these; whatever conclusions can be drawn for a material with a given combination of yield strength and strain hardenability, it is hoped can be drawn for other materials with similar properties. The strain hardenability can be written in terms of a Meyer strain hardening number  $n$ , and the yield strength may be called  $Y$ . Aside from internal pressure, stress applied to the gasket, the leakage, and the gasket and "flange" material properties, consideration of the leakage phenomenon requires a knowledge of surface finish of the mating surfaces. Hence, the last parameter to be included will be the surface finish, S.F.

Thus, the desired result would be a relationship such as

$$L = f(Y, n, \sigma, \Delta p, S.F.) \quad (1)$$

For both analytical and experimental investigations, flat surfaces in contact (flat annular gaskets) have been used as a model. In this manner, it becomes simple to isolate the effects of other parameters being varied.

The recommendations and conclusions which are made as a result of the experimental investigations are listed in subsection 31.2. Such conclusions are based on the results of both the experimental investigation and the analytical work.

The following sections of this report describe all of the analytical and experimental aspects of the investigation undertaken in this project.

In Section 32 is presented a description of the phenomena involved during the compression process between gasket and sealing surface. The description is based on classical theory of plasticity and is instructive for the interpretation of experimental results. Several separate regimes of material behavior are hypothesized.

The theoretical description and analysis of the leakage phenomenon is contained in Section 33. Predictions as to leakage rates and heights of gaps remaining between compressed sealing surfaces are made - each as functions of the material properties and surface finish. The analysis is based on a statistical model of the phenomenon, and hence includes some sweeping assumptions. The conclusions drawn from the analysis provide a basis and direction for the experimental work which is outlined further in the report.

The materials used in the experiments and their properties constitute the contents of Section 34. Strength properties, strain hardenability properties of metals, plastics, and the rubberlike materials used are included. Also incorporated is a description of the temperature transitional properties of some gasket materials.

All of the experimental apparatus and procedure used in the investigation is described in Section 35. The objectives, design concepts, techniques used are listed and explained.

Since the experimental work falls into three categories, those of the gasket materials used (metals, plastics, rubberlike materials), the results of each are contained in separate subsections of Section 36. Presented are leakage rates, surface finishes used, and all of the particulars of each gasket material test.

Section 37 is devoted to the observations made and conclusions drawn on all the experimental work. Comparisons with the predictions of Section 33 are drawn, as are comparisons with predictions as to leakage made by Fang (Section 22), who relates leakage with passage height for a uniform path. From the observations and conclusions of Section 37, are drawn the recommendations in Section 31.2.

## 31.2 Conclusions and Recommendations

Our principal findings to date in the study of the seal interface are briefly summarized below. As indicated by the references in parentheses, all of these results are discussed in more detail in Section 37.

### 31.2.1 Conclusions - General

1. The gross deformations of the flat annular gaskets obey plane strain criteria. (Section 37.1.1)
2. If the sealing of a gasket system is caused by plastic flow of the materials mated, then the seal is very insensitive to removal of the deformation-causing stress. (Section 37.1.7)
3. When gasket normal stresses are so severe as to cause gross sealing surface distortion, the surface asperities tend to be preserved. (Section 37.1.3)
4. The stress on the gasket is highest at the middle of the gasket width and becomes less at the edge. (Section 37.1.3)
5. Observations show that sealing of an annular gasket-sealing surface system is possible even when the asperities on the stronger material run in the direction of potential leakage flow. (Section 37.1.3)
6. The model of the flow passage being flat and of a given width and a given height is adequate for very smooth sealing surfaces and soft gaskets. (Section 37.1.4)
7. The concept of five regimes of metal deformation (Section 32) appears an adequate model for the smoother sealing surfaces. (Section 37.1.5)

### 31.2.2 Conclusions - Metal Gaskets

1. The best mating on the flat annular gasket-sealing surface system occurs at the gasket edge, the point of minimum normal stress. (Section 37.1.3)
2. The plastic flow of soft metal gaskets tends to start from regions internally within the gasket. The surface shear stress tends to control the mode of plastic flow. (Section 37.1.2)
3. Insensitivity of metal gasket seals to increases in pressure differential can be assured only if the gasket deformation producing the seal has been plastic in nature. Thus, from this standpoint, the soft gasket materials which experience gross plastic deformation at low stress levels appear to have better potential in static fluid connector design than harder metals. (Section 37.1.6)

4. Rough sealing surfaces cause sealing to be affected by elastic gasket deformation, and are quite unstable during removal of load. (Section 37.1.7)
5. Where metal gasket seals were found sensitive to internal pressure, it was possible to reduce the leakage rate by adding an increment of stress not more than 0.25 times the yield strength of the gasket material. (Section 37.1.6)
6. For all metal gaskets used, it has been possible to attain leaks as low as  $10^{-6}$  atm cc/sec for nominal normal stresses on annular gaskets equal to twice the stress level causing initial bulk flow of the gasket material (at a pressure differential of one atmosphere). (Section 37.1.5)
7. At the center of the gasket width, mating between gasket and sealing surface can be effected only by applying normal stress many times the yield stress. (Section 37.1.3)

#### 31.2.3 Conclusions - Plastic Gaskets

1. All plastic gaskets used attained a  $10^{-6}$  atm cc/sec seal at stress levels equal to 0.4 times the stress level which would cause bulk flow of the gasket. (Section 37.2.4)
2. Diffusion through plastic appeared in all tests conducted at leakage levels of  $10^{-6}$  atm cc/sec. (Section 37.2.4)
3. Plastic gaskets, even though visco-elastic in nature, retain mated surface geometries over long periods and can be considered as being in a state of plastic deformation. (Section 37.2.3)
4. Plastic gaskets are insensitive to internal pressure increases. Mating seems very complete between surfaces. (Section 37.2.5)
5. Because of cold flow, the problem of maintaining a plastic gasket in a pressurized system is present. (Section 37.2.2)
6. Plastic gaskets appear to be nearly completely insensitive to removal of normal stress. (Section 37.2.6)

#### 31.2.4 Conclusions - Elastomeric Gaskets

1. Elastomers (not silicone rubber) seal completely at very low stress levels regardless of the surface finish on the sealing surfaces. (Section 37.3.1)
2. Rubber, with its great compliance, seals primarily by elastic deformation - not plastic deformation. (Section 37.3.3)
3. Elastomer gaskets are insensitive to internal pressure and removal of load. (Section 37.3.2)

#### 31.2.5 Recommendations

1. Elastomeric (rubber-like) gaskets should be used wherever possible as the surface mating material. Based on pure leakage restraining characteristics, the elastomers offer the best possibility for zero-leakage gaskets. Hence, other criteria, such as temperature dependence of properties, incompatibility to certain fluids, and wear characteristics become the limiting factors in their use.
2. Plastics may be used in cases where low sealing stresses are available, and a certain amount of diffusion leakage can be tolerated. Plastics bonded to other materials in thin layers offer excellent prospects. Their cold-flow and diffusion characteristics hinder their successful use as a complete gasket.
3. Where metals are used, it is recommended that the softer materials which will grossly deform under available stress levels be employed in order to insure an insensitivity to loss of stress.
4. When metal gaskets are used, geometries which promote plastic shear deformation between the mating surfaces are recommended.

## 32. GASKET COMPRESSION PHENOMENON

by

Forrest O. Rathbun, Jr.

### 32.0 Summary

To understand the phenomenon of gasket compression, one can simplify the model for inspection to gain insight into the events taking place. In this section, the phenomenon of gasket compression is described in terms of classical elastic-plastic material behavior. While such an endeavor will not generally yield quantitative results extremely close to experimental observations, it does enable one to view the experimental observations with a better understanding. Also presented in this section is a hypothesis concerning the stages of compression of a gasket and their probable effect on leakage. The results of the experimental work are later reviewed in light of this hypothesis.

### 32.1 The Elastic-Plastic Compression Phenomenon

In cases where a small piece of metal with a low yield strength and little potential strain hardening is compressed between two larger pieces of metal with high yield strengths, it is possible to assume that the larger pieces are rigid. As the loads become very high or when strain hardening is appreciable, the assumption becomes less valid.

For the tests conducted in this program, the above assumption can be used in qualitatively explaining the phenomena which occur during a leak test. As an approximation, a quantitative explanation can also be given.

For the circular flat gasket shape resting between two flat rigid bodies and loaded normally by them, the directions of possible metal flow are reduced to the radial direction only. Metal must flow inward or outward; there is no circumferential displacement. Hence, the situation is approximately a plane strain case. As the gasket width is reduced or the radius increased, the approximation becomes better. Because of the inability of the metal to flow in both directions laterally under a normal load, the normal stress at which it yields will be higher than in a conventional compression test where no lateral constraints are used.

It can be shown (Ref. 1) that:

$$S = Y / \sqrt{1 - \nu + \nu^2} \quad (1)$$

where S is the normal stress to produce incipient yield, Y is the yield strength as gained by conventional testing, and  $\nu$  is Poisson's ratio. The above is based on the von Mises yield criterion. For metals, ( $\nu = 0.3$ ),

$$S = 1.127Y \quad (2)$$

A Tresca yield condition will give

$$S = Y \quad (3)$$

Hence, since the experimental data for ductile metals lies between the two yield criteria, but closer to the von Mises, we should expect yielding to occur in the annular shaped specimen at about

$$S \sim 1.1Y \quad (3a)$$

Besides the yielding of the gasket in bulk which should begin at a load described above, it must be recognized that at the interface between the surface of the rigid body and the surface of the gasket, asperities exist on both, and the area of contact between is initially small and grows with increased normal load. For a phenomenological explanation of the different phases of deformation which the softer material experiences, one can consider the gasket to have a certain surface geometry and to be a plastic-rigid body; i.e., the body is rigid until sufficient stress is produced at a point to cause plasticity. For that stress level and above, the material at that point is purely plastic. If the surface of the purely rigid body is devoid of irregularities (approximately



the diamond burnished case) then the following model can be surmised to explain the gasket deformation.

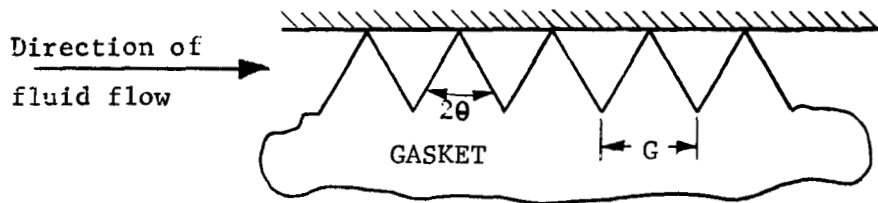


FIGURE 32.1 Model of Surface Asperities

The wedge shape, while not being exact, is a close approximation for the machined gasket surface. If one such wedge is considered, it can be shown (as is pointed out in Section 33 of this report) that the wedge deforms as shown below:

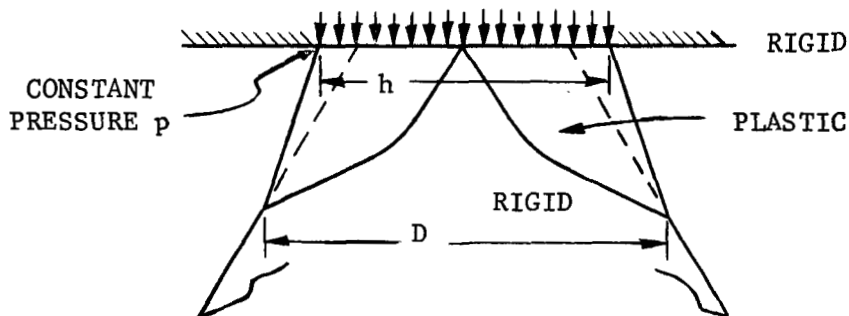


FIGURE 32.2 Plastic Wedge Deformation

The load bearing capacity of a deformation is known to be as shown in Figure 32.3.

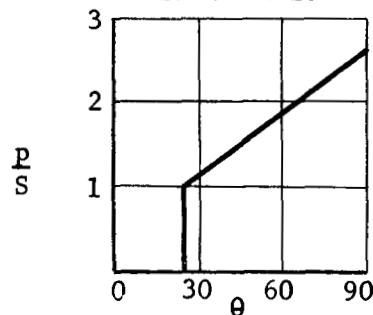


FIGURE 32.3 Variation of Wedge Stress With Wedge Angle (Ref. 1)

Hence for large angles  $\theta$  (which are conventional on finely ground surfaces,)

$$p \sim 2.63S \quad (4)$$

As  $\theta$  becomes close to  $180^\circ$ , the ratio of area over which the pressure acts to the total area of plastic deformation,  $h/D$ , becomes (Ref. 1)

$$h/D \sim 0.5 \quad (5)$$

Thus, it would appear that up to the load where  $D$  approaches the surface pitch  $G$ , (and interference between plastic regions from adjacent wedges occurs), we may predict the ratio  $h/G$ , the ratio of contact area to apparent area. The average normal stress acting the bulk of the gasket will be  $(h/G) \cdot p$ . Since  $p$  is a constant for a given angle  $\theta$ , then  $h$  will be linearly increasing with the total load  $F$  per unit thickness,

$$F \sim hp, \quad (6)$$

and the increase in area of contact ( $h/G$ ) will be linear with the mean normal stress  $Q$ .

$$Q = F/G = hp/G \quad (7)$$

At the point where  $h/D$  tends to  $h/G$ , then the average normal stress  $Q$  becomes

$$Q = 1.315S \quad (8)$$

for large angles  $\theta$ . Since this average stress would produce incipient bulk yielding, the phenomenon can be explained by this model only to the point where, from Ref. 1,

$$h/G \sim .4 \quad (9)$$

However, from the above, the earlier stages of mating are shown to produce a linearly increasing area of contact with increasing load. For the real case, this explanation is affected by the asperity shape being other than purely wedge shaped, the rigid surface having asperities, and the plastic material having an amount of strain hardening. We can, however, isolate a range of nominal normal stress in which

- a) only surface plastic deformation is produced, not bulk plastic deformation, and
- b) the increase in area with increasing stress is roughly linear.

### 32.2 Characterizing Regimes of Deformation

For purposes of discussing the leakage results, and in line with the above, five separate regimes of deformation are hypothesized during a given test.

Regime I - initial mating during which the extremely high asperities on the gasket which rise above the average height are plastically deformed under low average nominal stress. During this regime, little overall increase in contact area and little decrease in leakage should be noted.

Regime II - the deformation of the asperities only on the gasket - in line with the wedge analysis above. A rapid increase in contact area with nominal increases in normal stress is experienced. Leakage should be expected to decrease faster. This regime is only a good visualization when the rigid surface is very smooth. The terminal nominal stress for this regime would certainly be at a value equal to or less than S.

Regime III - Plastic flow of the asperities continues as a slower rate due the interference between the "pile-up" of plastic material. The gasket begins to flow in bulk. Strain hardening complicates both areas of deformation.

Regime IV - the gasket flows in bulk, increasing the area by shearing along the surface and by physically increasing the apparent area of contact. The amount of bulk flow is dictated to a large degree by the normal stress and the strain hardenability of the gasket material.

Regime V - the normal stress begins to cause bulk flow of the heretofore described rigid surfaces, i.e., the "flanges" deform grossly. This phase is to be avoided in order for the connection to be reusable. The original asperities on the "flange" do not suffer great deformations prior to this and even during this phase due to the containment of the asperities by the gasket material mated with them.

Under the above hypothesis, the experimental tests can be grouped as follows.

TABLE 32.1 Regimes of Gasket Mating

Gasket Material	Regime				
	I	II	III	IV	V
Indium				↔	
Lead			↔	↔	
Aluminum	↔			↔	
Copper	↔			↔	
Nickel	↔				*↔
Plastics			↔	↔	

\* in one instance only

It is to be noted that for indium, lead, and plastics, the test obviously includes the early regimes; however, no measurements of leakage can be taken at that time, since the minimum load which can be applied puts the material into a higher regime.

The rubber-like gasket tests defy such description due to the dominance of the elastic deformation.

### 32.3 References

1. R. Hill, The Mathematical Theory of Plasticity, Oxford University Press, 1956.

### 33. STATISTICAL ANALYSIS OF INTERFACE EFFECTS

by

T. P. Goodman

#### 33.0 Summary

The effect of surface finish, surface yield strength, and compressive stress on the leak-tightness of a fluid connector can be studied by a statistical analysis of the flow passages. This analysis, while based on many simplifying assumptions, nevertheless illustrates the advantages of using smooth surfaces, low-yield-strength gasket materials, and high compressive stresses to achieve a leak-tight connection.

The analysis shows how the ability of a sealing surface to reduce flow by plastic deformation is affected by the strain-hardening properties of the seal material. As expected, materials having only a small amount of strain hardening can seal with lower pressures than those with a greater amount of strain hardening. However, the analysis still shows that with or without strain hardening, a substantial plastic flow of at least one of the surface materials is necessary for effective sealing.

For surfaces having curved or wavy profiles in the direction of flow, the analysis shows that the sealing may be even more effective than for flat surfaces. This suggests that to insure good performance of a connector, it may be more important to control and inspect the surface-finish profile across the direction of flow than in the direction of flow.

Elastic deformations of sealing surfaces interact with plastic deformations in a complex way. The results obtained by neglecting elastic deformations are on the safe side for design, in that they predict less intimate surface contact, and hence greater leakage, than if elastic deformations were included in the analysis.

### 33.1 Introduction

While the surface finish of a machine part can be greatly improved by machining operations such as grinding, lapping, and burnishing, the surface asperities can never be completely removed. When the surface finish of a part is recorded on a profile recorder, the asperities appear as "hills" and "valleys." When two parts are pressed together in a fluid connector, the compressive load between the parts is taken by the "hills" as they come together, while the "valleys" provide passages through which the fluid can leak. In order to estimate the effective flow passage, the following steps are necessary:

1. The distribution of surface asperities must be found (Section 33.2).
2. The relation between the deformation of the surfaces and the resulting fluid-flow area, as the surfaces are pressed together, must be calculated (Section 33.3).
3. The load necessary to produce this deformation must be determined (Section 33.4).

With the present state of knowledge in all of these areas, some rather sweeping assumptions must be made in order to obtain numerical answers. The numerical results must, therefore, be interpreted as order-of-magnitude estimates. Still, the conceptual model which they provide should be helpful in interpreting the requirements of minimum-leakage connector designs.

### 33.2 Distribution of Surface Asperities

While there has been considerable interest during recent years (Ref. 1) in the rms surface finish of machine parts, there has been little published information on the statistical distribution of asperities. However, it is well known that a Gaussian distribution (Ref. 2) approximates many random physical phenomena, and Abbott and Firestone (Ref. 3) published some data on ground and lapped surfaces that can be matched by a Gaussian distribution, as shown in Table 33.1.

It will be noted that the ground surface is quite closely matched by a Gaussian distribution of surface heights between the 2% and 98% frequency levels. The long "tails" of the Gaussian distribution, which assert that there is a small but finite probability of having very high peaks and very deep valleys, are obviously unrealistic; however, values beyond the "three-sigma limit" (Ref. 2) are so improbable in a Gaussian distribution that their effect on the results given later in this section is probably negligible.

TABLE 33.1 Distribution of Surface Asperities

	<u>Measured Values (Ref. 3)</u>			<u>Calculated Values</u> <u>for Gaussian dis-</u> <u>tribution with 12.6</u> <u>microin. rms surface</u> <u>finish (microin.)</u>
	<u>Ground</u> <u>Surface</u> (microin.)	<u>Lapped</u> <u>Surface</u> (microin.)	<u>Johansson</u> <u>Block</u> (microin.)	
Peak roughness (Distance from plane with 2% of surface area above it to plane with 25% of surface area above it)	22	4	1	17.4
Medial roughness (Distance from plane with 25% of surface area above it to plane with 75% of surface area above it)	17	7	3	17.0
Valley roughness (Distance from plane with 75% of surface area above it to plane with 98% of surface area above it)	20	20	1	17.4

For the lapped surface, Table 33.1 indicates that the peaks have been largely removed, but that the valleys are still as deep as in a ground surface. Thus, for studying the flow through the valleys, the Gaussian model is still appropriate.

For a mirror-finish surface such as a Johansson block, the Gaussian distribution is no longer accurate; however, such a smooth finish may be impractical from a cost standpoint for fluid connectors. In addition, a

single scratch could negate the effect of the mirror finish as far as leakage is concerned.

The roughness numbers of Table 33.1 do not tell us how far apart the peaks and valleys are. Some idea of this can be obtained by looking at surface profile recordings (Ref. 3). In examining the recordings, it must be kept in mind that the vertical scale is usually made larger than the horizontal scale, so that the peaks and valleys look much steeper than they really are. If the two scales are made equal, the slopes appear much gentler, and it appears reasonable to represent the peaks by cones having a vertex angle between  $170^{\circ}$  and  $180^{\circ}$ . Also, it appears reasonable, in studying flow through valleys, to say that the valley cross-section changes only slowly, so that the flow through a valley is like the flow through a wide, shallow channel - that is, the sides of the valley have negligible effect in retarding the flow.



### 33.3 Relation Between Deformation and Flow Area

As two surfaces, each having surface asperities, are pressed together, the hills deform and the valleys are brought closer together. To determine how the compressive load affects the flow, we must study the deformation of the surfaces.

To relate the contact area to the cross-section area of the flow passage, some assumptions must first be made as to how the asperities are distributed in the direction of flow and in the direction perpendicular to flow. To visualize this situation, we may refer to the example used in Section 22,

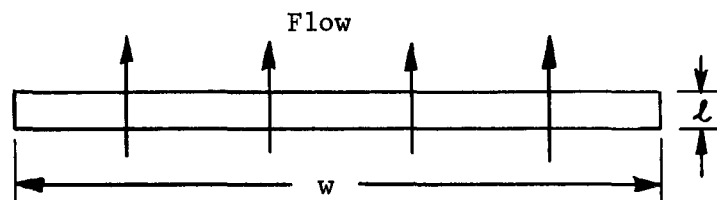


FIG. 33.1 Plan View of Developed Contact Area

with a flow passage having a perimeter  $w = 5$  inches and a length  $l = 0.1$  inch. We shall make the following assumptions about the distribution of asperities for the rectangular area of either of the two mating surfaces:

1. A surface-finish profile for any cross section perpendicular to the direction of flow has the same statistical properties.
2. The surface-finish profile changes slowly in the direction of flow; thus, the effects of meandering flow are negligible.

These assumptions are reasonable for surfaces finished by a non-directional grinding process, but they would not be valid for machine-finished surfaces in which the machine marks are predominantly in one direction. Surfaces of the latter type require a separate analytical treatment.

As the two surfaces are pressed together, an assumption must also be made about what happens to the material from the peaks of the two surfaces. Does it simply disappear, does it spread itself out uniformly over the two surfaces, or does it pile up between the peaks of the two surfaces? These three alternative assumptions will be designated as Assumption A1, Assumption A2, and Assumption B, respectively. They are illustrated by Fig. 33.2.

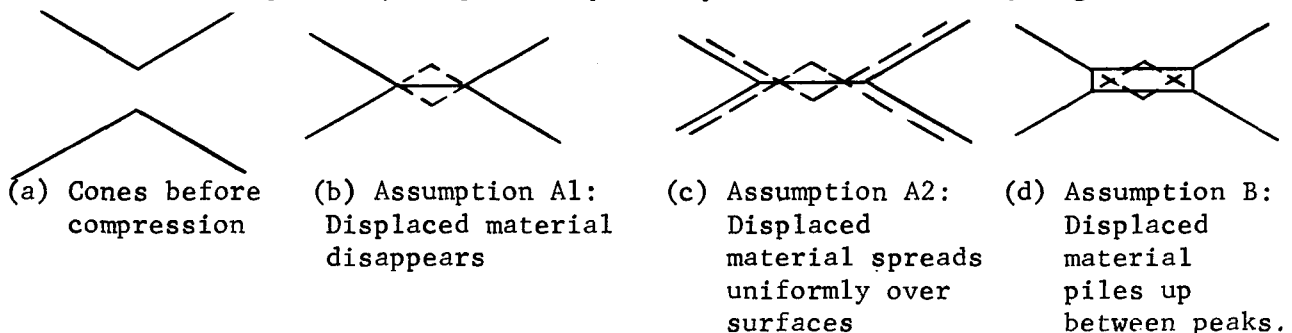


FIG. 33.2 Mutual Compression of Two Cones

For the relationship between contact area and flow area, Assumptions A1 and A2 give the same result; in the remainder of this section, when it is not necessary to distinguish between them, they will be designated together as Assumption A.

As might be expected, the actual situation, as derived from plasticity theory, is intermediate between Assumptions A and B. Fig. 33.3 shows the effect (Ref. 4) of compressing a wedge against a rigid plane, assuming fully developed plastic stress. When the wedge angle is small, the situation is more

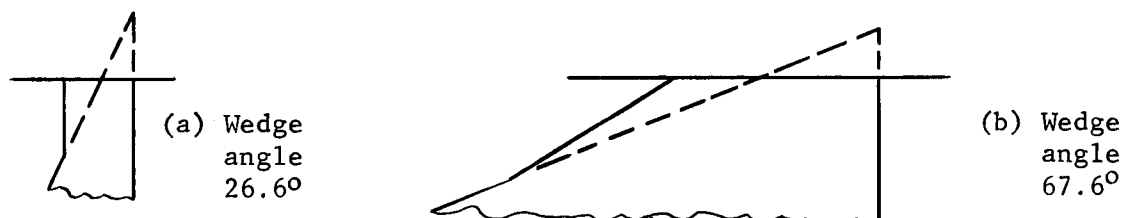


FIG. 33.3 Compression of Wedge Against Rigid Plane  
(Results from plasticity theory, Ref. 7)

like Assumption A. For our problem, therefore, Assumption A is more realistic. Also, Assumption A is much simpler to deal with analytically. It has been used for the calculations in the remainder of this section.

Assumptions A2 and B imply fully plastic flow at the asperities with no deformation of the supporting substructure of the mating parts. With plastic and/or elastic deformation of the substructure, some of the displaced material may, in effect, disappear, as in Assumption A1.

Proceeding under Assumption A, the relation between contact area and flow area can now be calculated. In a cross section perpendicular to the direction of flow, the two surfaces are shown schematically in Fig. 33.4.

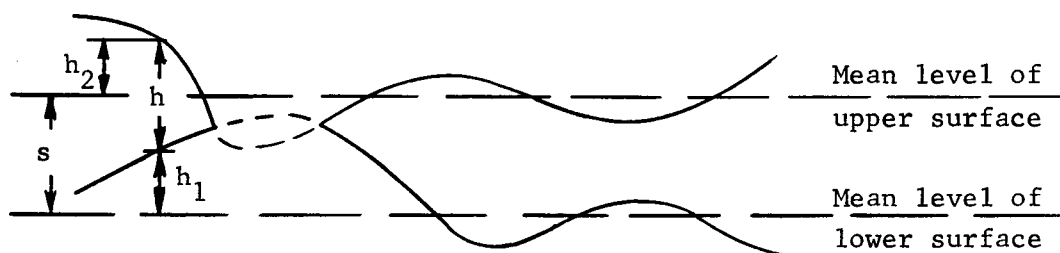


FIG. 33.4 Schematic of Flow Cross Section

As illustrated in Fig. 33.4, let

$s$  = mean separation between the two surfaces = distance between mean level of upper surface and mean level of lower surface

$h_1$  = height of lower surface above its mean level

$h_2$  = height of upper surface above its mean level

$h$  = height (clearance) of flow passage =  $s + h_2 - h_1$

$h_r$  = rms variation of  $h$  about its mean value.

It is evident that the mean value of  $h$  is  $s$ . If  $h_1$  and  $h_2$  are Gaussian random variables, then  $h$  will also be a Gaussian random variable, and its rms variation  $h_r$  will be the square root of the sum of the squares of the rms variations of  $h_1$  and  $h_2$  (Ref. 2). Thus, if each of the two surfaces has a 10-micro-inch<sup>rms</sup> finish,  $h_r = 10\sqrt{2} = 14.3$  micro-inches. This value was used in the example calculations that follow.

The Gaussian probability density function  $p(h)$  is shown in Fig. 33.5. The distribution is truncated at  $h = 0$ , since there can be no such thing as

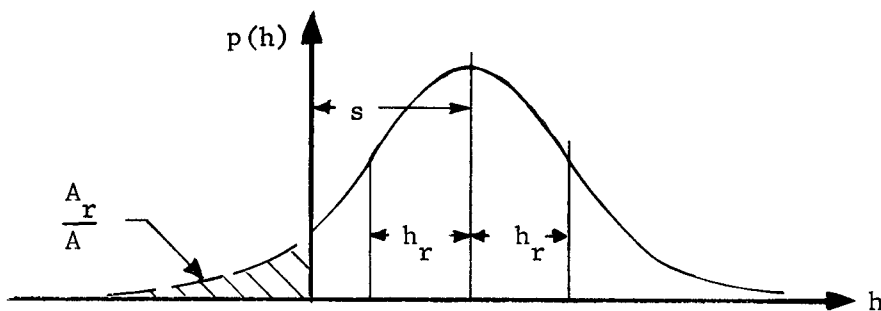


FIGURE 33.5 Probability Density of Flow Clearance  $h$

a negative clearance. However, the area under the curve to the left of  $h = 0$  is the contact area ratio  $A_r/A$ . Since viscous flow through a passage is proportional to the cube of the clearance, the effective clearance,  $h_e$ , which is the equivalent clearance of a uniform passage having the same flow rate, is found by taking the cube root of the weighted integral of the cube of the clearance  $h$  for all the flow passages.

The statements made in the preceding paragraph can be collected in the equations given below. To simplify the writing of these equations, the exponential function  $e^x$  is written as "exp  $x$ ", while the notation "erf  $x$ " is used for the Gaussian error function

$$\text{erf } x = \frac{2}{\sqrt{\pi}} \int_0^x \exp(-t^2) dt$$

With this notation,

$$p(h) = (1/h_r \sqrt{2\pi}) \exp \left[ -(h-s)^2 / 2h_r^2 \right] \quad (1)$$

$$\begin{aligned} A_r/A &= \int_{-\infty}^0 p(h) dh \\ &= (1/2) \left[ 1 - \operatorname{erf} (s/\sqrt{2} h_r) \right] \end{aligned} \quad (2)$$

$$\begin{aligned} h_e^3 &= \int_0^{\infty} h^3 p(h) dh \\ &= (s/2) (s^2 + 3h_r^2) \left[ 1 + \operatorname{erf} (s/\sqrt{2} h_r) \right] \\ &\quad + (h_r/\sqrt{2\pi}) (s^2 + 2h_r^2) \exp (-s^2/2h_r^2) \end{aligned} \quad (3)$$

If the flow is molecular rather than viscous (Sec. 21), then the flow rate is proportional to the square of the clearance, so that the effective clearance would be found by taking the square root of the weighted integral of the square of the clearance  $h$  for all the flow passages. Thus, for molecular flow, Equation (3) would have a different form, but the order-of-magnitude conclusions of this section would not be altered.

### 33.4 Relation Between Load and Deformation

Having found the relationship between deformation and fluid-flow area under the assumption of plastic flow of the metal at the mating asperities, we must now determine the relation between the deformation and the compressive load required to produce it.

The deformation of surface asperities under load has been of interest in studies of friction between solids (Refs. 4-7). The mechanism of friction is now generally understood to consist in the welding together of surface asperities by normal compressive force and the breaking of this force by a shearing load. As normal force is applied to two surfaces in contact, the real area of contact is found to increase linearly with normal force. Electrical resistance measurements and microscopic examination of surfaces have shown that the real area of contact,  $A_r$ , is a surprisingly small fraction of the total area,  $A$ , of the two surfaces. The increase of  $A_r$  with normal load,  $N$ , cannot continue to be linear as  $N$  increases indefinitely, since even with an infinite load,  $A_r$  cannot exceed  $A$ .

The ratio  $N/A_r$  is the compressive stress  $\sigma^*$  on the asperities. The value of  $\sigma^*$  at the beginning of compression may be denoted by  $\sigma_0^*$ . Assuming, as seems reasonable, that a fully plastic state of stress is developed at the real area of contact, the plastic stress for a cone deformed by contact with a rigid plane approaches  $3Y$  as the cone angle approaches  $180^\circ$ , according to plasticity theory. Here  $Y$  is the yield stress of the material. Thus we may take  $\sigma_0^* = 3Y$ , using  $Y$  as the lower of the two yield stresses when the two materials in contact have different yield stresses. Bowden and Tabor (Ref. 5), in their experiments with mild steel on mild steel, found that  $\sigma^*$  is about  $10^4$  kg/cm<sup>2</sup>, or about 143,000 psi. Finnie and Shaw (Ref. 6), in their experiments with 1020 steel on 18-4-1 HSS tool material, found that  $\sigma_0^* = 318,000$  psi. In the example calculations of this Section, we have rounded off Finnie and Shaw's value to 300,000 psi. However, it should be kept in mind that much lower values are possible with softer materials - particularly with plastics which may be used in gaskets.

When cones projecting from two plane surfaces approach each other, the real area of contact will be parallel to the surfaces only if the tips of the cones from the two surfaces match up exactly. Otherwise, the real area of contact will be oblique to the surfaces. However, for cone angles between  $170^\circ$  and  $180^\circ$ , the difference between the real area of contact and the projected real area of contact will be negligible for our purposes. Hence, in this Section, we assume that these two areas are equal.

As the two surfaces are compressed together, the value of  $\sigma^*$  is affected both by strain hardening and by the mutual interaction of asperities. These effects are both difficult to include in the calculations in a rigorous way, but the actual situation can be bracketed by two extreme cases, both of which are illustrated by Figs. 33.6 and 33.7. First, we may assume that  $\sigma_0$  remains constant until  $A_r = A$ ; this is tantamount to assuming no strain hardening and no mutual interaction of asperities. Second, following Ref. 6, we may assume an exponential function for the relation between  $N$  and  $A_r$ . Then, as  $N$  increases indefinitely, the area-vs.-load

curve, Fig. 33.6, becomes asymptotic to a horizontal line with  $A_r = A$ .

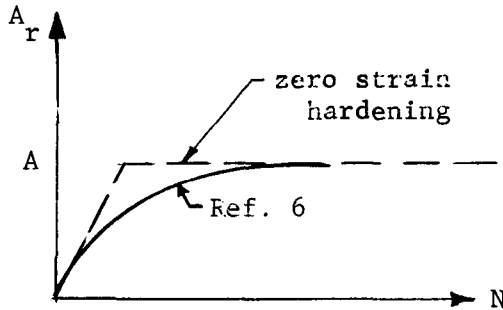


FIG. 33.6 Relation of Real Area of Contact  $A_r$  to Normal Load  $N$  (Ref. 6)

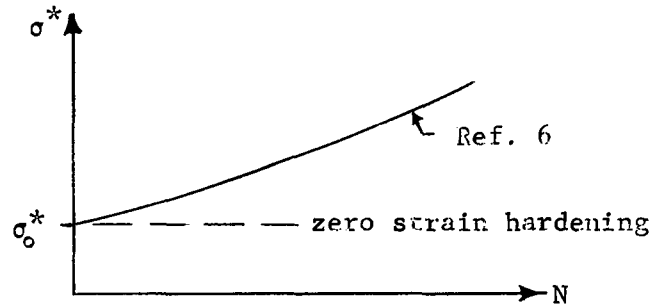


FIG. 33.7 Relation of Compressive Stress  $\sigma_o^*$  to Normal Load  $N$  (Ref. 6)

The decreasing slope of this curve with increasing load represents a strain-hardening effect that can also be illustrated by the curve of stress vs. load shown in Fig. 33.7. Experimental verification has been obtained for the curves of Figs. 33.6 and 33.7 (Ref. 6) up to an  $A_r/A$  ratio of about 0.6. Using the symbol "exp x" for the exponential function  $e^x$ , the equations represented by the curves given in Ref. 6 are:

$$A_r/A = 1 - \exp(-N/A\sigma_o^*)$$

$$\sigma_o^* = \frac{N}{A_r} = \frac{N}{A(1 - \exp(-N/A\sigma_o^*))}$$

As  $A_r/A$  approaches 1, the exponential assumption implies that  $N$  becomes infinite, and this leads to a very pessimistic conclusion about the load required to achieve "zero leakage." On the other hand, the assumption of constant  $\sigma_o^*$  leads to a more optimistic conclusion. To provide a family of curves between these two extremes, we may consider the strain-hardening phenomenon in more detail.

A review of the literature of strain-hardening (Ref. 8) indicates that for some materials the yield stress increases substantially with plastic deformation, while for other materials the yield stress is essentially independent of plastic deformation. For annealed metal specimens, the yield stress generally increases with deformation, but for cold-worked specimens, the initial yield stress is higher than for annealed specimens of the same material, but shows little further increase as a result of

additional plastic deformation. The effect of strain hardening on yield stress may be represented approximately by

$$Y = b\epsilon^m \quad (4)$$

where

$Y$  = yield stress, psi

$b$  = a constant

$\epsilon$  = true unit strain (elongation/instantaneous gage length, not elongation/original gage length)

$m$  = strain-hardening coefficient

The exponent  $m$  and the constant  $b$  may be chosen to match an experimental stress-strain curve. Typical values of  $m$  for metals would be in the range 0.1 to 0.3; a purely plastic stress-strain relation, with no strain-hardening, would be indicated by  $m = 0$ , while a purely elastic stress-strain relation would correspond to  $m = 1$ . The exponent  $m$  is related to the Meyer strain-hardening coefficient  $n$  (Ref. 8; see also Section 32. of this report) by the approximate relationship  $n = m + 2$ . While other investigators have urged caution in applying the exponential relationship of Eq. (4) to plastic-stress problems, it still gives results that are closer to reality than either a purely plastic ( $m = 0$ ) or purely elastic ( $m=1$ ) analysis. (Refs. 9,10).

To illustrate the effect of the amount of strain hardening on the sealing ability of a fluid connector, Fig. 33.6 has been re-plotted for a range of strain-hardening relationships. In the mutual compression of two rough surfaces, it is not possible to determine the actual amount of strain  $\epsilon$ , so some modification of Eq. (4) is necessary. A convenient measure of the amount of strain or work-hardening that has taken place at any point on the surfaces as they are compressed is the "negative clearance,"  $-h$ , at each point where the surfaces have been pushed together (Fig. 33.5). Then the stress  $\sigma$  at any point on the surface is given by

$$\sigma = b (-h)^m, \quad h < 0 \quad (5)$$

Obviously the stress is zero when  $h \geq 0$ , since a positive value of  $h$  at any point indicates that the surfaces have not yet come together at that point.

The values of  $b$  and  $m$  in Eq. (5) are not necessarily the same as those in Eq. (4); however, it is to be expected that for a series of materials with different amounts of strain-hardening, the relative ranking of values of  $m$  from the compression tests represented by Eq. (4) would correspond to the relative ranking of values of  $m$  for the surface interactions represented by Eq. (5).

Now, for any given separation  $s$  between the mean heights of the two surfaces, the total sealing force  $N$  may be obtained by integrating the stress  $\sigma$  over the area of real contact  $A_r$ . Referring to Eqs. (1) and (2),

$$N/A = \int_{-\infty}^0 \sigma p(h) dh = c_m \int_{-\infty}^0 h_o^m \exp \left[ - (h_o - s_o)^2 \right] dh_o \quad (6)$$

$$\text{where } h_o = h / \sqrt{2} h_r$$

$$s_o = s / \sqrt{2} h_r$$

$$c_m = b (\sqrt{2} h_r)^m / \sqrt{\pi} = \text{constant for a given } m$$

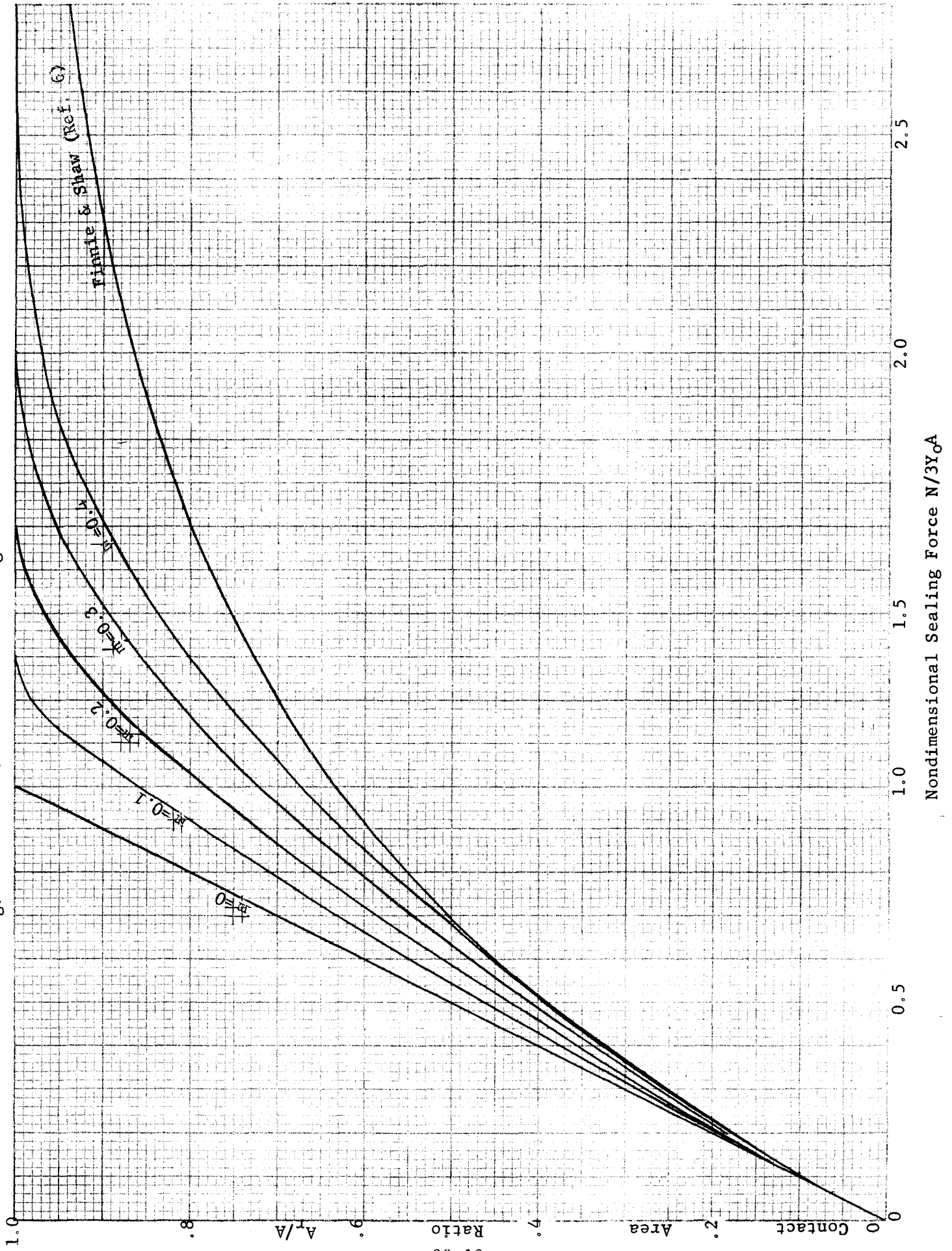
The integral of Eq. (6) was evaluated numerically, using the General Electric 225 digital computer, for a range of values of  $s_o$  and with  $m$  equal to 0.1, 0.2, 0.3, and 0.4. The results were used to plot the curves of  $A_r$  vs.  $N$  shown in Fig. 33.8. For these plots, the constant  $c_m$  was evaluated for each value of  $m$  from the condition that  $N/A_r = 3Y_o$  for initial deformations, in agreement with experimental results reported in the literature (Refs. 5, 8).  $Y_o$  is the yield stress in the absence of strain-hardening.

It must be noted that there is a logical inconsistency in defining  $Y_o$  as "the yield stress in the absence of strain-hardening" when Eqs. (4) and (5) assert that the yield stress in the absence of strain-hardening should be zero. Actually, Eqs. (4) and (5) are approximations that do not apply all the way down to zero strain but which begin to become valid when a small amount of strain has taken place. The relation  $N/A_r = 3Y_o$  was obtained experimentally (Refs. 5, 8) for materials with a well-defined yield point; for materials such as plastics that have no clearly defined yield stress, further experiments are needed to determine the initial relationship between  $N$  and  $A_r$ .

For comparison, the curve of Finnie and Shaw (Ref. 6) and the curve for zero strain-hardening are also shown in Fig. 33.8. Finnie and Shaw's curve was intended as an approximation to an experimental curve for values of  $A_r/A$  up to about 0.6, and it will be noted that for this range, their curve is a reasonable approximation to our calculated curves based on Eq. (6), especially for  $m$ -values of 0.3 and 0.4. However, for the values of  $A_r/A$  near 1.0, which were not of interest to Finnie and Shaw but are of crucial interest to our present investigation, the Finnie-Shaw curve gives quite pessimistic results about the load necessary for tight sealing.



Fig. 33.8 Effect of Strain Hardening on Real Area of Contact



The curves including the effect of strain-hardening, but neglecting the mutual interaction of asperities, indicate that essentially "perfect" sealing can be obtained with nominal stresses somewhat greater than  $3Y_0$ , as summarized in the table below:

<u>Stain-hardening coefficient m</u>	<u>Sealing force for "perfect" sealing</u>
0	3.0 $Y_0A$
0.1	3.9 $Y_0A$
0.2	4.8 $Y_0A$
0.3	6.0 $Y_0A$
0.4	7.5 $Y_0A$

### 33.5 Relation of Load to Flow Passage

The equations of Sections 33.3 and 33.4 can now be combined to give the relation between load and equivalent flow passage based on viscous flow and Assumption A. The results of this calculation are plotted in Fig. 33.9. Then the flow can be computed as in Section 22. This computation has been carried out for the flow passage used in Sec. 22, using an internal pressure of 100 atmospheres, and the result is plotted logarithmically in Fig. 33.10. The abscissa scale is given both in terms of the unit load for steel on steel and in terms of the yield stress,  $Y$ , of the material. This latter scale can be used for other materials, using the assumption that the plastic stress is  $3Y$  over the real area of contact. The ordinate scale can be converted to flow rates for other surface finishes by observing that when all other conditions are equal, the flow rate is proportional to the cube of the rms surface roughness. When the roughnesses of the two surfaces are unequal, the flow rate is proportional to the  $3/2$  power (i.e., to the cube of the square root) of the sum of the squares of the rms roughnesses of the two surfaces. Thus, the rougher of the two surfaces has greater influence on leakage than the smoother surface.

In the design of connectors, the question arises whether it is desirable to reduce the length of the flow passage for the sake of increasing the normal sealing stress, using a given total normal force. This question can be answered from Fig. 33.10. In this example, if the normal force were 150,000 lb., a reduction in the length,  $\ell$ , of the flow passage from 0.1 in. to 0.05 in. would halve the apparent contact area and hence increase the sealing stress from 300,000 psi to 600,000 psi. For a given sealing stress, the flow is inversely proportional to the passage length; therefore, for a given total load, a decrease in length increases the flow when the slope of the flow-vs.-stress curve is greater than  $-1$ , and reduces the flow when the slope of the flow-vs.-stress curve is less than  $-1$ . Referring to Fig. 33.10, it can be seen that for all values of the strain-hardening coefficient  $m$ , the slope is greater (algebraically) than  $-1$  for stresses less than about  $0.8Y$ , and less (algebraically) than  $-1$  for stresses above this value. Hence, it is advantageous to reduce the length of the flow passage provided that the stress level is already above  $0.8Y$ .

It should be remembered that the stresses used for the abscissas of Figs. 33.9 and 33.10 are nominal stresses obtained by dividing the total load  $N$  by the apparent area of contact  $A$ . The assumed actual stress on the real area of contact is  $N/A_r$ .

It must be reiterated that this conceptual model of flow is based on many sweeping generalizations and fraught with many uncertainties. Nevertheless it should prove useful in understanding the problem and in suggesting further analytical and experimental work. A comparison between the results of this analysis and the experimental results is given in Section 37.1.8.

FIGURE 33.9 Calculated Effect of Sealing Pressure on Equivalent Passage Height for Viscous Flow

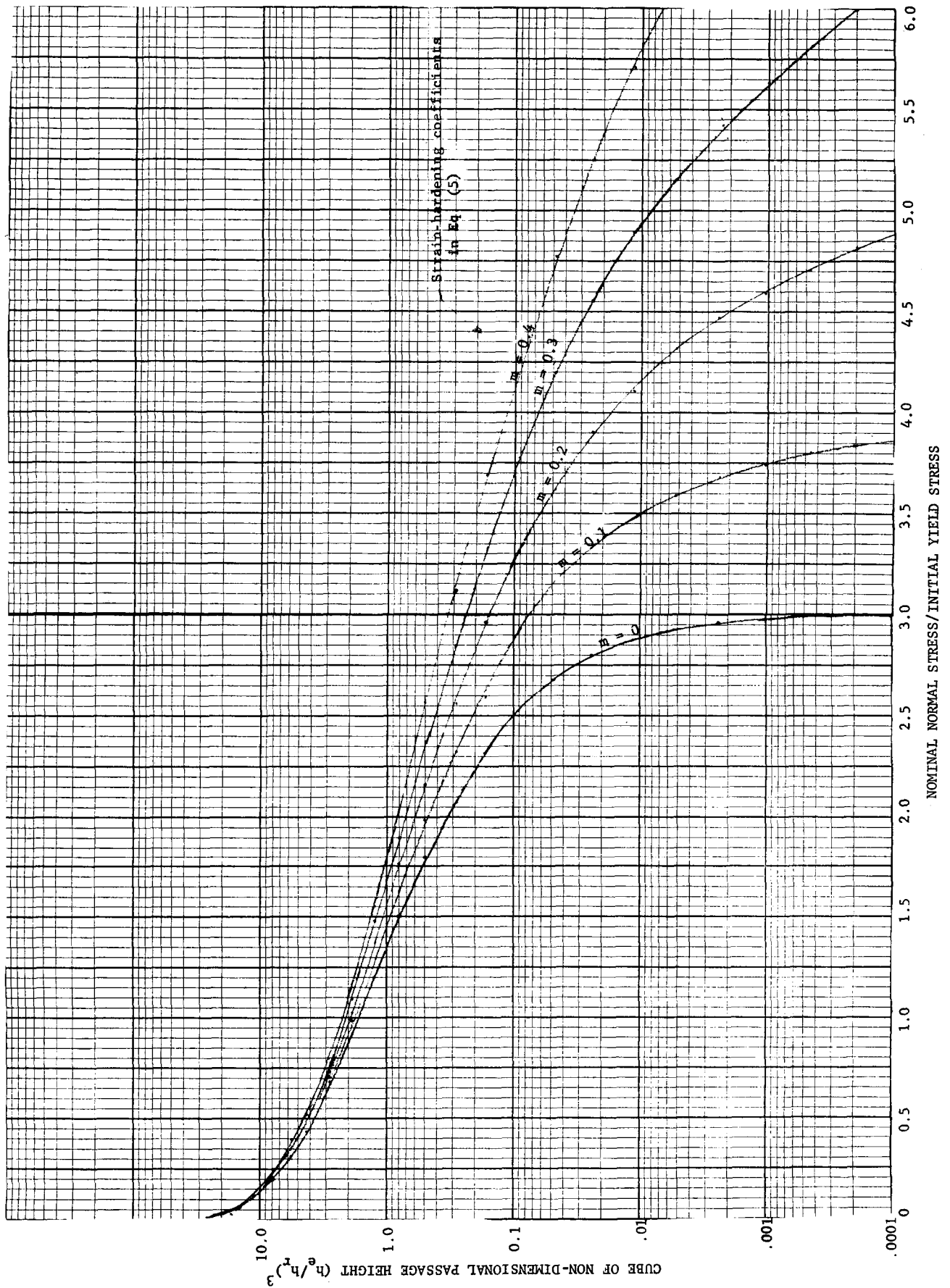
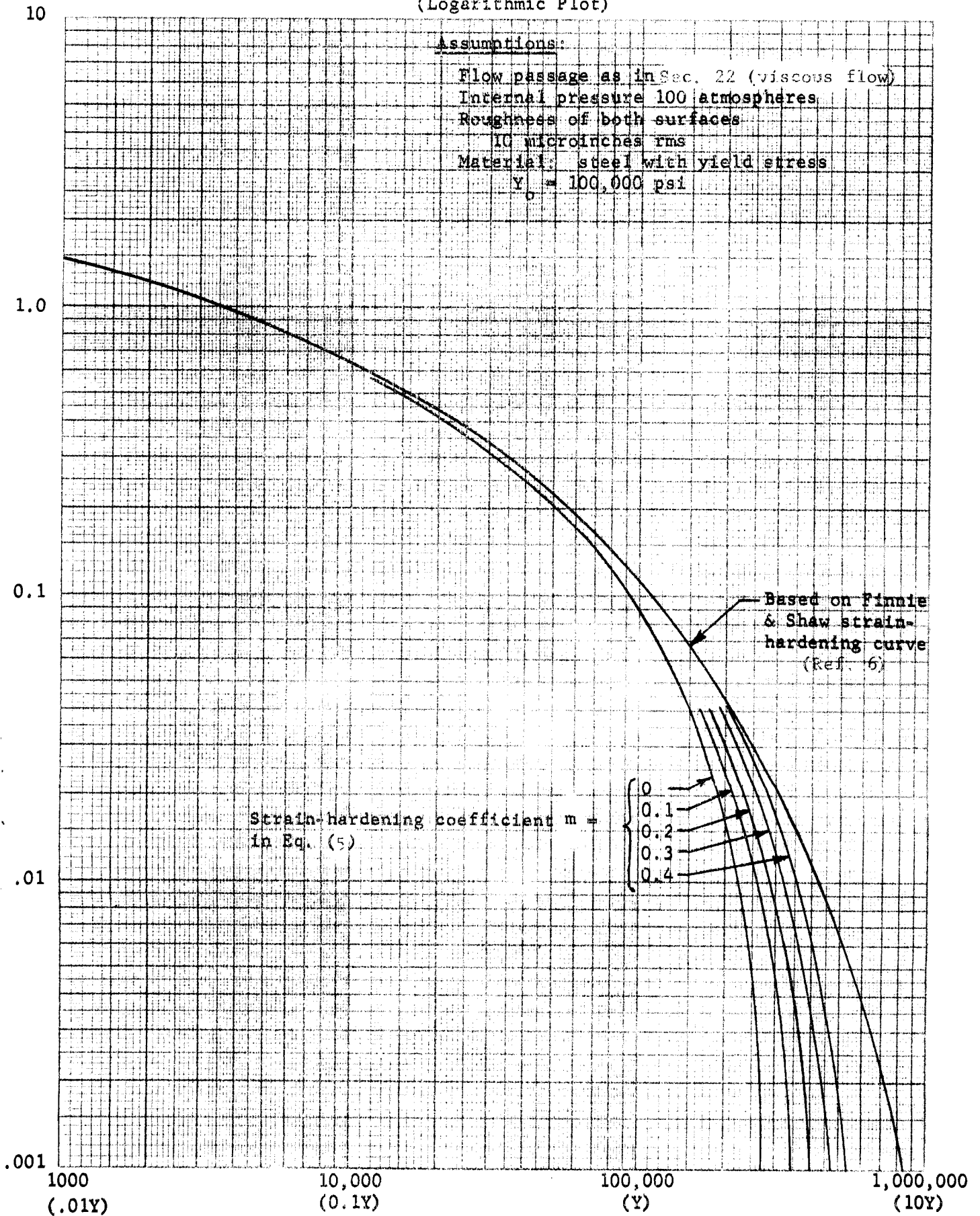


Fig.33.10 Calculated Effect of Sealing Force on Flow Rate for a Typical Joint  
(Logarithmic Plot)



### 33.6 Effect of Surface Waviness

In addition to the smaller asperities that are called "roughness", a machined surface can have larger peaks and valleys known as "waviness" (Ref. 1). The direction parallel to the ridges and valleys of the waviness is called the "lay" direction (Ref. 1). When the lay direction of the flange surfaces is normal to the direction of flow, waviness may have a beneficial effect in reducing leakage by reducing the effective flow-passage length, as discussed at the end of Section 33.5. However, when the lay direction is parallel to the direction of flow, the effect of waviness on leakage can be catastrophic. For this reason, specifications for flange connectors often stipulate that the lay of machining marks should be circumferential rather than radial.

The flow analysis of the preceding sections does not apply directly to surfaces having appreciable waviness. However, the analysis can be extended to include the effect of waviness by treating each crest of the waviness as a separate area of apparent contact.

### 33.7 References

1. American Standards Association, "Surface Roughness, Waviness, and Lay," ASA Standard B46.1-1955.
2. C. E. Weatherburn, A First Course in Mathematical Statistics, Cambridge University Press, 1949, Chapter III.
3. E. J. Abbott and F. A. Firestone, "Specifying Surface Quality," Mechanical Engineering, Vol. 55, No. 9, September 1933, pp. 569-572.
4. F. F. Ling, "Some Factors Influencing the Area-Load Characteristics for Semismooth Contiguous Surfaces Under 'Static' Loading," Trans. ASME, Vol. 80, 1958, pp. 1113-1120.
5. F. P. Bowden and D. Tabor, The Friction and Lubrication of Solids, Oxford University Press, 1950.
6. I. Finnie and M. C. Shaw, "The Friction Process in Metal Cutting," Trans. ASME, Vol. 78, 1956, pp. 1649-1653.
7. F. F. Ling, "On Asperity Distributions of Metallic Surfaces," Jl. Appl. Phys., Vol. 29, No. 8, August 1958, pp. 1168-1174.
8. D. Tabor, The Hardness of Metals, Oxford University Press, 1951.
9. A. Winzer and W. Prager, "On the Use of Power Laws in Stress Analysis Beyond the Elastic Range," J. Appl. Mech., 1947, pp. A-281 to A-284. Discussion and Authors' Closure, 1948, pp. 185-187.
10. A. Nadai, Theory of Flow and Fracture of Solids, McGraw-Hill, 1950.

## 34. MECHANICAL PROPERTIES OF FLANGE AND GASKET MATERIALS

by

F.O. Rathbun, Jr., G.W. Sarney, and J.E. McConnelee

### 34.0 Summary

One of the important areas of study in the gasket leakage investigation is that of gathering information on the pertinent properties of the materials used in the system, as both gaskets and the sealing surfaces on which the gaskets rest. In order to use material characteristics as parameters in the leakage investigation rather than investigating different combinations of materials separately, it is necessary to establish quite accurately the properties of the materials used experimentally. Many characteristics of materials play important roles in the leakage phenomenon - creep under high temperature, relaxation under continued loading, the outgassing of some of the materials, the susceptibility of materials to the diffusion of gases through them, the temperature dependence of all properties, the strain hardenability, and the static strength properties such as the yield strength and the modulus of elasticity.

In the experimental and analytical work performed, however, changes of properties with temperature and time are not considered as such; but rather the assumption is made that when properties do change with temperature or time, then the system response can be determined by the new properties at that time or temperature. Since tests at room temperature are made for various static strength properties, it is assumed that this information can be extrapolated to other temperatures.

One time consideration does enter the investigation, however, that of short-time cold flow of some plastic gasket materials.

This section deals primarily with the static strength properties of the materials under investigation. The sealing surface materials (347 Stainless Steel and 2024(24S)T4 Aluminum) have been chosen because of the vast utilization of these materials as fuel containers in missile applications.

The gasket materials, which are listed in Section 34.2, were determined on the basis of several factors. Three categories of materials were selected - metal gaskets, plastic gaskets, and rubber-like gaskets. The metals were selected on the basis of securing a large range of yield stress. Materials were included which have proved at least partially successful in gasket applications. The plastics and rubber-like materials selected have, for the most part, been used in connectors prior to this investigation, and span the characteristics for these categories quite well.



### 34.1 Sealing-Surface Materials

Two materials have been selected for use as sealing surfaces (flange materials). Both are currently in use in connector test facilities at the G.C. Marshall Space Flight Center. A stainless steel and an aluminum have been selected:

- (1) 347 stainless steel
- (2) 2024(24S)T4 aluminum

The steel used is a tough, difficult-to-machine material with an ASTM listed yield strength of from 35,000 to 40,000 psi. The aluminum has an ASTM listed yield strength of 47,000 psi. To insure a precise knowledge of the actual yield strength of the specimens used in leakage tests, room-temperature tensile tests have been accomplished on one-half-inch-diameter specimens of each material. Normal room-temperature ASTM testing procedure was utilized. The resulting stress-strain curves are shown in Figure 34.1. It will be noted that the aluminum has the higher yield strength. Two standard yield strengths are evaluated for each material - the 0.2% yield strength and the 0.02% yield strength. The tensile strength was also evaluated in the same experiment. Table 34.1 lists the resultant strength properties.

TABLE 34.1 SEALING SURFACE MATERIALS

<u>Material</u>	<u>0.02% Yield Strength</u>	<u>0.2% Yield Strength</u>	<u>Tensile Strength</u>
347 S.S.	30,750 psi	39,125 psi	85,000 psi
2024(24S)T4 aluminum	50,000 psi	51,750 psi	69,000 psi

Also of interest, and hence evaluated for the sealing surface metals (and metal gasket materials), is the Meyer strain-hardening index  $n$ .

The parameter  $n$  is an empirical quantity initially used in the equation

$$W = kd^n \quad (1)$$

where  $d$  is the diameter of a hole made by a fixed-radius ball indenter under a load  $W$ . This relationship was first observed by Meyer (1908). (Ref. 1)

Subsequent work showed that  $n$  is almost independent of the ball indenter diameter. Experiments show equation (1) to be quite valid for many metals within a certain range of  $d/D$  ( $D$  being the ball indenter diameter). The lower limit of  $d/D$  was fixed by Meyer to be about 0.1, and the upper limit is near 1.0 for many metals. Most metals are known to have values of  $n$  between 2.0 and 2.5, with fully annealed metals having values near 2.5 and fully worked metals near 2.0.

The value of  $n$  can be measured by successive Brinell hardness tests on the same metal with the same ball indenter. Discrete increases in load are applied. From equation (1), we can write

$$\ln(W) = (n)\ln(d) + \ln(k) \quad (2)$$

Thus, by plotting W and d on log-log paper for successive values of W, the slope of the resulting line will be equal to n.

For values of d outside the applicable limits, the resulting plot cannot be approximated by a straight line.

For 347 stainless steel, the resultant value of n is 2.35. For 2024(24S)T4 aluminum, the experimentally found value is 2.27. This value of n finds utilization in section 33, where strain hardening is a factor in the analytic leakage predictions.

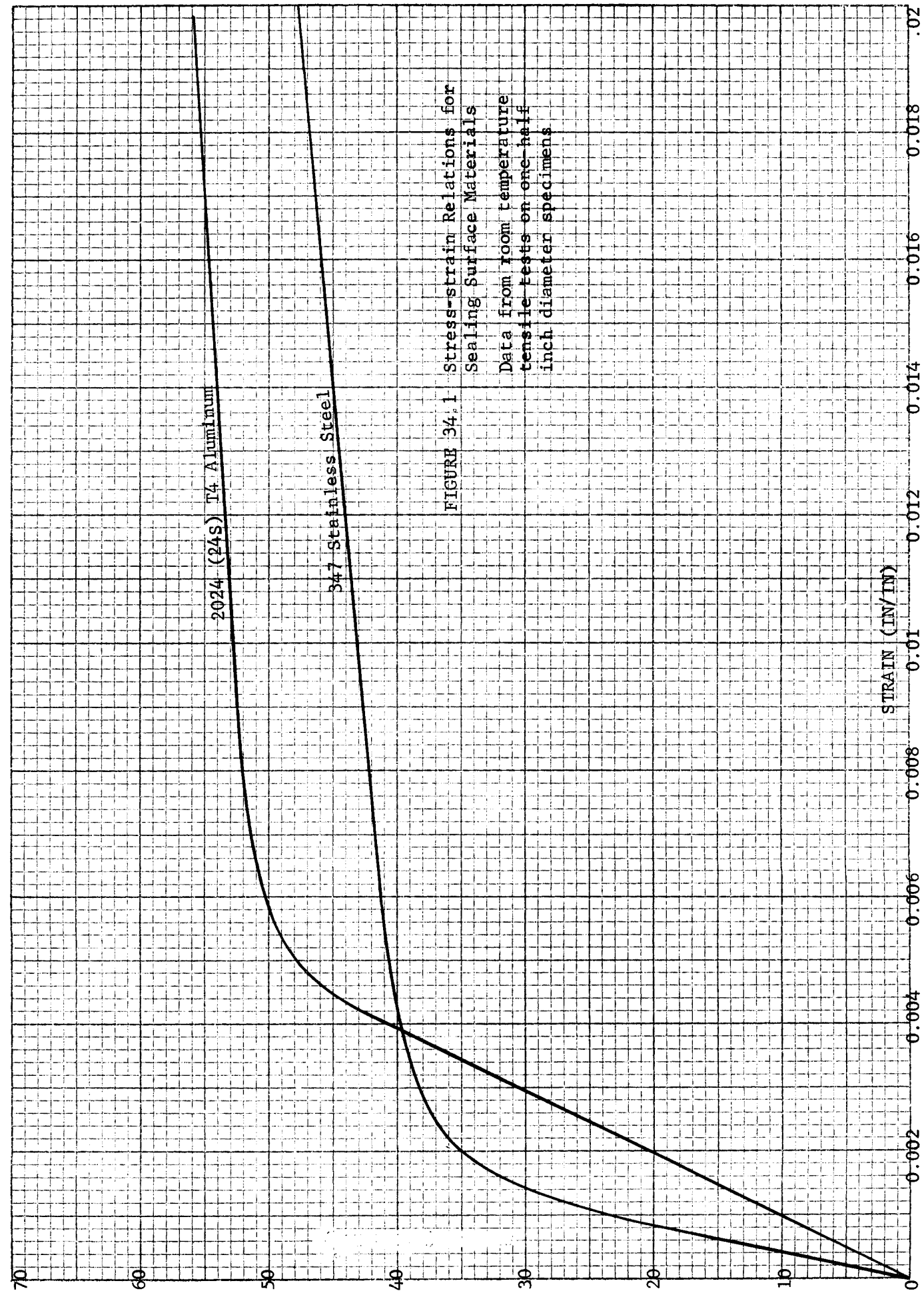


FIGURE 34.1 Stress-strain Relations for Sealing Surface Materials  
Data from room temperature tensile tests on one-half inch diameter specimens

## 34.2 Gasket Materials

### 34.2.1 Metal Gaskets

All gasket metals utilized are much weaker than the materials used for sealing surfaces. Five metals have been used:

- |             |   |
|-------------|---|
| 1. Indium   | 99.97% pure                                 |
| 2. Lead     | 99.90+% pure, ASTM B29.55                   |
| 3. Aluminum | 99.6+% pure, 1060-0 Temper. ASTM209-61      |
| 4. Copper   | 99.9+% pure, federal specification QQ-C-576 |
| 5. Nickel   | 99.4% pure, ASTM B160-58T                   |

Material for gaskets was procured in flat stock. Hence, yield strength data for these metals have been gained from specimens cut from flat stock. Since the gaskets cut from the stock are loaded normal to the plane of the stock, the possibility of the yield strength being different for the application and the test exists. Anisotropy of strength of flat rolled stock is possible.

However, tensile test data are indicative of relative strength. Experimental results of tensile data are shown in Table 34.2.

TABLE 34.2 GASKET METAL STRENGTHS

<u>Metal</u>	<u>0.02% Yield Stress</u>	<u>0.2% Yield Stress</u>	<u>Tensile Strength</u>
Indium	41 psi	82 psi	202 psi
Lead	1040 psi	1425 psi	2000 psi
Aluminum	3388 psi	4400 psi	10000 psi
Copper	6140 psi	7770 psi	29100 psi
Nickel	10200 psi	13230 psi	45300 psi

The tensile tests for indium and lead were done as prescribed in ASTM Standard 1961, Part 3, ASTM Designation E21-58T (tensile tests for metals at high temperatures). Since at room temperature, indium and lead creep, a prescribed rate of strain was employed consistent with rates for other metals tested within their creep ranges.

The stress-strain curves attained from the above mentioned tensile tests are presented in Figures 34.2 and 34.3.

The approximate yield strengths of the actual gasket materials used can be obtained also by inspection of the load-deflection curve associated with the leakage experiment. Since three linear differential transformers are used around the periphery of the gasket to monitor the uniformity of gasket compression, it is possible to ascertain the location of the yield point of the gasket material loaded normal to the plane of the gasket. Hence, any effects of anisotropy of the gasket material will not be seen. Since the tensile tests conducted on specimens cut in the plane of the gasket give the yield stress in that direction, but offer no guarantee that the characteristics are the same for the material used as a gasket, the evaluation of a yield strength during the actual leakage test provides a check on the tensile test value and becomes a more meaningful parameter for study.

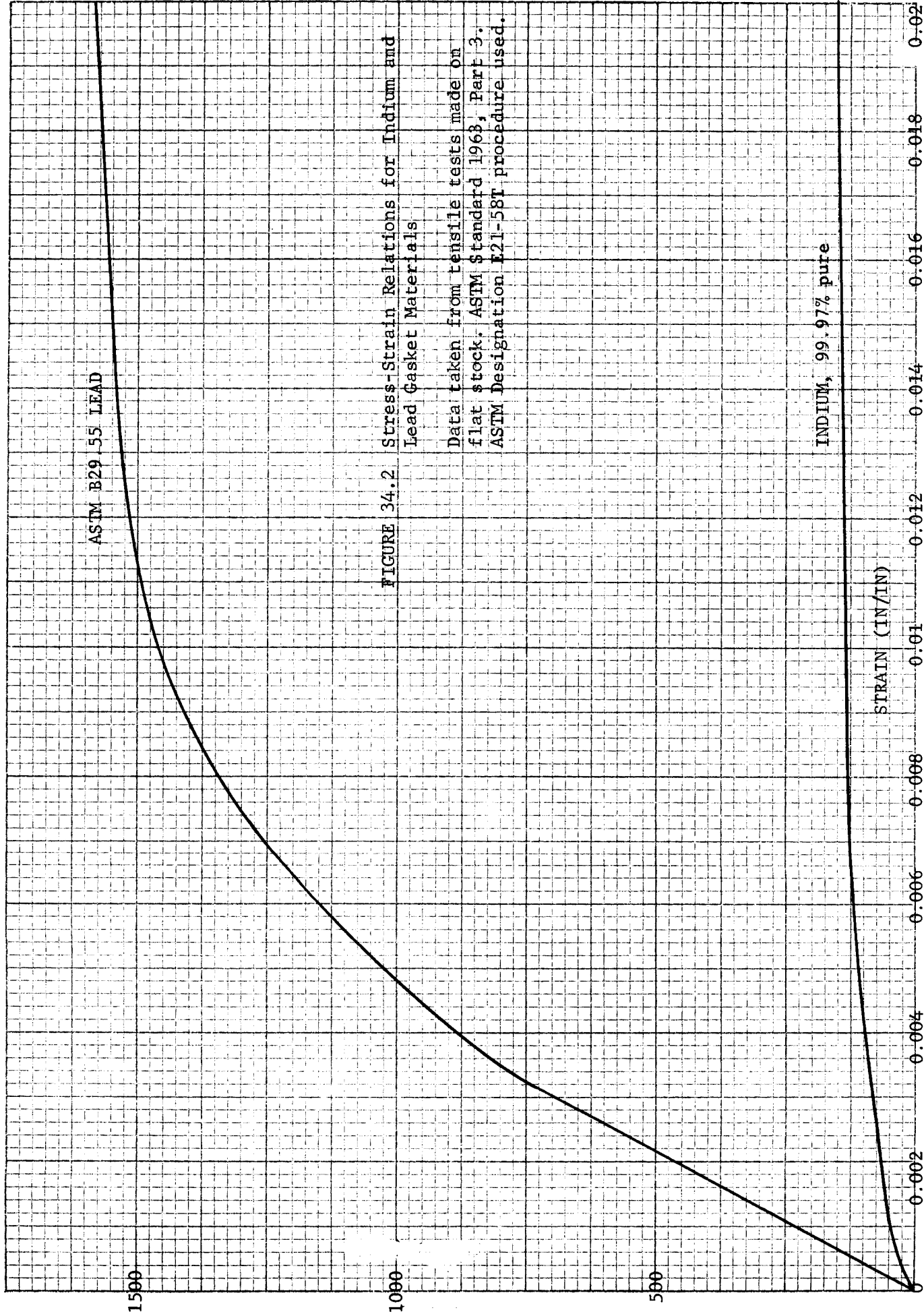
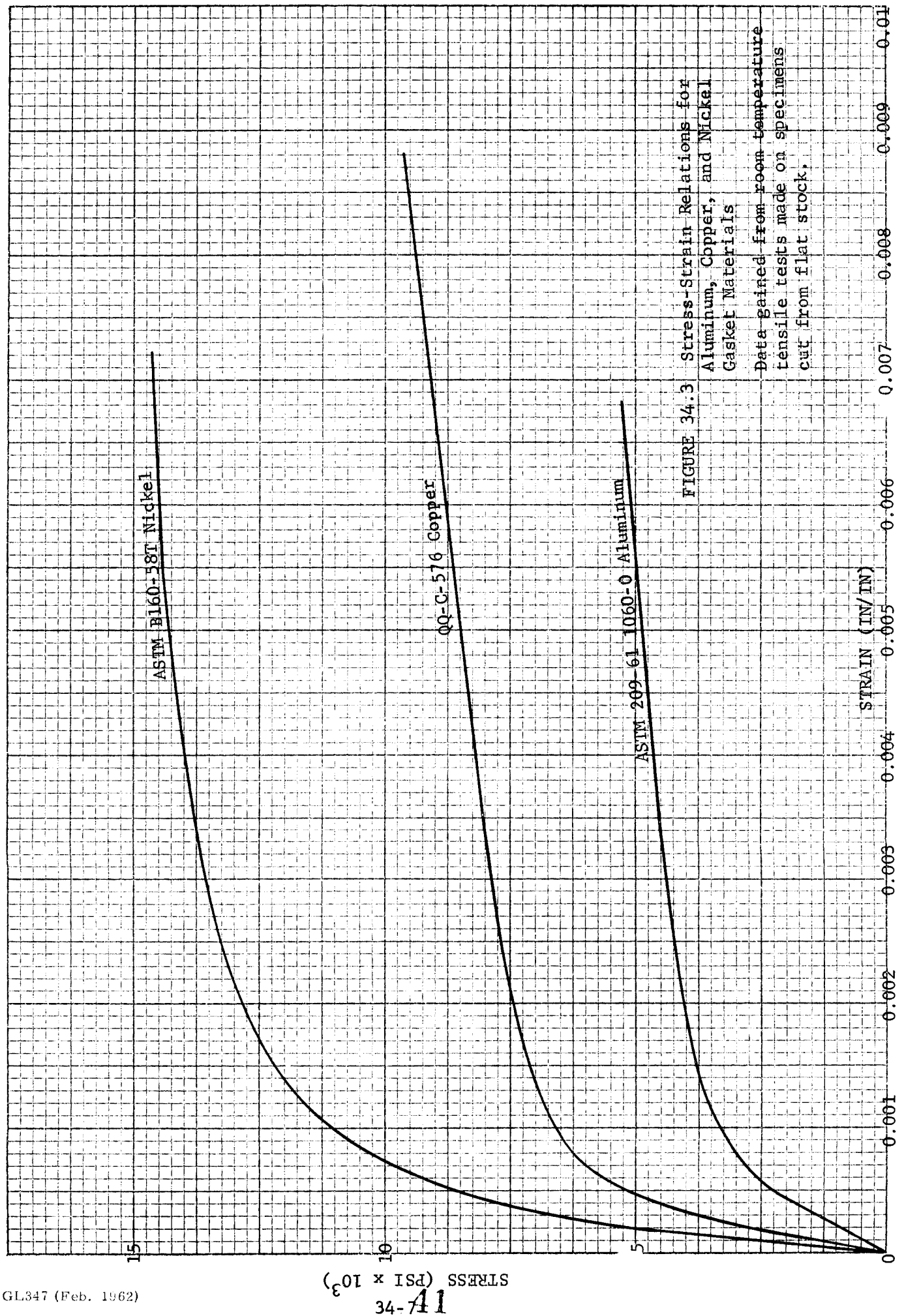


FIGURE 34.2 Stress-Strain Relations for Indium and Lead Gasket Materials

Data taken from tensile tests made on flat stock. ASTM Standard 1963, Part 3. ASTM Designation E21-58T procedure used.



Because of the gasket height-to-area ratio, the specimen shape is not ideal for compression testing. Friction plays an unusually high role in the compression phenomenon. Also, as has been mentioned in Section 32, the compression of a flat annular gasket approximates the plane strain problem; i.e., the material flow will be radial only (no tangential displacement). Hence, the yield strength noted from load-deflection data associated with the actual leak test will be approximately 1.1 times the yield strength as measured in a normal tensile test. Of course, it is assumed that the yield strength does not vary from the tensile to the compression case.

Also, any data gained from the leak test load deflection curve can be used only to evaluate strength properties independent on magnitude of strain (such as a yield strength evidenced by a distinct change in slope of the load deflection curve). Due to the flexibility of the supporting structure and the local deformation of surface asperities, the relationship between stress and strain will not resemble the true case; e.g. Young's modulus could not be attained. However, the phenomenon does not detract from the yield-strength evaluation as long as the parameter is evaluated consistently for each test.

For the metal-gasket leak tests, data have been accumulated concerning the load-deflection relationship; load-deflection curves have been plotted for each of the three linear differential transformer readings for every test. The indium tests produced no significant data since the yielding occurred before enough data points could be accumulated.

The tests utilizing lead as a gasket material produced a mean yield strength of 2300 psi. The 2300 psi value is that gained directly from the test and hence is approximately 1.1 times the desired yield strength. Thus, by the leak-test evaluation, the yield strength of lead is approximately 2090 psi. Also, it must be stated that the selection of a yield strength by these means is not as refined as the selection of an 0.02% or an 0.2% yield strength. The method used is that of selecting the intersection of the extensions of two straight lines coincident with the elastic line and the yielded load-deflection curve. The resultant load is then divided by the instantaneous area, thus giving a yield-strength value.

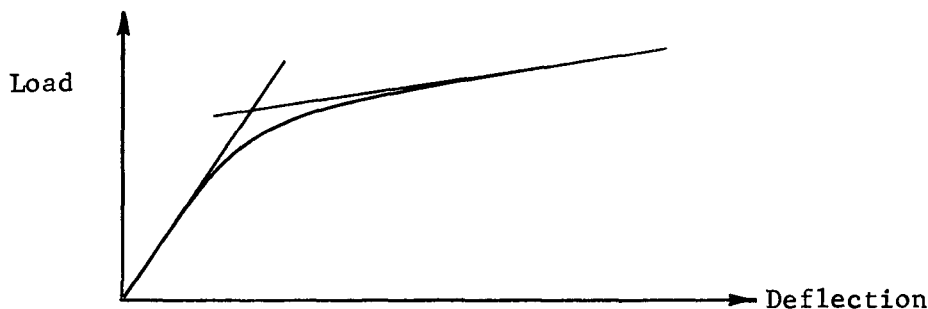


FIGURE 34.4 Determination of Yield Point from Gasket Compression Tests

Comparing this point geometrically to a similar procedure used on the tensile-test data, it can be seen that the method gives approximately the same results as the 0.2% yield-strength criterion.

Hence, for the case of lead, it can be seen that anisotropy or the effect of friction was a factor. The 0.2% yield strength of the lead in the direction normal to the gasket would be approximately 2090 psi. Extrapolation of these data to an 0.02% yield strength gives a 1525 psi magnitude.

Similar evaluations have been made for copper, aluminum, and nickel. The results of each are listed in Table 34.3.

TABLE 34.3 YIELD STRENGTHS OF GASKET MATERIALS

Material	Tensile Test Data			Leak Test Data			
	0.02%Y.S.	0.2% Y.S	Y*	1.1 Y*	Y*	0.02% Y.S. <sup>x</sup>	0.2% Y.S. <sup>x</sup>
Lead	1040	1425	1518	2300	2090	1433	1960
Aluminum	3388	4400	3930	5700	5350	4620	6000
Copper	6140	7770	7200	14000	12700	10820	13600
Nickel	10200	13230	12530	32000	29100	23700	30800

Y\* gained directly from load-deflection curves: intersection of extensions of elastic and plastic portions of the curves.

x same ratio of 0.02% Y.S. to Y\* as in tensile test data.

It is to be noted that the data gained from the leak tests concerning yield point are averaged in the above table. The dispersion of data was such from test to test to allow such an averaging technique in the case of metals. Since each gasket was cut from the same piece of material, it is reasonable to assume that variances are due to non-uniformity of loading, and that a single value of yield strength is to be expected. It is noted in all cases that the yield strength evidenced in leak tests is much larger than that evidenced in a tensile test. For lead and aluminum, the increase is approximately 37%; for copper, 77%; and for nickel, 137%. Obviously, both the geometry and large friction between surfaces plays a large role; also, anisotropy affects each case differently.

Whatever the reasons, the leak test results are more indicative of the phenomenon of yielding during the actual test; hence, these results are more meaningful as standards of comparison.

The same type Meyer strain coefficient tests were accomplished on the metal gasket materials as were done on the sealing surface metals. The results are shown in Table 34.4.



TABLE 34.4 MEYER INDICES FOR GASKET METALS

<u>Material</u>	<u>Meyer Index</u>
Indium	2.19
Lead	2.25
Aluminum	2.3
Copper	2.29
Nickel	2.18

### 34.3 Plastic Gasket Materials

Plastic gasket materials have been tested in mating with stainless steel and aluminum flange material to determine the sealing characteristics of the plastics. The following plastic materials have been tested:

TABLE 34.5 PLASTIC MATERIALS

<u>Trade Name</u>	<u>Composition</u>
KEL-F81	chlorotrifluoroethylene
Saran	polyvinylidene chloride
Teflon-FEP	fluorinated ethylene-propylene
Teflon-TFE	tetrafluoroethylene
Duroid-5600	60% Teflon - 40% Ceramic fiber

The teflon TFE is a compressed powder, and the teflon FEP is formed by molding.

The stainless steel and aluminum materials are relatively rigid with respect to the plastic gaskets, so that the interface sealing will be a function of the soft gasket material properties only. The material properties affecting leakage may be classified as those chemical properties affecting permeation through the gasket material and those mechanical properties affecting the deformations necessary for sealing at the interface.

The calculation of leakage rates due to permeation depends on the gasket geometry, the gas pressure differential and the permeation rate. The permeation rate is a function of the gas - material combination and the system temperature. The following permeation rates have been reported for room temperature:

TABLE 34.6 PLASTIC MATERIAL PERMEATION RATES

<u>Gasket Material</u>	<u>Gas</u>	<u>Permeation Rate</u> - $\frac{\text{cm}^3 - \text{mm}}{\text{sec} \cdot \text{cm}^2 - \text{atm}}$
Kel - F81 **	Air	$4.0 \times 10^{-7}$
Saran *	H <sub>2</sub>	$.23 \times 10^{-7}$
Teflon *	H <sub>2</sub>	$3.4 \times 10^{-7}$
Duroid		not available

\* Private conversations with Dr. F.J. Norton, General Electric Research Lab.  
 \*\* Computed from data in Section 23

The interface. sealing will be a function of the visco-elastic properties of the gasket. The yield stress which is indicative of gross deformations is the most meaningful parameter for surface asperity deformations.

The yield stress for plastic materials is a pronounced function of temperature, strain rate, nature of loading (compression, tension, torsion) and the directional properties of the material. Also for gaskets used in these tests with low height-to-area ratios the surface roughness, friction and plane strain loading affect the gross deformations.

The deflection and load data obtained during the test provided a reliable measure of the yield stress for each test. All of these tests were conducted at room temperature and with very low strain rates. The variation of yield stress among different tests of the same gaskets material is a function of the mating surface finish, as shown in Table 34.7. The value of the yield strength is determined for a .2% strain offset. The yield stress of the gasket is higher for the rougher mating surface. This effect is less pronounced for teflon, probably due to its very low coefficient of friction.

TABLE 34.7 LEAKAGE TEST .2% YIELD STRESS

<u>Gasket Material</u>	<u>Surface Finish</u>	<u>.2% Yield Stress -psi</u>
KEL-F81	Circumferential Machining	7400
KEL-F81	Radially Ground	6350
KEL-F81	Diamond Burnish	6100
Saran	Circumferential Machining	5300
Saran	Radially Ground	4000
Saran	Diamond Burnish	3000
Teflon-FEP	Circumferential Machining	3050
Teflon-FEP	Radially Ground	3100
Teflon-FEP	Diamond Burnish	2850
Teflon-TFE	Circumferential Machining	2800
Teflon-TFE	Radially Ground	2050
Teflon-TFE	Diamond Burnish	2100
Duroid-5600	Circumferential Machining	2350

Separate compression tests have been run at room temperature for the same configuration gasket cut similarly from the same plastic sheet as the leakage test samples. The results of these mechanical tests in which the strain rate was accurately controlled are shown in Table 34.8.

TABLE 34.8 PLASTIC MATERIAL .2% YIELD STRESS

<u>Gasket Material</u>	<u>Strain Rate,</u> <sup>mil</sup> <u>min</u>	<u>.2% Yield Stress, psi</u>
KEL-F81	50	7250
KEL-F81	50	6800
KEL-F81	20	6750
Saran	100	7200
Saran	50	6400
Saran	20	5650
Saran	2	4850
Teflon-FEP	100	3275
Teflon-FEP	50	3600
Teflon-FEP	20	3750
Teflon-TFE	100	2500
Teflon-TFE	50	2525
Teflon-TFE	20	2375

The general trend is for higher yield-stress values at the faster strain rates. The yield-stress values at the low strain rates compare favorably with the values obtained in the leakage test which was conducted over a relatively long time period. The value of the yield stress which is most meaningful is that obtained from each test, since it includes the effects of all the actual test variables.

Evaluation of the strain-hardening characteristic of the plastic materials is not practical due to their visco-elastic properties. The Meyer strain-hardening coefficient, which is obtained by measuring the indentation of a ball under load on the surface of the material, would be a function of the rate of loading and the indenter ball diameter.

#### 34.4 Rubber Gasket Materials

##### 34.4.0 Elastomer Gasket Material Properties

The sealing ability of rubber-like gaskets is discussed in terms of the material properties of the gasket and the restraint on Bulk flow of the gasket.

##### 34.4.1 Rubber Gasket Material Properties

The sealing characteristics of four rubber-type gasket materials have been investigated. The mating stainless steel and aluminum flange materials are stiff relative to the rubber, so that the sealing for various flange surfaces will be a function of the material properties of the rubber.

TABLE 34.9 - RUBBER MATERIALS

<u>Trade Name</u>	<u>Composition</u>
Viton-A	co-polymer of vinylidene fluoride and oride and hexafluoropropylene
Neoprene	chloroprene
Hypalon	chorosulfurated polyethylene
Silicone	polysiloxane

The material properties affecting leakage may be classified as those chemical properties affecting permeation through the gasket material and those mechanical properties affecting the deformations necessary for sealing at the interface.

The following permeation rates have been reported (Section 23) using air at room temperature.

TABLE 34.10 RUBBER MATERIAL PERMEATION RATES

<u>Rubber Material</u>	Permeation Rates, $\frac{\text{cm}^3 \cdot \text{mm}}{\text{sec} \cdot \text{cm}^2 \cdot \text{atm}}$
Silicone	$2.2 \times 10^{-5}$
Neoprene	$6.0 \times 10^{-8}$
Viton - A	not available
Hypalon	not available

The mechanics of deformation of rubber-like materials is in general extremely complicated. The durometer system is the only general approach at classifying the mechanical behavior of elastomers. This provides a basis for comparison of the stiffness of one rubber with respect to another but can not be related to other types of materials. The stiffness of each elastomer decreases with decreasing durometer value. The durometer value is presented for the rubber materials tested in Table 34.11.

TABLE 34.11 RUBBER MATERIAL HARDNESS

<u>Rubber Material</u>	<u>Durometer - A</u>
Silicone	40 - 85
Neoprene	40 - 95
Viton-A	60 - 95
Hypalon	40 - 95

However, rubber-like materials have a very low stiffness in relation to the metal and plastic gaskets used in this series of tests. It is expected that deformation and compliance at the interface will occur at a correspondingly low normal pressure.

#### 34.4.2 Effect of Gasket Constraint on Behavior of Rubber (Refs. 2,3,4)

The composition of rubber-like materials is such that wide variations in mechanical behavior occur as a function of temperature and bulk constraint. To demonstrate these effects on the sealing ability of the gasket an analysis of some simple mechanical models is included. This analysis shows that gasket constraint is a primary consideration for rubber-like materials. Virtually all of the organic gasket materials exhibit rubberlike properties in the sense that:

- (1) They exhibit a critical or transition temperature at which abrupt changes occur in certain of their physical properties.
- (2) Their mechanical behavior is basically that of a two-phase material (mechanical mixture) in which the first phase is elastic and the second phase is visco-elastic at room temperature. (These two phases will hereafter be referred to as the elastic and visco-elastic phases respectively).

The changes in the physical properties of these organic materials at their transition temperature are basically the result of an abrupt change in the mechanical properties of the visco-elastic phase only. The elastic phase does not exhibit any abrupt changes in properties at the transition temperature.

In passing through the transition temperature (in the direction of decreasing temperature), the viscosity of the viscoelastic phase increases so greatly that this phase exhibits almost purely elastic behavior below the transition temperature. The modulus of elasticity of the visco-elastic phase,  $E_2$ , is many times the modulus of elasticity of the elastic phase,  $E_1$  (For example, for neoprene  $E_2$  is of the order of  $10^5$  psi while  $E_1$  is of the order of  $10^3$  psi). This is the reason for the abrupt change in certain of the physical properties of the composite, since above the transition temperature the long-time deformations of the composite are controlled by the elastic phase, whereas below the transition temperature the visco-elastic phase controls the deformation characteristics of the composite.

One would, therefore, expect to see abrupt changes in the effective modulus of elasticity,  $E^*$ , of the composite as well as in its hardness, elongation and other mechanical properties.

Since there are several orders of magnitude between the values of  $E_1$  and  $E_2$  ( $E_2 > E_1$ ), what one actually obtains in measurements of the mechanical properties of these materials are primarily the properties of the elastic phase above the transition temperature and primarily the properties of the visco-elastic phase below the transition temperature.

A notable exception is the bulk modulus, which does not vary appreciably through the transition temperature. The bulk modulus of the composite is of the order of  $10^5$  psi for many of these materials (Refs. 2 and 3). This is basically in agreement with all of the existing theory used in plasticity and visco-elasticity, since plastic or viscous deformations are always considered to be associated with the deviatoric strains and not with the isotropic portion of the strain (dilatation). The importance of this will be illustrated by the following analysis.

Although there are an almost unlimited number of organic gasket designs in use, for purpose of the present analysis they can all be covered by two simple categories. These categories are:

- (1) Gaskets constrained so as to permit volumetric precompression.
- (2) Gaskets which are not sufficiently constrained to permit volumetric precompression.

In order to illustrate the inherent difference between these two categories, the simplified models\* in Figure 34.5 are analyzed. Figs. 34.5a and 34.5d show a simple model of a gasket of groups (1) and (2) respectively in the unstrained condition. The dotted region in each case represents the visco-elastic phase of the material characterized by its bulk modulus,  $K_2$ , while the spring represents the elastic phase characterized by a linear spring constant,  $k_1$ . (The elastic phase is considered to be incompressible

\* see following page

and therefore  $K = K_2(1 + V_1/V_2)$  where  $V$  denotes volume.)

If each gasket is given an initial linear precompression of amount  $\delta$  (Figs. 34.5b and 34.5e), the force required to accomplish this will be as indicated in the figure.\*\* For the constrained gasket, this force is composed of term  $k_1\delta$  associated with the linear compression of the elastic phase and the term  $K\delta/h$  associated with the volumetric compression of the gasket, whereas for the unconstrained gasket there can be no volumetric compression and hence no force involving the bulk modulus of the gasket.

Consider now the case in which Figs. 34.5b and 34.5e represent the situation existing in a gasketed assembly at a temperature just above the transition temperature. Next, let the cooling proceed to a temperature just below the transition temperature. In the process, the viscoelastic phase has become essentially purely elastic in nature with a modulus of elasticity considerably higher than that of the elastic phase.

If in addition the drop in temperature is accompanied by a differential thermal expansion between the parts of the gasket assembly such that the precompression is relaxed by an amount  $\epsilon$  ( $\epsilon > \delta$ ), the situation will be as indicated by Figs. 34.5e and 34.5f. In the case of the constrained gasket, a sealing force proportional to the remaining volumetric compression  $(\delta - \epsilon)/h$  remains. In the case of the unconstrained gasket, all of the sealing force has been lost and a gap exists, since the viscoelastic phase has "hardened," thereby restraining the relatively small restoring force of the elastic phase linear spring.

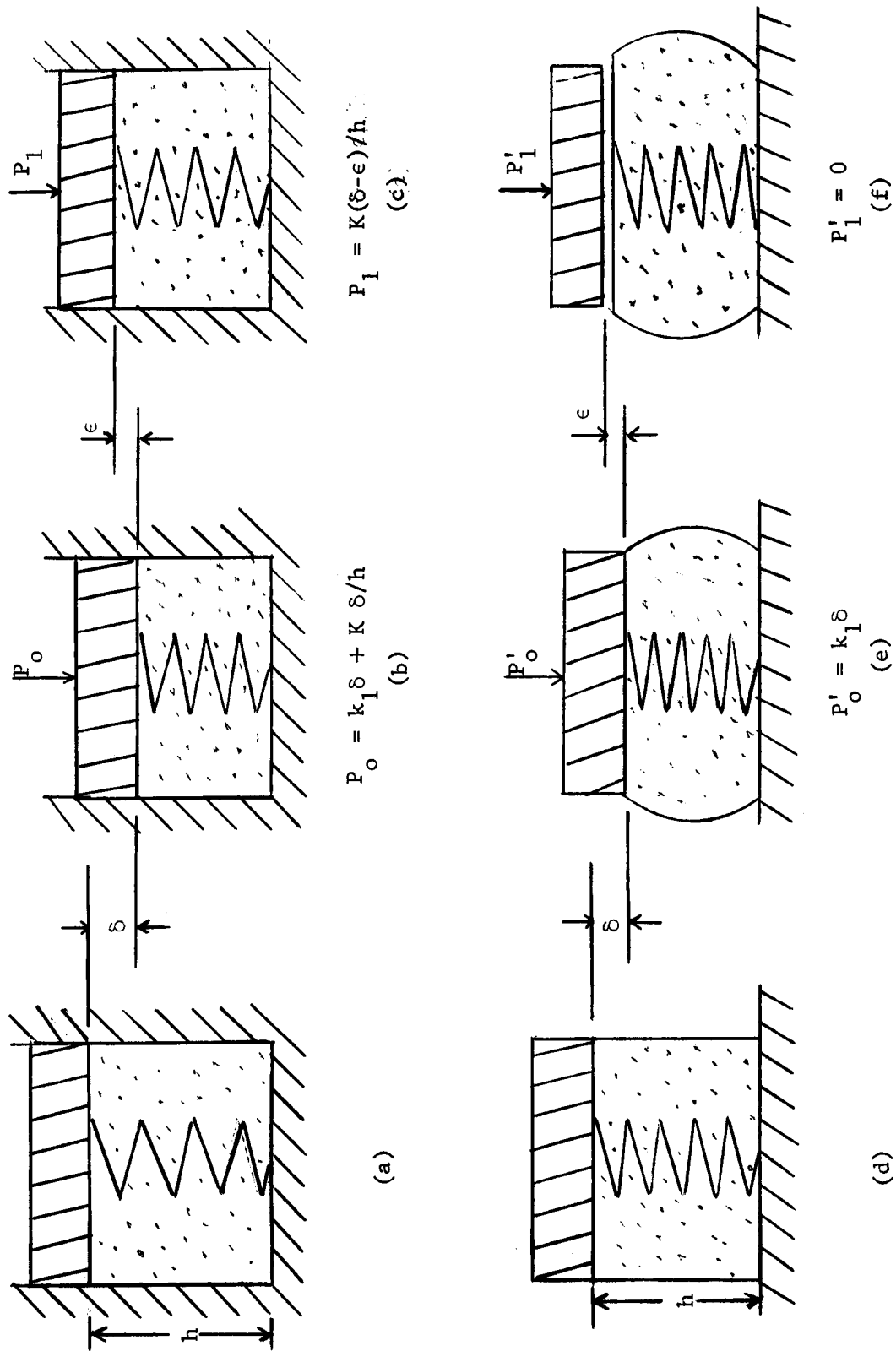
To place the problem in clearer perspective, consider the numerical values involved in the foregoing example if the gasket is a one-inch cube of neoprene rubber. The bulk modulus of neoprene is approximately  $10^5$  psi and the modulus of elasticity of the elastic phase is about 1500 psi. Therefore

---

\* The mechanics of deformation of rubber-like materials are in general extremely complicated and for a detailed discussion the reader is referred to reference 4. However, these simplified models are used here since they are sufficient to illustrate the basic deformation properties in gasket design. More sophisticated mathematical models may be required at a later date to evaluate some of the finer points of gasket designs.

\*\* Provided the load is applied slowly. If the load is applied rapidly, there will also be a viscous component of load present, but this is of no practical importance to this analysis.





Mechanical Models for Rubber-like Gasket Materials

FIG. 34.5

$$K = 10^5 \text{ psi}$$

$$k_1 = 1500 \text{ psi}$$

$$h = 1 \text{ in.}$$

Assume  $\delta = 0.1 \text{ in.}$

$$\epsilon = 0.01 \text{ in.}$$

Therefore:

$$P_o = 10,150 \text{ psi}$$

$$P_1 = 9,000 \text{ psi}$$

$$P_o' = 150 \text{ psi}$$

$$P_1' = 0.$$

The foregoing example illustrates two important advantages of using the constrained gasket design for organic gasket materials.

- (1) Above the transition temperature, where the organic materials are generally very "soft," it is possible to obtain large sealing pressures.
- (2) The available elastic "spring-back" remains virtually unchanged in passing through the transition temperature.

The constrained type of gasket design is vastly superior to the unconstrained type for organic gasket materials. Further investigation is needed to determine to (1) permit easy assembly and yet provide sufficient volumetric precompression to insure continued sealing and (2) insure that the constraint is present throughout the full range of possible operating conditions.

34.5 References

1. D. Tabor, The Hardness of Metals, Oxford University Press, 1951.
2. K.H. Meyer, Natural and Synthetic High Polymers, Interscience Publishers, Inc., New York 1942.
3. G.S. Whitby, Synthetic Rubber, John Wiley and Sons, Inc., New York, 1954.
4. T. Alfrey, Jr., Mechanical Behavior of High Polymers, Interscience Publishers, Inc., New York 1948.

## 35. EXPERIMENTAL PROGRAM

by

Forrest O. Rathbun, Jr.

### 35.0 Summary

The experiments performed in order to gain an understanding of the relationships among the various leakage parameters and to provide an evaluation of the analytical endeavors are of three distinct types. First, a qualitative and quantitative evaluation has to be made of the surface finish on the sealing surface, prior to using that surface in a leakage test. Such is done by recording the surface profile through use of a profile indicator (Section 35.1). The leak test is then made, using the now known sealing surface along with the chosen gasket material. The experimental apparatus and procedure is outlined in Section 35.3. When the leakage test for any sealing surface - gasket system has been completed, the third aspect of the experimental program is accomplished - a qualitative evaluation of the degree of mating attained during the just-completed leakage test. Such is accomplished using high-magnification photographs of the gasket surfaces and sealing surfaces. The use of the interference microscope in this evaluation is outlined in Section 35.2.

### 35.1 Evaluation of Surface Finishes

A Taylor-Hobson "Talysurf" stylus-type profilograph has been used to obtain profiles of the various finishes used. Such an instrument will yield single-line profiles of surfaces which have as little as two-micro-inch asperities. Not only are traces of the profiles in a given direction gained, but an electronic integrator circuit produces, for any surface of a certain minimum length, a center line average (CLA) roughness. While the "Talysurf" (Ref. 2) is basically simple to utilize, a thorough understanding of the interpretation of the traces is required.

When inspecting "Talysurf" profilometer traces, it is necessary to insure that:

- (1) the direction in which the trace was made is known, and
- (2) the different scales present on the trace in the vertical and horizontal directions are understood

Since the "Talysurf" trace is merely the record of a stylus motion following the contours of the surface in a straight-line travel, the information attained about the surface is limited. Any asperities on either side of the trace are not recorded; nor is there any surety that a trace made parallel to the trace at hand would resemble the recording at hand. Hence, something must be known about the surface prior to producing the trace. The stylus must be moved in the lay direction - the direction across which the asperities run. If a surface has a random asperity distribution, traces in two directions can be made. There is no guarantee that a single trace will yield information indicative of the true character of the surface. For machined parts, and some ground parts, the lay direction is perpendicular to the direction of the tool motion.

The utility of the profilometer tracing lies in the magnification of the record of the stylus displacement in the vertical direction. Since an equal magnification in the travel (horizontal) direction would result in extremely lengthy traces, the horizontal scale is fixed; on all traces the scale is 20:1. Each small division on the paper (0.2 inch) equals 0.01 inch of stylus travel. The vertical magnification can be changed to suit the surface at hand; six magnifications are possible.

<u>Number</u>	<u>Magnification</u>	<u>Each Small Division Equals</u>
1	1,000X	100 microinches
2	2,000X	50 "
3	5,000X	20 "
4	10,000X	10 "
5	20,000X	5 "
6	50,000X	2 "

Hence, for all cases, the vertical magnification is different from the horizontal magnification. The scales utilized are noted for each trace presented herein.

Because of the scale variances, the asperities are much less severe than are shown in the traces. It must be recognized that the enclosed angle for a "peak" will generally be greater than  $170^\circ$ . Hence, while the traces yield a great deal of useful information, they do not represent an actual visual picture of the surface.

With regard to the CLA average, such a characterizing quantity is defined by

$$CLA = \frac{1}{\ell_0} \int_{x=0}^{x=\ell_0} |y| dx \quad (1)$$

The CLA system, now an American standard, is sometimes supplemented by the more common rms system. While the CLA value of a surface is automatically computed by the Talysurf, the rms value is not.

The rms value, defined by

$$rms = \frac{1}{\ell_0} \left[ \int_{x=0}^{x=\ell_0} y^2 dx \right]^{1/2} \quad (2)$$

must be gained from a knowledge of the details of the surface profile or be estimated from the CLA value. In both cases,  $y$  is the height of the surface from the mean line describing the surface

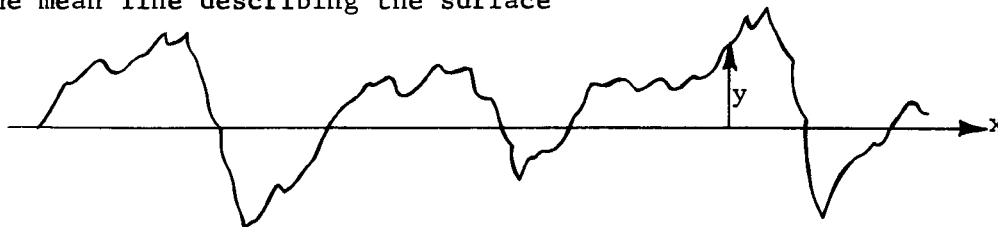
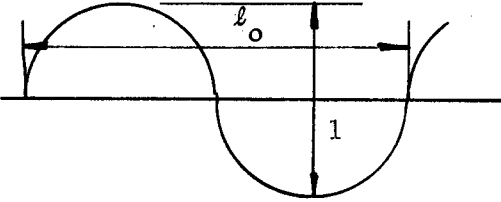
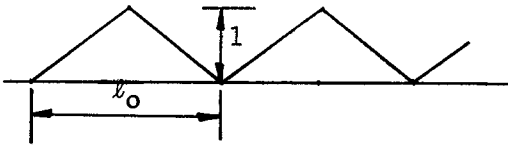
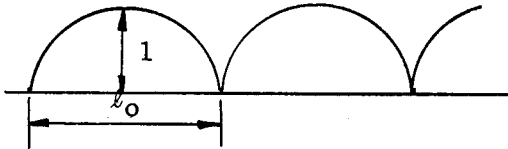
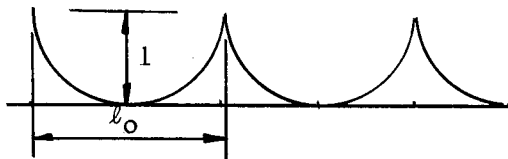
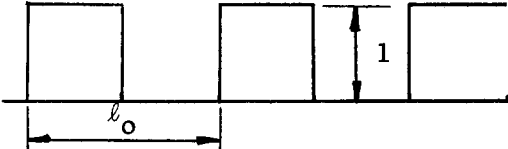


FIGURE 35.1 Typical One Dimensional Surface Profile

Following are listed in Table 35.1 the CLA and rms values from several mathematically described surface geometries. The variations between rms and CLA are given as aids in estimating rms values from CLA values.

TABLE 35.1 Mathematical Surface Profiles

Profile	rms	CLA	rms > CLA
(1) Sine Wave 	0.318	0.354	11.2%
(2) Saw Tooth 	0.25	0.289	15.6%
(3) Parabola 	0.256	0.298	16.3%
(4) Parabola 	0.256	0.298	16.3%
(5) Step Function 	0.5	0.5	0%
(6) Gaussian Distribution of Surface Asperities	$1.0\sigma^*$	$0.796\sigma$	25.8%

\* $\sigma$  = Standard deviation

### 35.2 Evaluation of Degree of Mating of Surfaces

When the leakage test has been completed for a given combination of gasket and sealing surface, and the resultant quality of such a combination as a fluid connector is known, it becomes of interest to evaluate, independently of the rate of flow through the seal, the degree of mating of the gasket and sealing surface. For the case of metals, and some plastics, where the seal has been formed by plastic deformation of the gasket such that the surface of the gasket mirrors to some extent the surface of the sealing surface, it is possible to view matching locations on each surface under high magnification. If the mating is due to plastic deformation for the most part, the degree of mating which existed during the leak test will be evident during post-experiment observation. Further, if the difference between the yield strengths of the gasket material and the sealing-surface metal is great enough, then the plastic deformation will be predominantly present in the softer gasket material. Hence, for such a combination, the sealing surface need be viewed only after the leak test, since its profile will not have varied. For most of the tests conducted in the experimental program, such was the case, and only post-leak-test surface observations were made.

The apparatus used for such observations is the Zeiss interference microscope (Ref. 1) with a polaroid camera attachment. Both ordinary magnified photographs and magnified interference photographs are possible.

In order to precisely locate matching points on the two mated surfaces, local scribe marks were made in the sealing-surface profile with a stylus. Such a mark becomes noticeable on the softer material as a result of the plastic flow; photos in the region of this mark are then compared.

In order to interpret the interference photographs, it is necessary to understand the phenomenon which causes the interference lines. Considering light to propagate as a wave, we can speak of the frequency of the light and of the wave length of the light. If two light sources of the same frequency and magnitude are directed along the same path, then the magnitude of the resultant wave produced by the addition of the two waves will depend on the phase between the original two waves. The addition of two light waves to produce a new wave of different magnitude characteristics is called interference. If, by optical devices, the light from a single source is split, then the possibility of interference exists. By reflecting one wave from the object to be seen, and the other from a mirror at a known distance and angle to the object, then the two reflected waves will interfere in a manner so as to produce the interference profile of the object surface.

The resultant lines can be envisioned as contour lines on the object surface as seen if the surface were slightly off normal to the line of vision. Such is shown for a flat surface in Figure 35.2. The bands formed can be viewed as contour lines of the surface seen from a direction perpendicular to the parallel planes shown. The vertical distance between planes (and hence bands) is one-half the wave length of the light used. As the angle between line of sight and surface changes, the distance between bands varies; however, the vertical distance between the bands taken as contour lines remains  $\lambda/2$  (one-half the wave length of the light).



Were a groove to exist in the surface, then the bands would show up as in Figure 35.3. Again, the direction of light is perpendicular to the planes shown, and the bands are  $J/2$  apart in a direction perpendicular to the line of sight.

Figure 35.3 also illustrates the interpretation of the interference bands. Measuring from the center of a dark band to the center of the same band in a location where the band has changed direction, we can note what portion of a half wave length of light the band has displaced. In Figure 35.3, the displacement is  $(0.3 \times J/2)$ . Thus, the depth of the groove is  $0.3 \times (J/2)$ .

If the surface had been tipped in a direction  $90^\circ$  to its present direction, a different band pattern would emerge.

Both surface topograph shape and depth can be ascertained by this method.

For the results shown in this report, white light has been used; a value of 11.8 microinches can be taken as a half wave length.

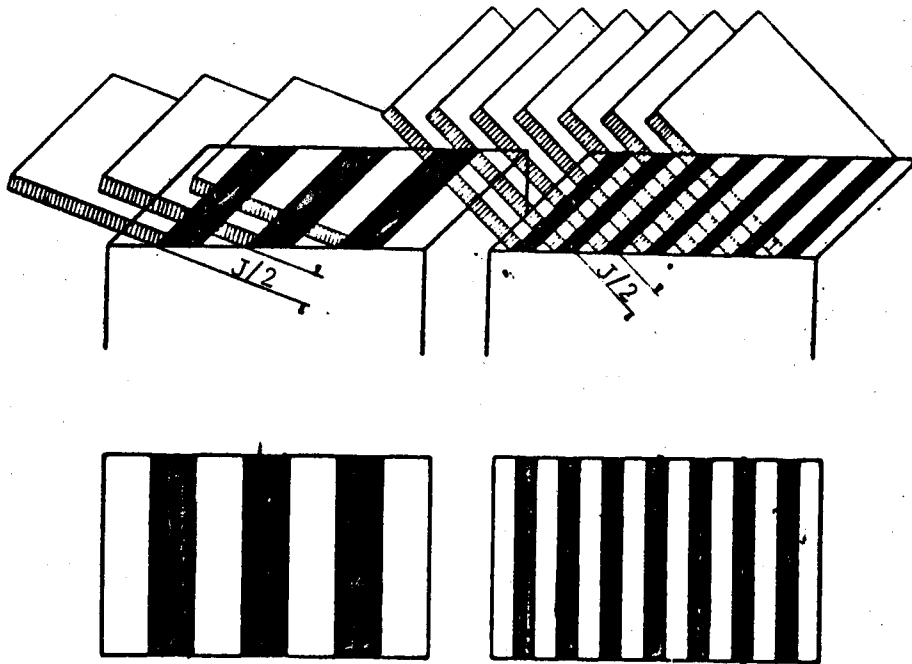


FIGURE 35.2 Interference Pattern for Flat Surface

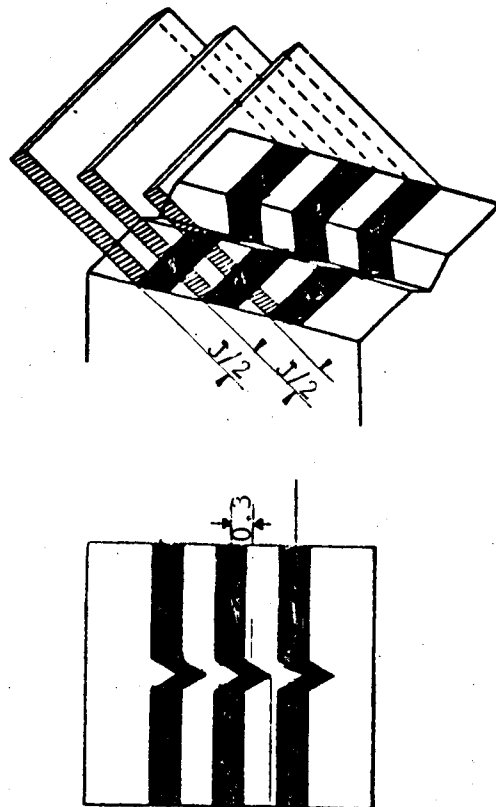


FIGURE 35.3 Interference Patterns for Flat Surface with Groove

### 35.3 Leakage Experiment

#### 35.3.0 Introduction

The main effort in the experimental program has been to measure accurately, for a given combination of gasket material properties and sealing surface finish, the relationship between leakage through such a sealing system and such functions as gasket load and internal pressure. Such an experiment has been conceived to evaluate the validity of analytic investigations (Section 33) and to promote a greater understanding of the leakage phenomenon itself. Since analyses have shown that the fundamental leakage phenomenon can be studied in terms of a limited number of parameters which do not include the response of the supporting structure, the experimental apparatus used to study the leakage problem has been designed to exclude the problems of flange deformation, bolt load uniformity and bolt relaxation. The concept of the experimental work has been to isolate the leakage phenomenon in terms of those parameters which are absolutely needed to evaluate the problem, namely, sealing surface finish, material properties, gasket stress, and internal pressure. Hence, the task assigned to such an experimental apparatus is to:

- (a) Support two sealing surfaces in such a manner that the inherent flexibility of the sealing surface material will be present, but such that no geometric flexibilities are present. The surfaces should be parallel, one above the other, such that a flat annular gasket can be compressed between them.
- (b) Provide a means of compressing the annular gasket uniformly between the sealing surfaces. Means should be available to monitor the magnitude and uniformity of gasket compression. The compressive load should be applied under control at known levels.
- (c) Provide a means of internally pressurizing the sealing system with helium. It should be possible to vary the pressure through a given range, and also to maintain such a pressure over finite time intervals.
- (d) Provide a means to measure quantitatively the leakage of helium through the gasket system.

In line with the above objectives, an experimental apparatus was designed and is described in Section 35.3.1. The experimental procedure is outlined in Section 35.3.2; and the degree of accuracy attainable in measurements taken is described in Section 35.3.3.

#### 35.3.1 Experimental Apparatus

The entire leak test apparatus is shown in Figure 35.4 and the ensuing photographs.

Components (3) and (4) (the head and body) have machined or ground onto them the prescribed test surface finishes, locations (12) and (13). Item (11) is a locator pin to insure that the head and body seat concentrically. Two safety devices are incorporated, an internal safety ring (2) to protect the vacuum bellows (6) and an external safety ring (7) to protect the experimenters

in case of a catastrophic gasket failure at high pressure.

The testing machine used for the applications of load was a Baldwin Southwark load-regulated testing machine with a 60,000-pound capacity. The machine has been equipped with a load maintaining device to allow testing of gaskets at given load over long time periods.

Figure 35.5 shows the test body surmounted by the test gasket in the correct test position. Two locating pins are placed in drilled holes to properly locate the mating head. Three linear differential transformers are shown in position to monitor gasket deflection. Shown to the left of the photo is the vacuum line which draws all helium leaked through the seal to a mass spectrometer. The electrical leads shown are for the differential transformers.

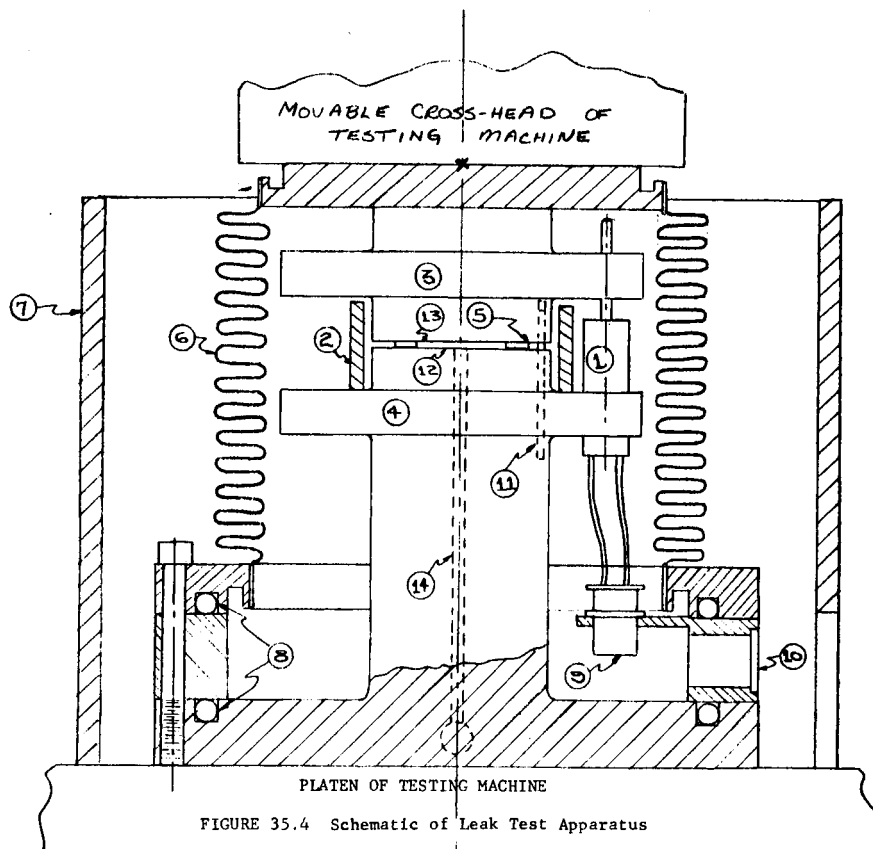
Figure 35.6 shows the internal test facility ready for operation. Affixed to the head are three linear differential transformer cores which ride freely in the transformers themselves. The safety ring is shown in position in the gasket region between head and body. The rectangular grooves in the head (and body) are for positioning the pieces exactly on the "Talysurf" profile recording device. The internal helium pressurizing system is partially shown. The valve and tube in the upper right-hand corner of the photo are the purge line and outlet valve. Shown on the face of the sealing surface are the two passages for helium flow--inward and outward. The tube in the lower left-hand corner is the inlet tube, which has an inlet valve. A helicoid pressure gage, a dry gas filter and a pressure regulator mounted on a 2000 psi helium tank complete the pressurizing system. The dry gas filter used will prevent passage of 98% of all particles 0.4 microns in diameter and 100% of all one-micron-diameter particles.

The final photograph, Figure 35.9, shows the entire testing facility, including the testing machine, linear differential transformer instrumentation, General Electric mass spectrometer leak detector (supplemented by a Kiethley 410 micro-microammeter), and the apparatus already described.

### 35.3.2 Leakage Measurements

In order to measure accurately the leakage from the gasket system, a vacuum is drawn between the outside of the seal and the flexible bellows. A constant pumping action draws the helium molecules escaping from the seal into the leak detector. A vacuum of approximately 4 microns of mercury can be attained within the bellows after the system has been made leaktight itself. The leak detector ideally produces a current proportional to the number of helium molecules passing through it. However, the sensitivity of the system varies from day to day slightly, and the absolute ratio factor between leakage and current is not initially known. Thus, a daily calibration is made on the leak measuring equipment.

Six constant-value leaks have been manufactured. Each day, prior to and after leakage measurements on our test facility, each leak is placed in the leak detector system, and a value of current associated with that leak is recorded.



#### NOTES ON LEAK TEST APPARATUS

- (1) Three standard Schaevitz variable differential transformers, model 100-MS-L, located 120° apart - to measure uniformity and magnitude of gasket compression.
- (2) Safety cylinder - placed outside gasket-sealing surface system to prevent damage to apparatus by a sudden gasket blowout.
- (3) Head of sealing surface fixture - has circumferential lip to support Schaevitz transformer cores.
- (4) Body of sealing surface fixture - has lip to support Schaevitz transformers.
- (5) Gasket to be tested.
- (6) Vacuum system - a U.S. Flexible Bellows (stainless steel), welded to a cover plate and base ring.
- (7) Metal cylinder placed around system as a safety precaution in the event of gasket blowout.
- (8) Precision #430 O-Rings - for sealing vacuum system.
- (9) Three AMPHENOL miniature socket and plug No. 78 S-6-S and 71-S, with retainer rings - to receive leads from Schaevitz transformers.
- (10) Instrumentation rings - has three STUPAKOFF multiterminal glass headers, CAT. No. 971606, to receive leads from Schaevitz transformers; has orifice for vacuum pump.
- (11) Two holes drilled in fixture body and head, outside gasket live - to receive pins to locate head and body positively.
- (12) Sealing surface of fixture body - can be refinished several times to desired roughness.
- (13) Sealing surface of fixture head - can be refinished several times to desired roughness.
- (14) Two holes drilled axially in fixture body, each to an orifice in the body base - one for pressuring system with helium and one for purging air from system.

X on movable crosshead of testing machine denotes point through which load passes (ball and socket fixture).

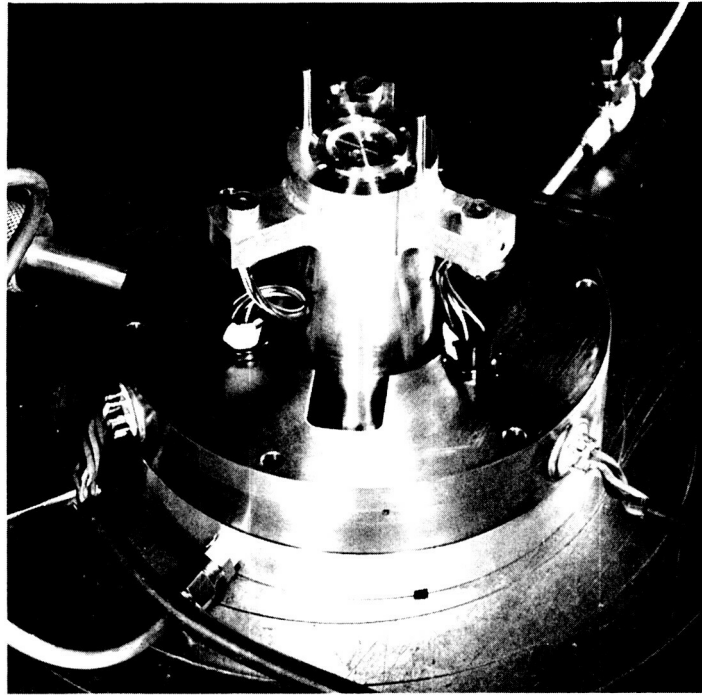


FIGURE 35.5 Body of leakage testing apparatus showing linear differential transformers in place, gasket resting on body sealing surface, and head locating pins.

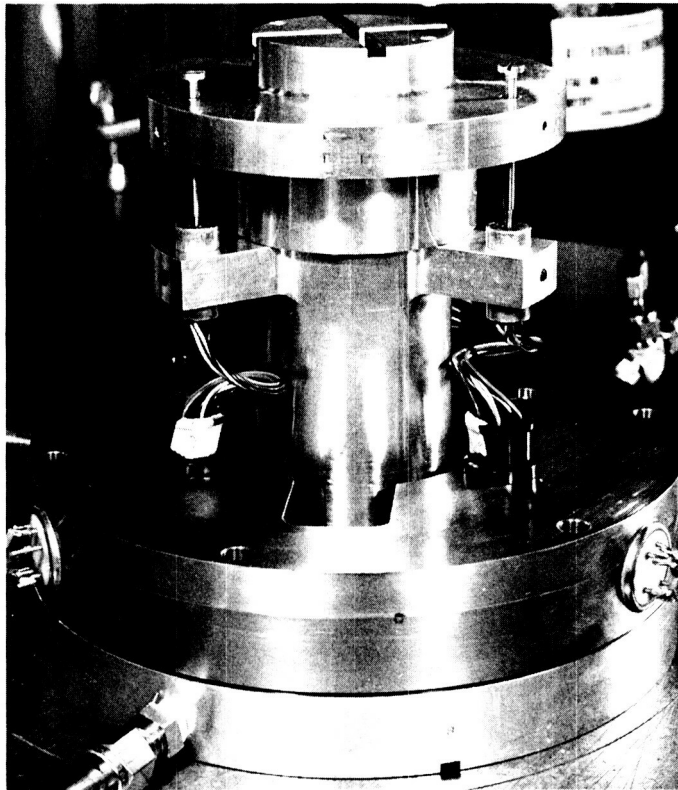


FIGURE 35.6 Leakage testing apparatus (without vacuum container), showing linear differential transformers connected to head and body. Safety cylinder surrounds gasket region.

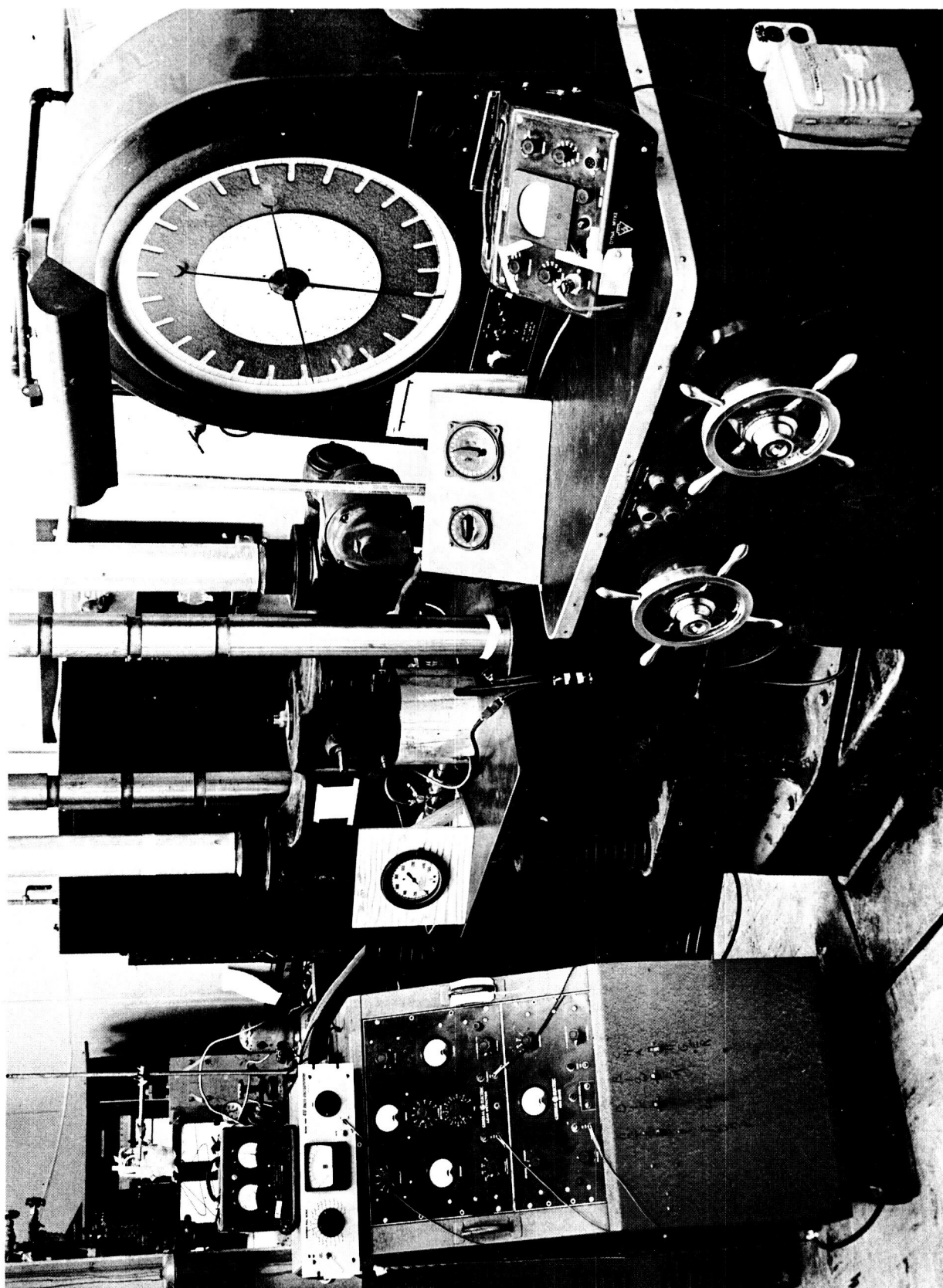


FIGURE 35.7 Entire leakage testing facility, showing General Electric mass spectrometer, testing machine, linear differential transformer instrumentation, and leakage testing apparatus covered by external safety cylinder.

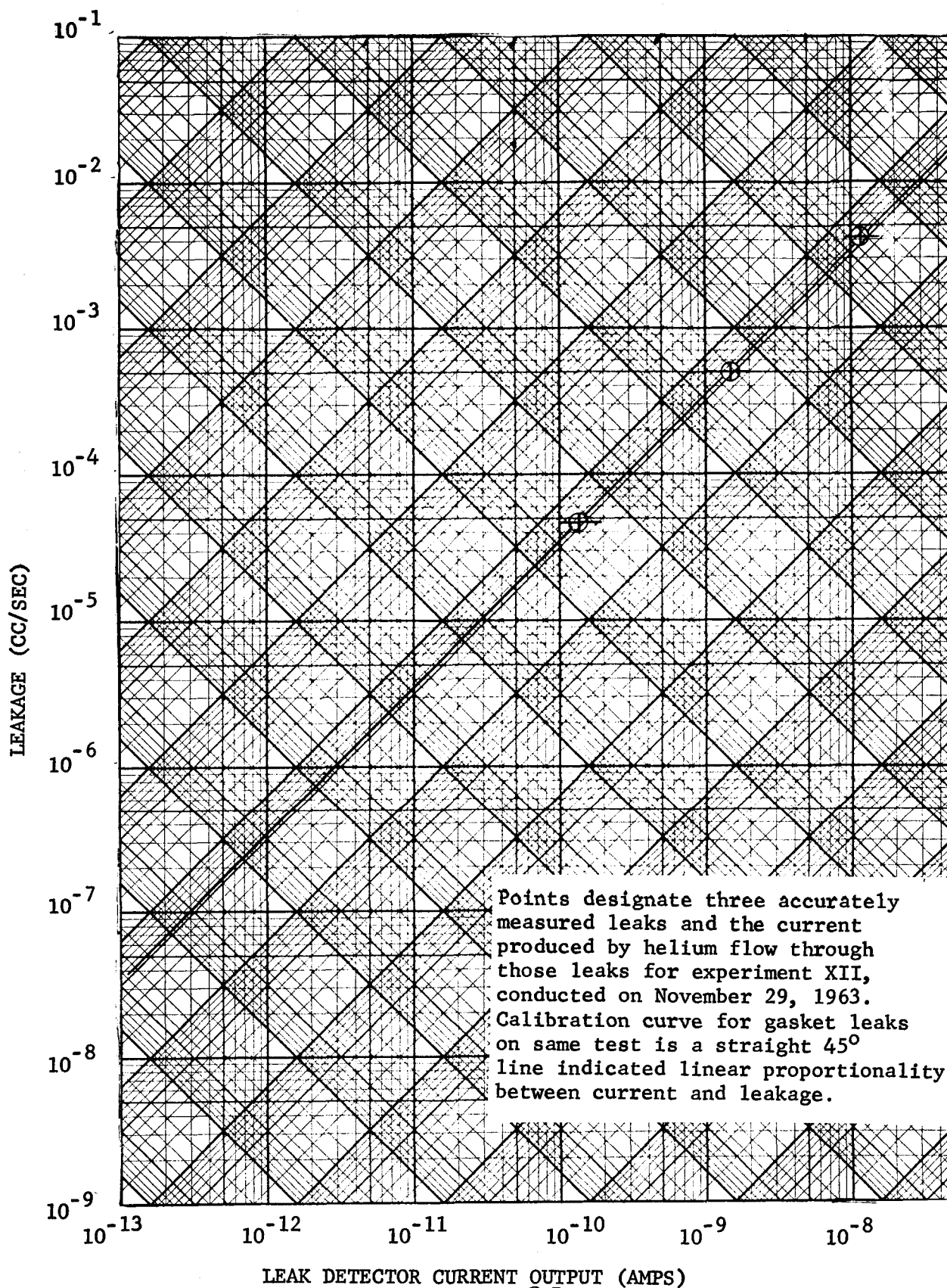
A separate endeavor has been made to evaluate the size of the six leaks by other means. By the method of causing a one-atmosphere pressure differential across the leak, helium is made to flow through the leak. The volume from which the helium flows is maintained constant by allowing a slug of liquid to flow through an affixed capillary tube toward the leak to make up the volume lost by flow through the leak. By monitoring the rate of motion of the capillary slug, the leakage flow rate can be ascertained.

This study was successful in evaluating standard leaks through a range of four decades. A constant ratio was found to exist between leakage and current. Hence, a calibration curve for each day was determined. Extrapolation of the linear curve was necessary in the  $10^{-8}$  cc/sec leak range. A typical resulting calibration curve is shown in Figure 35.8.

67



FIGURE 35.8 TYPICAL CALIBRATION FOR LEAK DETECTOR



### 35.3.3 Test Procedure

For any given experiment, the sealing surface material, gasket material and surface finish are each fixed. The variables of each test then become the normal load  $P$  applied to the system and the internal pressure  $p_i$  (helium) within the system. The data gained from the experiment is the leakage for various combinations of  $P$  and  $p_i$ .

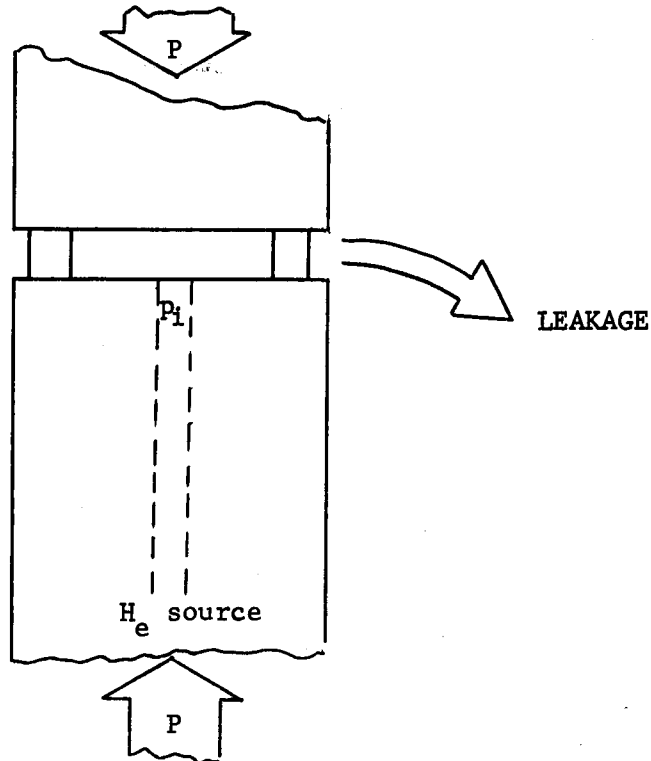


FIGURE 35.9 A Leakage Flow Path (schematic)

The chronological order with which load and internal pressure are applied becomes important in the evaluation of the data.

In each test, three phenomena which occur in a bolted connector are reproduced in the test.

#### 35.3.3.1 Phase I

A vacuum is drawn around the outside of the connector system. A helium flush is maintained within the system; hence, a one atmosphere pressure differential exists across the potential leak. The sealing load P is then applied in increments as the reduction of leakage at each increment is recorded. Since the response time of the leakage measurements is in the order of several seconds, and the load-deflection response of the gasket is not always immediate (particularly in the case of lead and indium, which creep at room temperatures), the leakage is recorded after all transients die out. The time at which the leakage is recorded and the load increment applied is recorded. Increments of loads are applied until the leakage is reduced to the  $10^{-7}$  cc/second range (or below).

The object of this test is to gain information as to the mating of the surfaces and its effect on leakage. The load at the end of Phase I remains the highest load applied to the system; hence, the deformation at the conclusion of the test can be associated with the leakage at the end of Phase I. (In the case of lead and indium, the possibility of cold flow exists; but the amount of deformation during the remainder of the test can be checked, since the compression of the gasket is monitored with linear differential transformers during the entire test.)

### 35.3.3.2 Phase II

At the conclusion of Phase I, the leakage is very low; however, it is caused by a pressure differential of one atmosphere only. As the internal pressure is increased, more leakage is expected. If the gasket system has attained a low leakage by good mating of the interfaces, then the increase in leakage with increasing pressure should flow a smooth curve. If the low leakage is attained by a foreign particle in a potential leak path or by a thin mating barrier, then it is possible for the leakage to increase drastically with pressure. To insure that the low leakage is due to proper mating and to gain a leakage-pressure relationship for a given applied normal stress, Phase II is included in the test. Pressure  $p_i$  is increased in increments up to 1150 psi. The leakage-internal pressure relation also shows whether the leakage flow is in the viscous or molecular range. (Viscous flow exhibits a leakage  $\sim$  pressure squared relationship while molecular flow shows a linear leakage-pressure relation.)

It can be adjudged from the Phase II test how good a seal exists under the terminal mating and peak stress for a practical internal pressure. Under certain conditions these data can be extrapolated to show leakage for even higher internal pressures.

If, at the conclusion of Phase II, the leakage at that time is very high ( $>10^{-3}$  cc/sec), then the load is increased to reduce the leak to a tolerable one (say  $10^{-6}$  cc/sec). A new terminal deformation is achieved, along with a new terminal load.

It must be noted that the nominal normal gasket stress is not kept truly constant during the test; however, it does not vary by more than about 10%. As the internal pressure is increased, the resultant downward force for a given testing machine load decreases by the (pressure X area) vertical load. However, to show the phenomenon, the normal stress can be assumed constant.

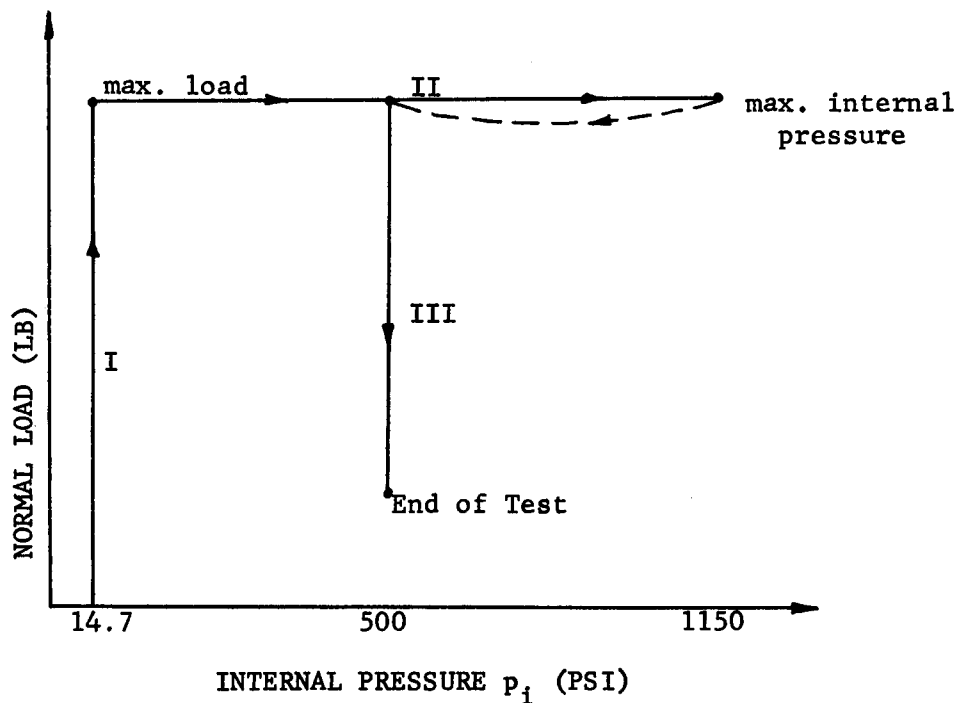
### 35.3.3.3 Phase III

In a conventional flat gasket connector, a common occurrence is that the normal load on a gasket decreases with time. Such can occur due to creep of the bolt, creep of the gasket, external forces being applied, changes in temperature, changes in internal pressure, and a host of other phenomena.

Hence, for a given plastic deformation of a gasket (which has deformed to attain a low leakage rate of the joint), it is of interest to discern the sensitivity of the joint to removal of load. Thus, Phase III consists of removal of normal load in increments while recording the leakage at each stage. To reduce the possibility of a "catastrophic tragedy" should the seal blow out, the internal pressure is reduced to 500 psi (or lower in some tests). Hence, at a constant pressure, load is removed down to approximately twice the internal-pressure vertical load (for safety reasons).

At the end of Phase III, the internal pressure is dropped and the residual load is removed, thus concluding the test. Figure 35.10 shows graphically the chronological phases of the experiment.

FIGURE 35.10 Testing Procedure



#### 35.4 References

1. Instruction Book, Zeiss Interference Microscope
2. Operating Instructions for Model 3, "Talysurf" Surface Measuring Instrument

## 36. EXPERIMENTAL DATA AND RESULTS

by

F.O. Rathbun, Jr. and G.W. Sarney

### 36.0 Summary

The experimental work has been accomplished in three phases - each phase associated with a different type of gasket material. Metal gaskets were first utilized, followed by plastics and then rubber-like materials. The data accumulated from the tests are presented in this section. The results for each gasket material group are presented separately. Observations, comparisons with theory, evaluation of test data, and recommendations are made in Section 37.

## 36.1 Experimental Results - Metal Gaskets

### 36.1.1 List of Experiments

For each metal gasket material utilized, four different sealing surfaces were employed. Both 347 stainless steel and 2024(24S)T4 aluminum base material were employed for sealing surfaces. The yield strengths of each being much higher than the gasket yield strengths, random combinations of sealing-surface specimens and gasket materials were made. No attempt was made to match a particular gasket material to a particular sealing-surface material.

Efforts have been made, however, to insure that the surface finishes used for each gasket were nearly identical (for a given type finish). Whenever the sealing surface was damaged in the gasket compression process, a new surface finish was placed on the sealing surface. Profilometer traces were made of each surface used to insure its adequacy and similarity with previous surfaces of that type. The four surfaces employed in the metal gasket tests were

- (a) Diamond burnished surfaces (DB) with approximately a 4 micro-inch rms surface finish, diamond burnishing accomplished circumferentially. A typical radial profile of such a surface is shown in Figure 36.1.
- (b) Radially ground surface (RG), with approximately a 55 micro-inch rms finish. Grind marks run in 2-inch-diameter arcs from the center of the test apparatus to the edge, resulting in approximately straight radial asperities across the gasket width. A typical circumferential profile of such a surface is shown in Figure 36.2.
- (c) Fine circumferentially machined surface (FM); purely concentric profile, no lead used in the machining process, pitch equal to 0.002 inch, nearly a wedge-shaped profile with a 100 micro-inch rms finish. A typical radial profile is shown in Figure 36.3.
- (d) Coarse circumferentially machined surface (CM) purely concentric profile, no lead used in the machining process, pitch equal to 0.003 inch, nearly a wedge-shaped profile with a 300 micro-inch rms finish. A typical radial profile is shown in Figure 36.4.

The surface profile on the annular gaskets was recorded only in the case of aluminum, copper, and nickel (the three with the highest yield strengths). For these gaskets, the profile was a normally machined circumferential profile, roughly wedge-shaped, with approximately a 33 micro-inch rms finish. The machining was done with a normally applied lead of 0.001 inch. Such a typical profile is shown in Figure 36.5. No surface machining was attempted on the lead and indium gaskets due to the softness of the material and the ready deformation of the surface under compression.



The initial gasket geometry was the same in all cases:

inside diameter       $0.937 \pm 0.0005$  in.  
outside diameter       $1.187 \pm 0.0005$  in.  
thickness               $0.060 \pm 0.001$  in.

The combinations of metal gaskets and surfaces tested, and producing useful data, are listed in Table 36.1. Early tests with indium were helpful in establishing experimental procedure. The Roman numerals listed are the test numbers.

TABLE 36.1 Material-Surface Finish Combinations

Gasket Material	Sealing Surface				Material Surface			
	347 S.S.				2024(24S)T4 Al			
	Surface Finish				Surface Finish			
	D.B.	R.G.	F.M.	C.M.	D.B.	R.G.	F.M.	C.M.
Indium					XI	III		
Lead	IX				VI	VII, VIII		
Aluminum		XVI			XIII		XX	XVII
Copper		XIV		XVIII	XV		XXI	
Nickel	X	XII		XIX			XXII	

### 36.1.2 Experimental Leakage Rates - Metal Gaskets

As outlined in Section 35.3.3, the leakage experiment is accomplished in three phases: Phase I - increasing gasket stress with a one-atmosphere pressure differential across the seal; Phase II - increasing internal pressure for a given gasket stress; and Phase III - decreasing gasket stress while internal pressure is maintained at a constant level. So that the leakage phenomenon occurring during each phase can be evaluated, separate traces of leakage rate in terms of the varied parameter during each phase have been plotted.

During Phase I, leakage rate varies as a function of the increasing nominal gasket stress. Since the quantity to be viewed as a possible meaningful parameter is the yield strength of the gasket material, the stress has been normalized by division of each stress by the yield strength of the gasket material under test. During each test, two parameters have, by necessity, been constant: surface finish of the sealing surfaces and gasket material. Hence, it is of interest to observe the effect of each of these when making comparisons. As is described in Section 34.2, the stress at which yielding occurred during the tests varied as compared with the yield strength as determined by tensile tests. Thus, for Phase I data, the compressive yield stress as determined during the tests was used as a normalizing factor. The Phase I results are plotted in Figs. 36.6 through 36.9.

During Phase II, the leakage rate varied as a function of the internal pressure. In each case, the internal pressure at the start of Phase II was 14.7 psi. In all cases, 1150 psi was a goal for the ultimate pressure. However, in some cases, such a peak could not be attained due to extremely high leakage rates at lower pressures. Also, in some cases, no increase in leakage was evidenced until the internal pressure exceeded 14.7 psi by a large amount. In still other cases, leakage dropped off at high pressures due to the closing off of some passages. The data are again grouped, as was the case for Phase I. It must be noted that the terminal testing-machine load during Phase I is maintained during Phase II. Hence, two points must be considered. The load during Phase II is different for each test, since it is a function of what load caused sealing across a one-atmosphere pressure differential. Also, since it is the testing-machine load which is maintained constant, the actual normal gasket stress will decrease slightly due to the increasing pressure during Phase II. The change in normal stress is quite small, however, so that this stress can be considered roughly constant during this test. Such is true due to the high machine load existing at this time and the small area over which the internal pressure acts. Since the stress existing during Phase I is nearly constant, it is seen that Phase II shows the sensitivity of a constant seal geometry to increasing pressure. The results of this phase are plotted in Figs. 36.10 through 36.13.

For Phase III, in which the sensitivity of the seal to decreasing normal load is explored, the leakage rate is plotted as a function of normal gasket load. During this phase, the internal pressure was maintained at an arbitrary value of 500 psi. The data are grouped by sealing-surface finish. In this case, the stress has been normalized by the tensile-test yield strengths. It must be noted that, chronologically, the events graphed read from right to left, i.e., from high stress toward low stress. The results of Phase III are plotted in Figs. 36.14 through 36.17.

### 36.1.3 Visual Inspection of Mated Surfaces

Each sealing surface, regardless of surface finish, was marked with a stylus in four locations prior to the leakage experiment. The marks were positioned, one in each quadrant, such that they lay either near the center of the gasket area or at a point near a gasket edge. In all cases, the mark was very small compared with the gasket width, thus precluding a potential continuous leakage path across the seal.

During the gasket compression, the entire sealing surface was impressed onto the gaskets to a certain degree. The stylus mark also became a feature on the gasket. Hence, upon completion of the leakage experiment, inspection and comparison of both the gasket surface and the sealing surface could be made at four points of mating. In areas near the stylus mark, the actual mating of the surfaces could be examined. Such was done in all cases; high-magnification photographs were taken of both sealing surfaces and both sides of the gasket. Where possible, interference photos were

taken (not possible when the sealing surface was extremely rough). All of the photographs yielded information concerning the degree of mating attained in the experiments. In this report, however, only selected photographs are presented to illustrate some of the conclusions drawn.

Figures 36.18 through 36.25 show diamond burnished sealing surfaces after mating with four different gasket materials. The mated gasket materials are also shown, along with the nominal normal stress which caused the degree of mating attained.

Figures 36.26 and 36.27 show the degree of mating attained with a radially ground sealing surface and a lead gasket.

Figures 36.28 through 36.34 show an aluminum gasket after a leakage test with a radially ground stainless-steel sealing surface. Two locations are shown, one near the center of the gasket area, and one near the edge. A comparison can be made as to the variation in mating at the two locations. Three different magnifications are shown to illustrate the phenomenon.

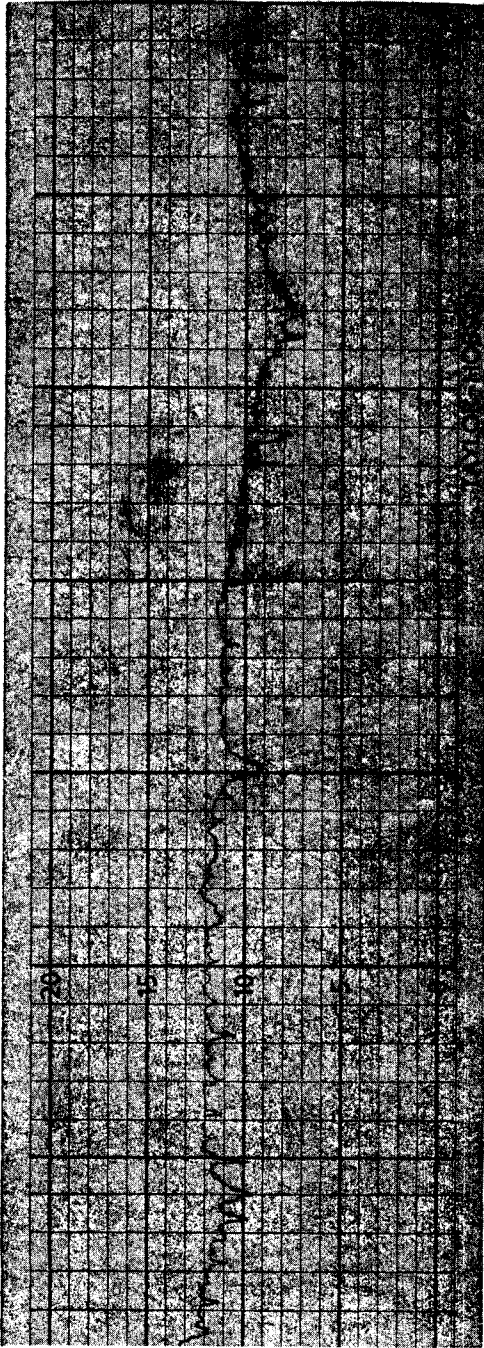


FIGURE 36.1

Typical radial profile of diamond burnished sealing surface.

Vertical Scale: 10 micro-inches  
between light lines.

Horizontal scale: 0.01 inch  
between heavy lines.

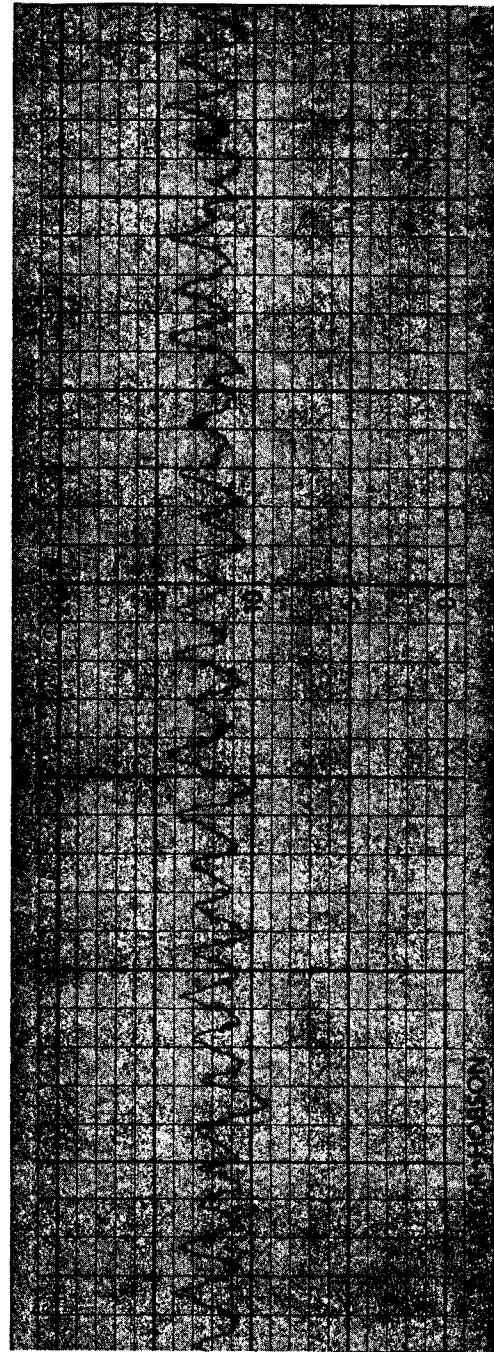


FIGURE 36.2

Typical circumferential profile  
of radially ground sealing surface.

Vertical Scale: 50 micro-inches  
between light lines.

Horizontal Scale: 0.01 inch  
between heavy lines.

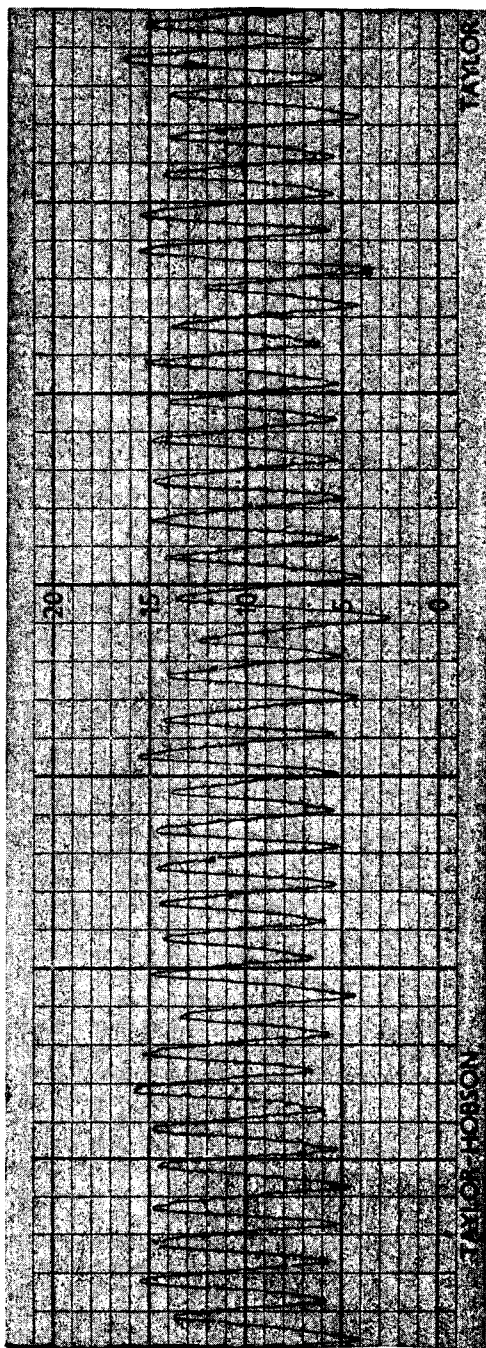


FIGURE 36.3

Typical radial profile of fine machined sealing surface.

Vertical Scale: 50 micro-inches between light lines.

Horizontal Scale: 0.01 inch between heavy lines.

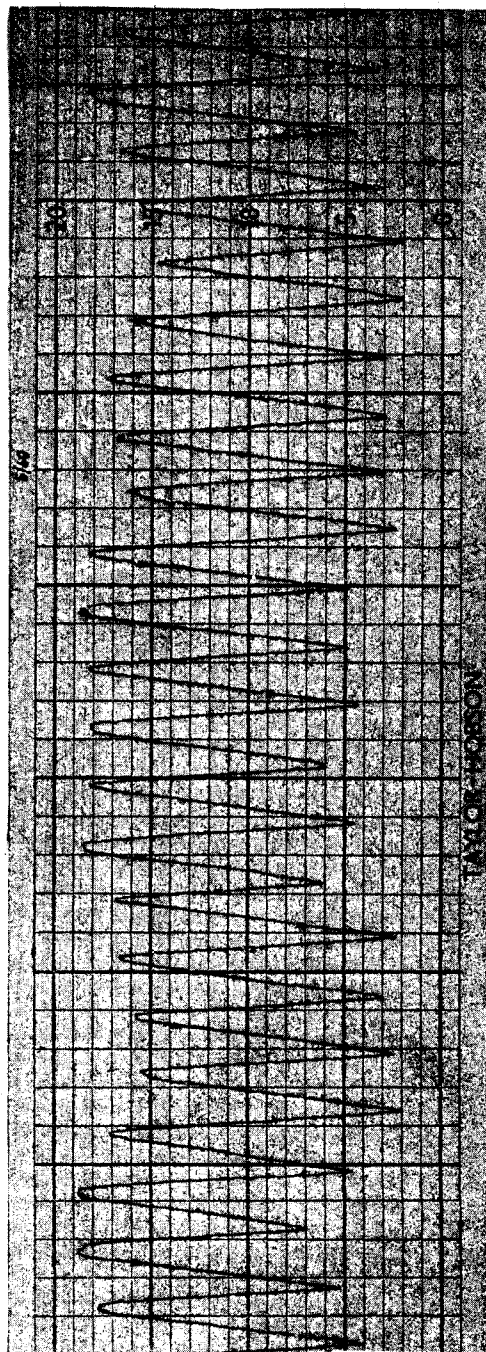


FIGURE 36.4

Typical radial profile of coarse machined sealing surface.

Vertical Scale: 100 micro-inches between light lines.

Horizontal Scale: 0.01 inch between heavy lines.

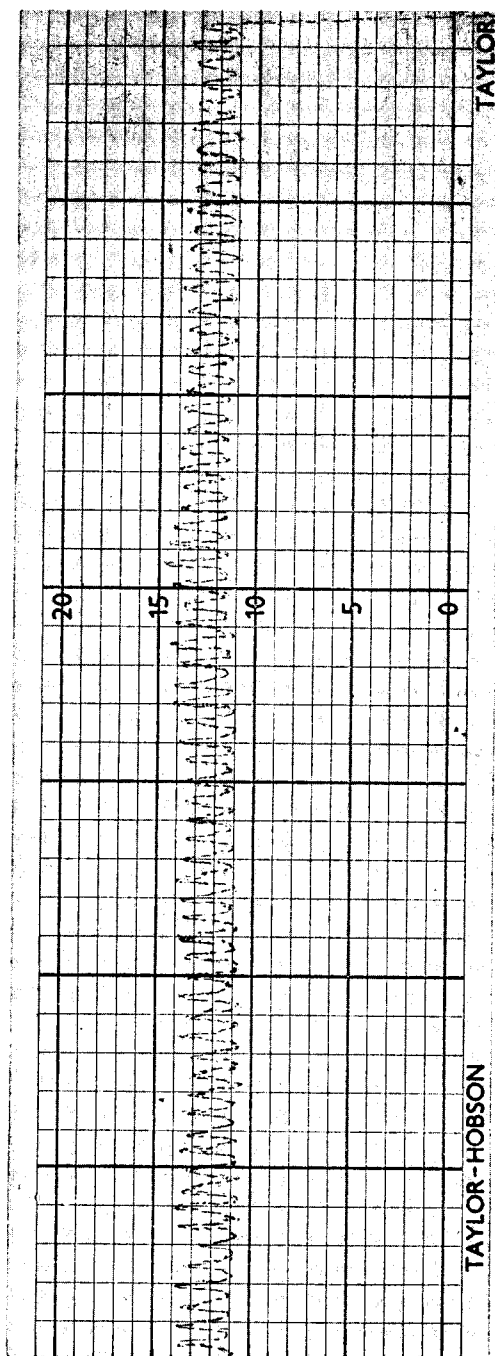


FIGURE 36.5

Typical radial profile of Al, Cu  
and Ni gaskets.

Vertical Scale: 50 micro-inches  
between light lines.

Horizontal Scale: 0.01 inch  
between heavy lines.

FIGURE 36.6 LEAKAGE RESULTS - PHASE I, DIAMOND BURNISHED SURFACE FINISH

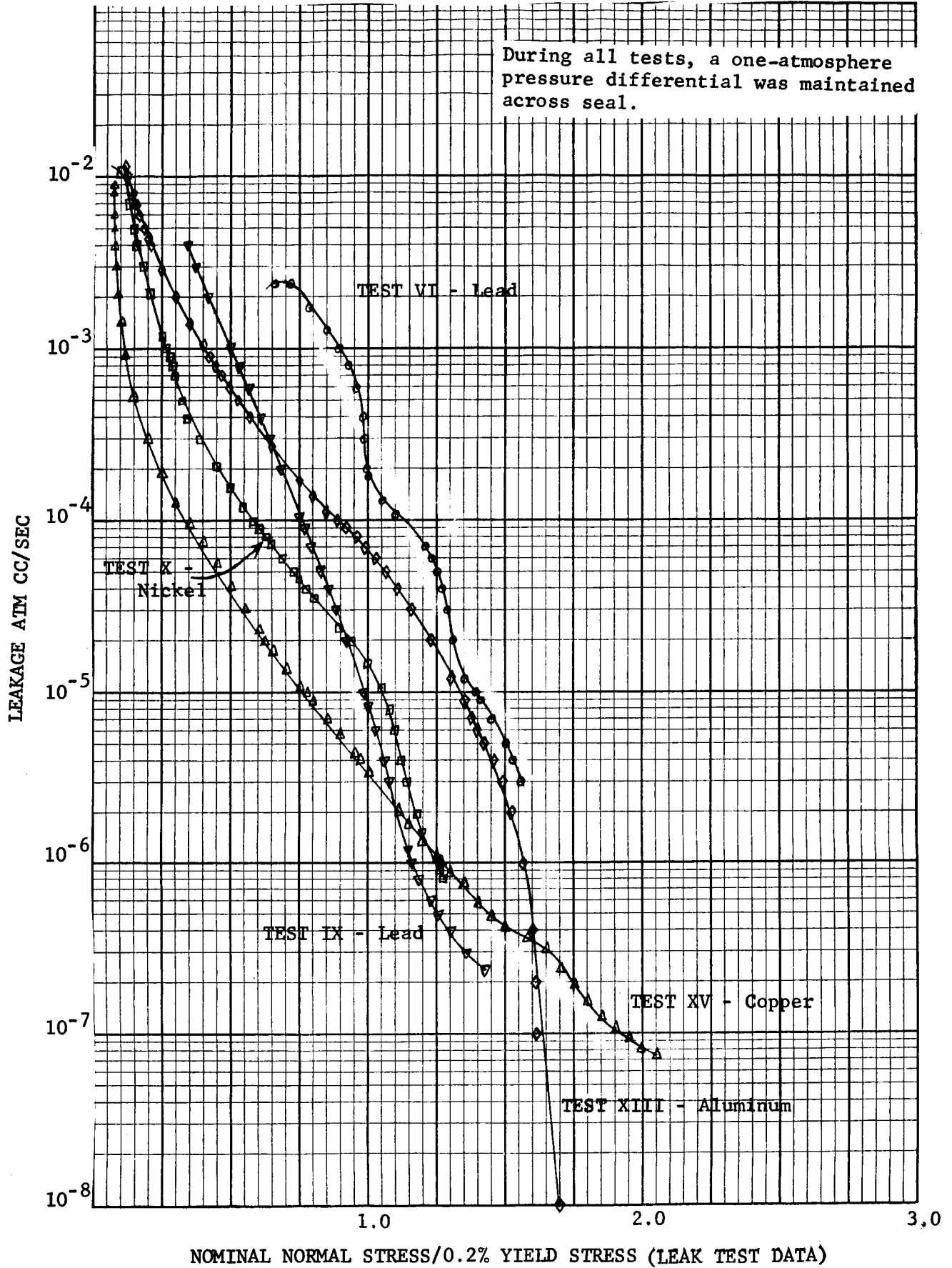
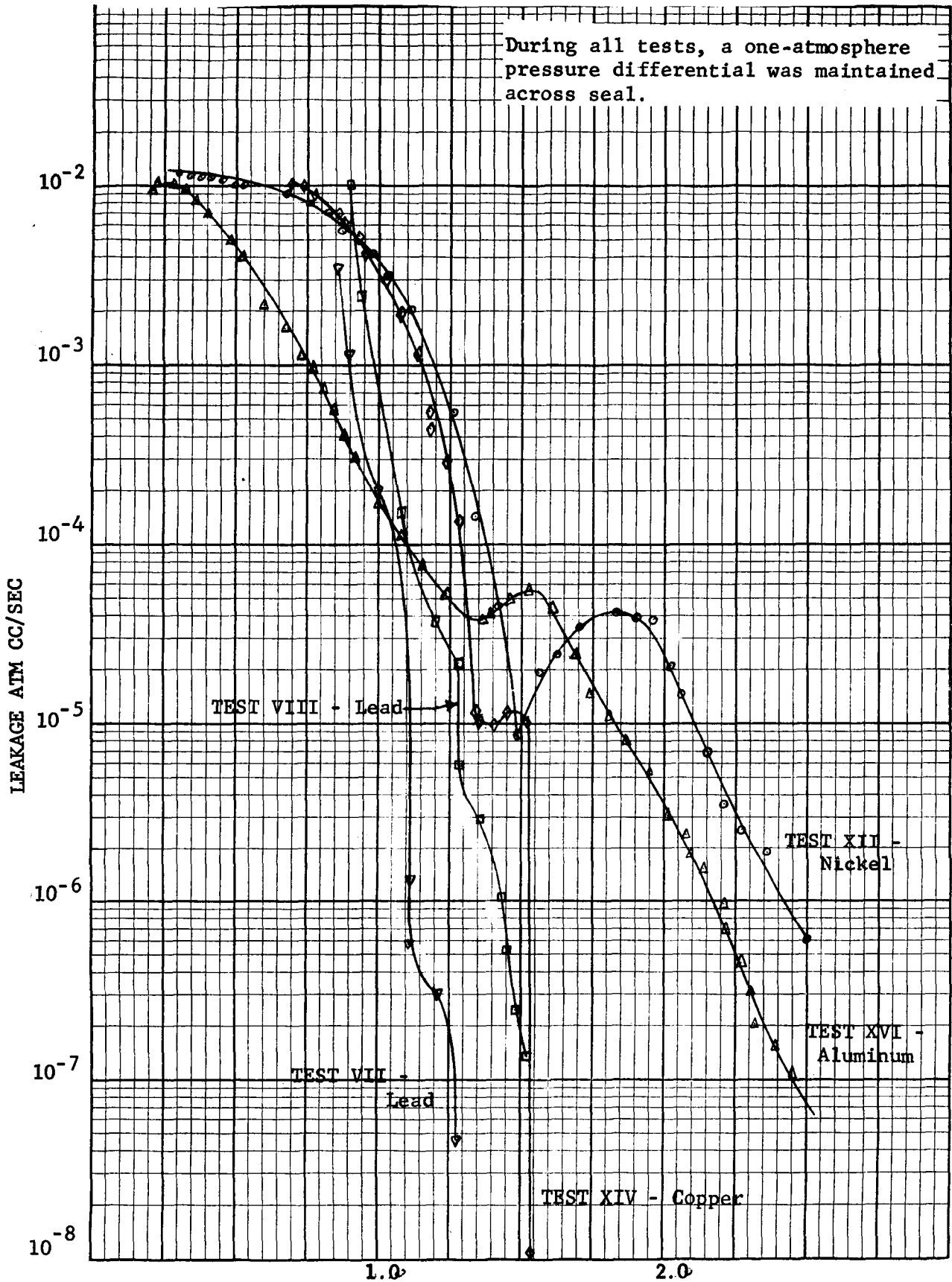


FIGURE 36.7 LEAKAGE RESULTS - PHASE I, RADIALLY GROUND SURFACE FINISH



83



FIGURE 36.8 LEAKAGE RESULTS - PHASE I, FINE MACHINED SURFACE FINISH

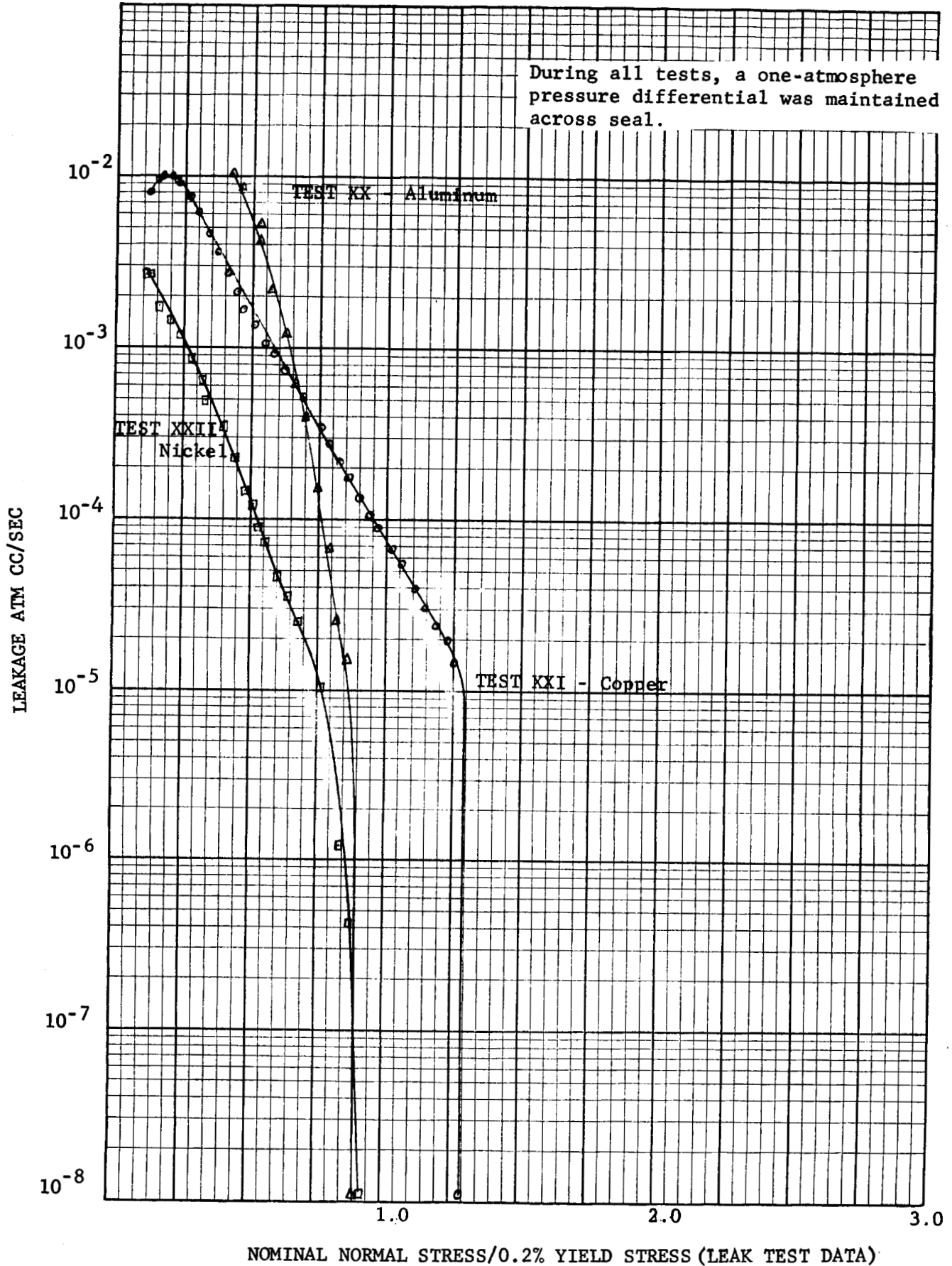


FIGURE 36.9 LEAKAGE RESULTS - PHASE I, COARSE MACHINED SURFACE FINISH

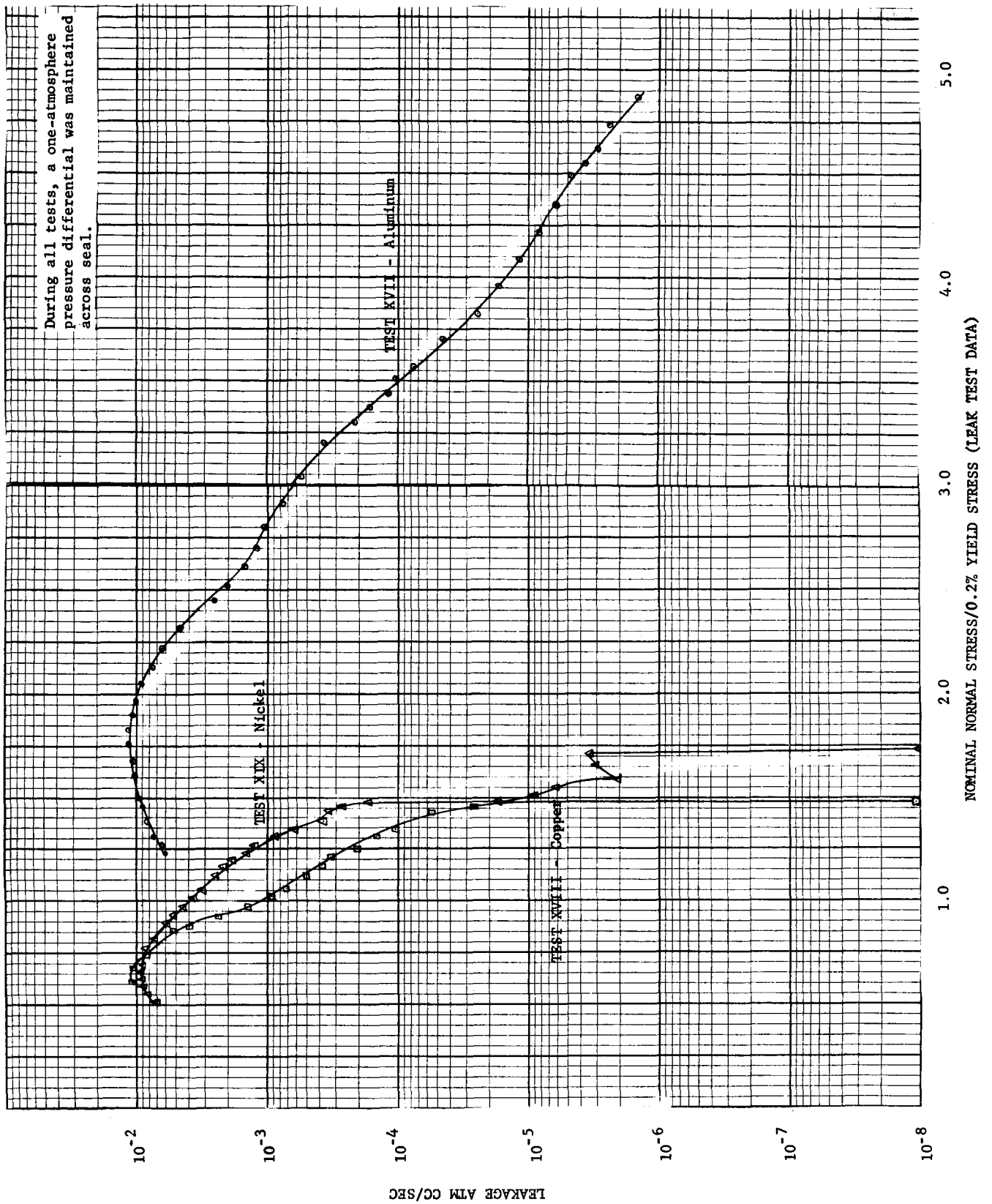


FIGURE 36.10 LEAKAGE RESULTS - PHASE II, DIAMOND BURNISHED SURFACE FINISH

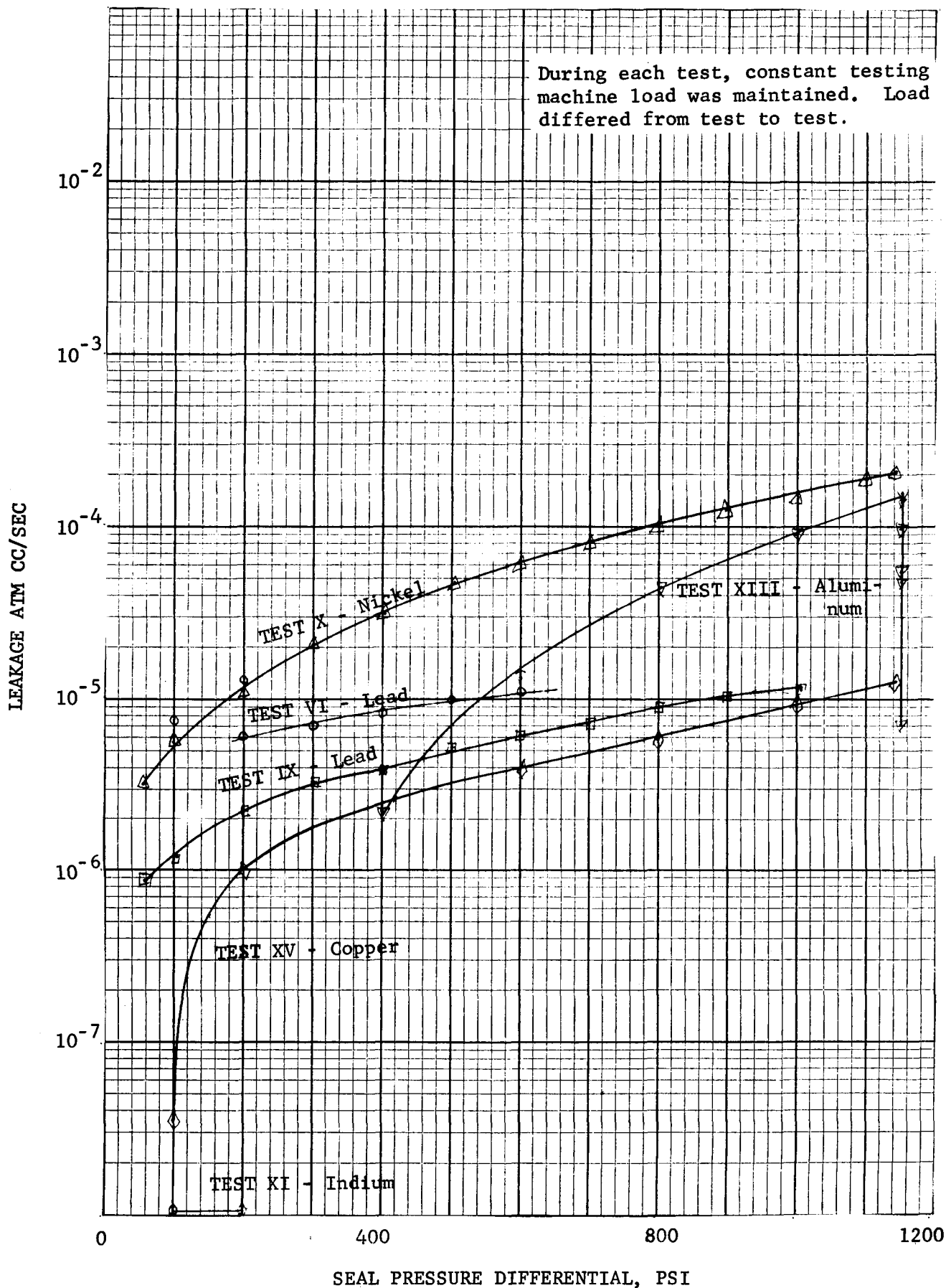


FIGURE 36.11 LEAKAGE RESULTS - PHASE II, RADIALY GROUND SURFACE FINISH

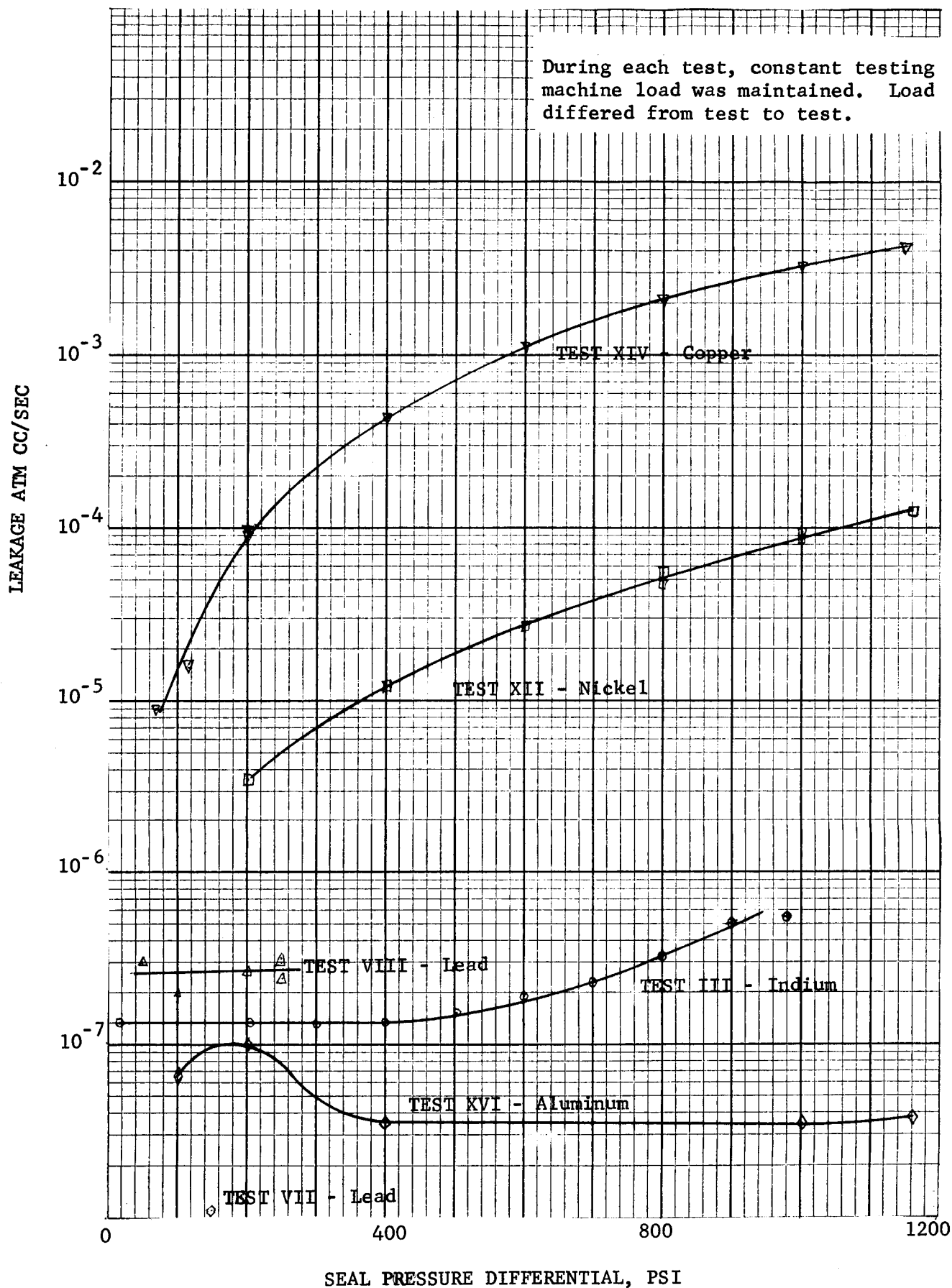


FIGURE 36.12 LEAKAGE RESULTS - PHASE II,  
FINE CIRCUMFERENTIAL MACHINED SURFACE FINISH

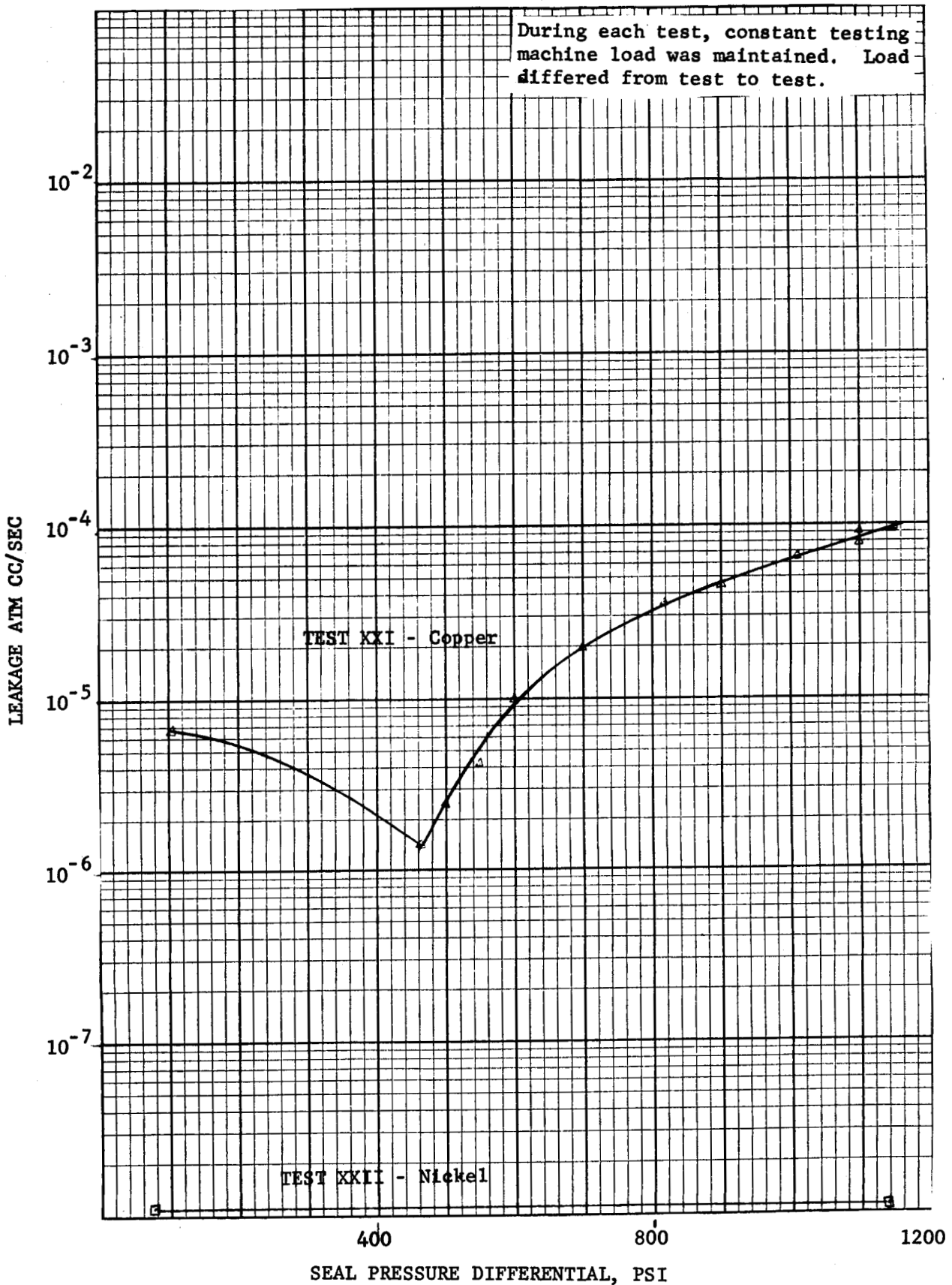


FIGURE 36.13 LEAKAGE RESULTS - PHASE II,  
COARSE CIRCUMFERENTIAL MACHINED SURFACE FINISH

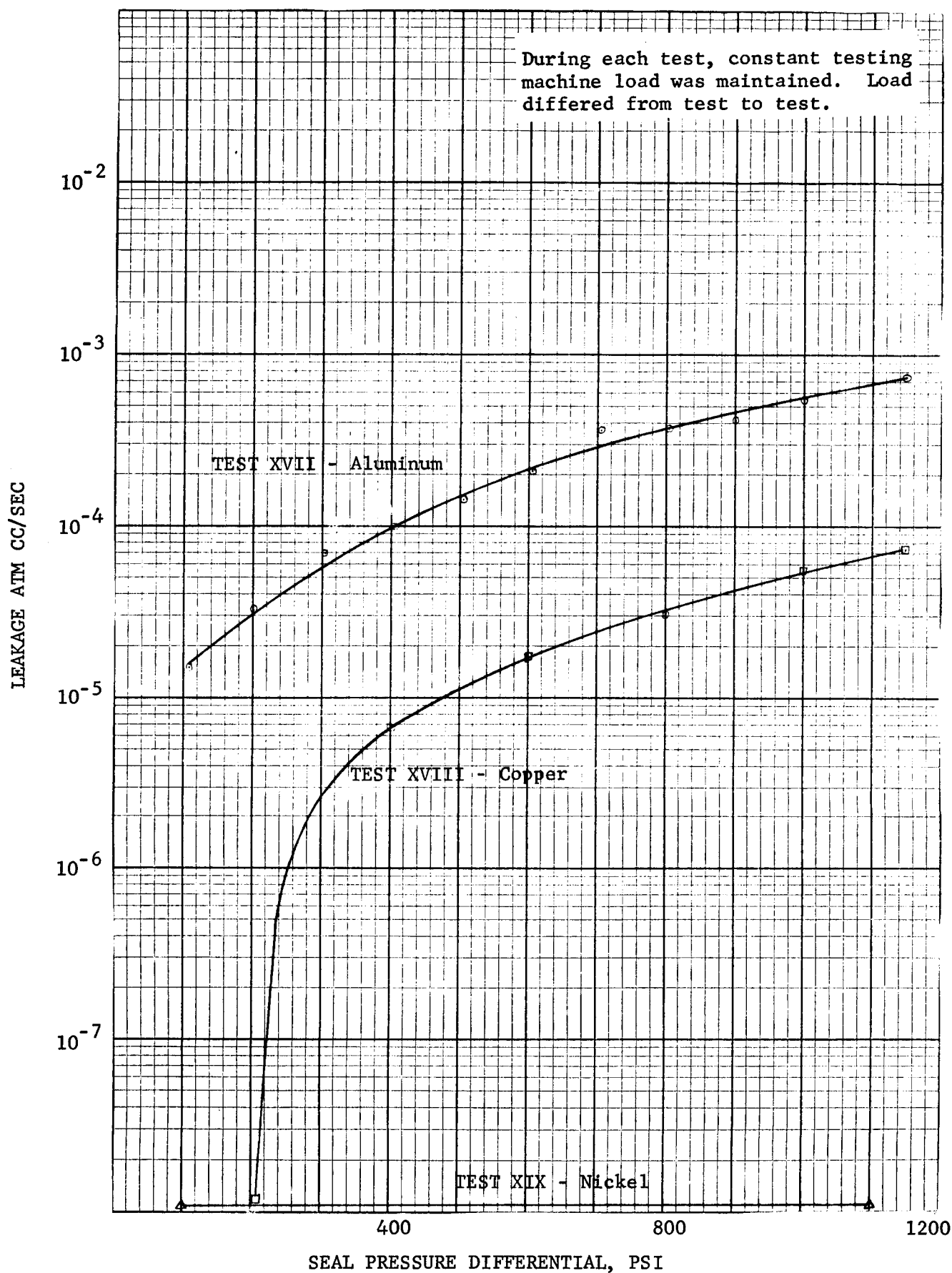


FIGURE 36.14 LEAKAGE RESULTS - PHASE III, DIAMOND BURNISHED SURFACE FINISH

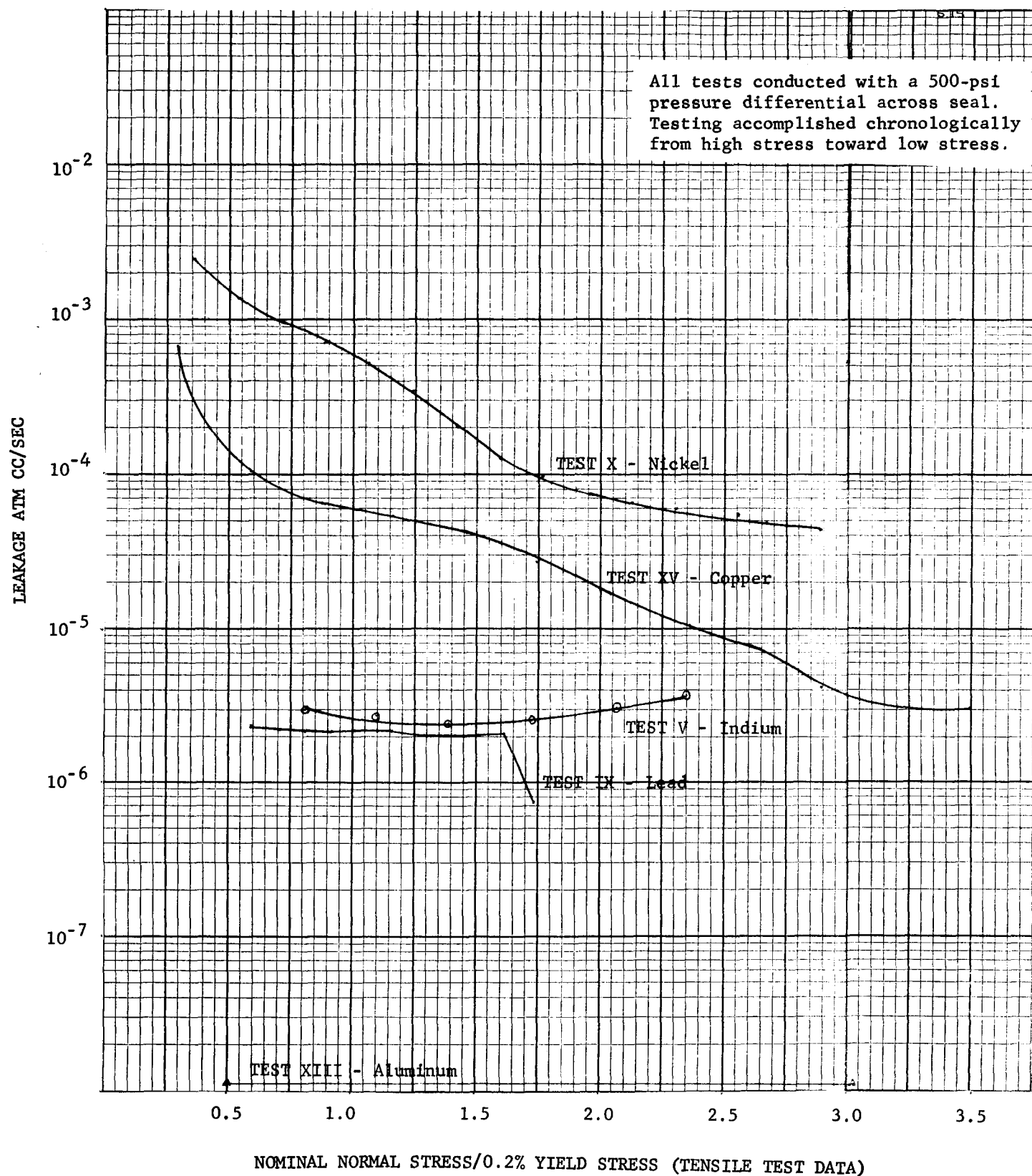


FIGURE 36.15 LEAKAGE RESULTS - PHASE III, RADIALLY GROUND SURFACE FINISH

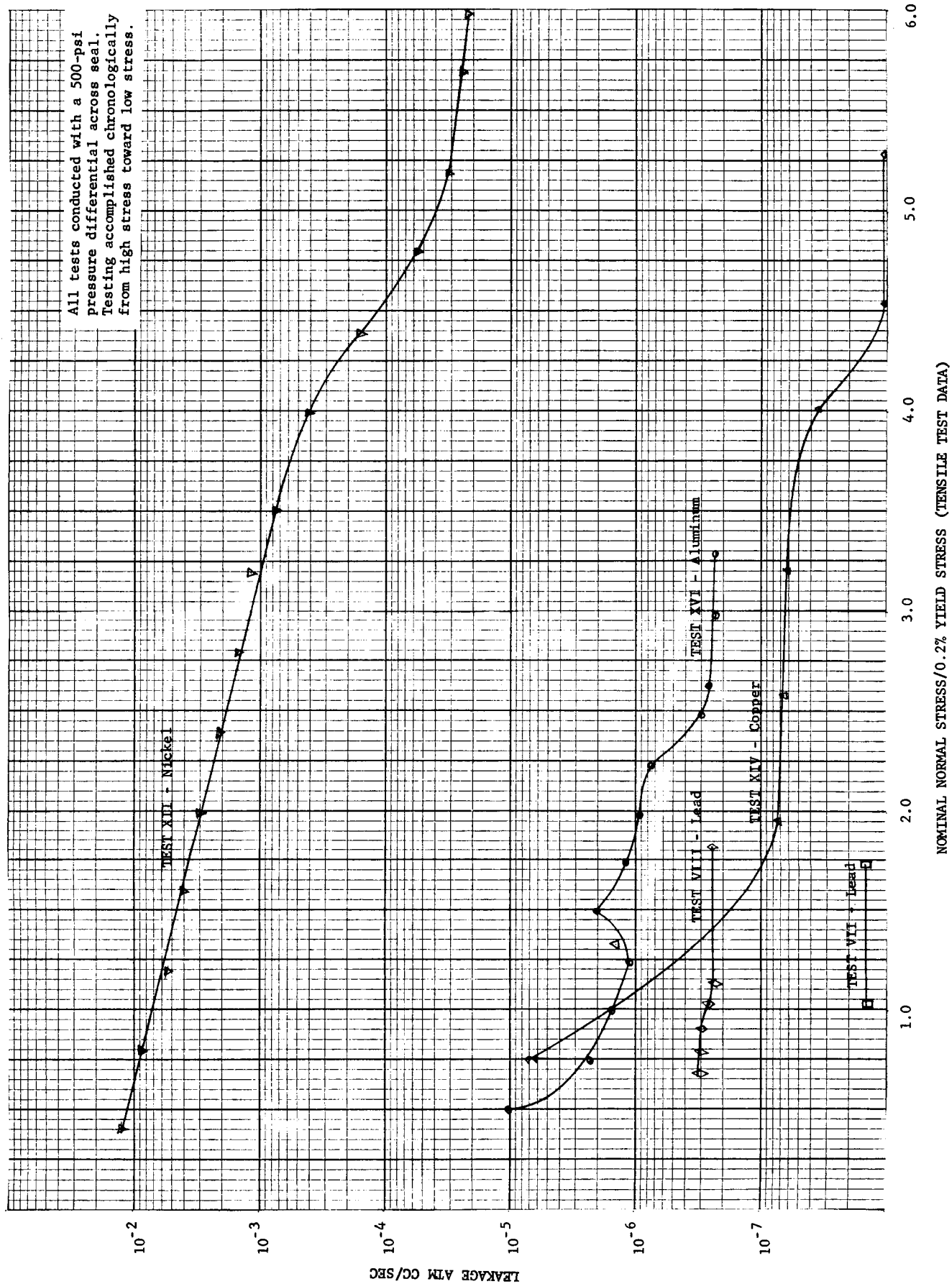




FIGURE 36.16 LEAKAGE RESULTS - PHASE III,  
FINE CIRCUMFERENTIAL MACHINED SURFACE FINISH

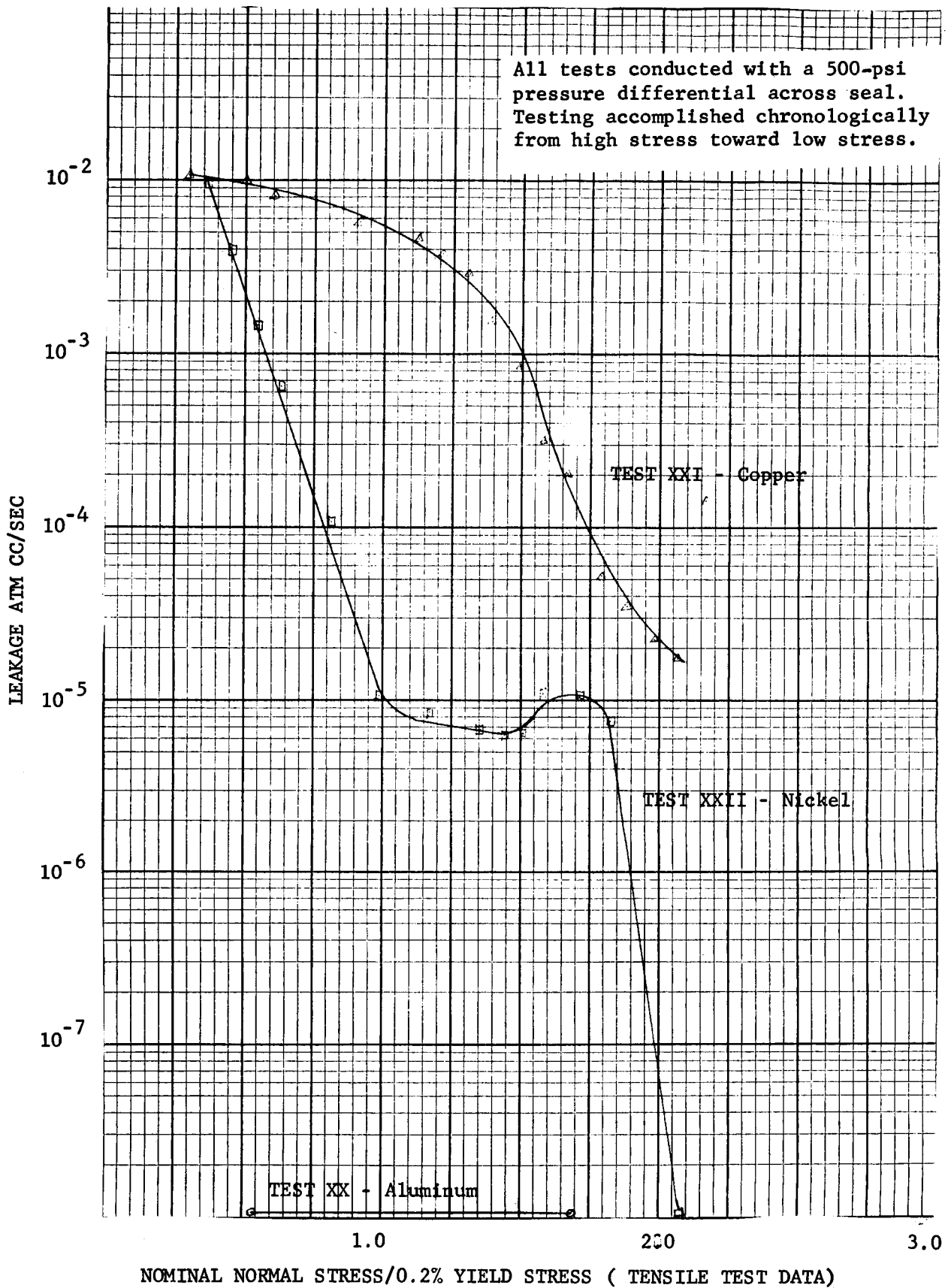
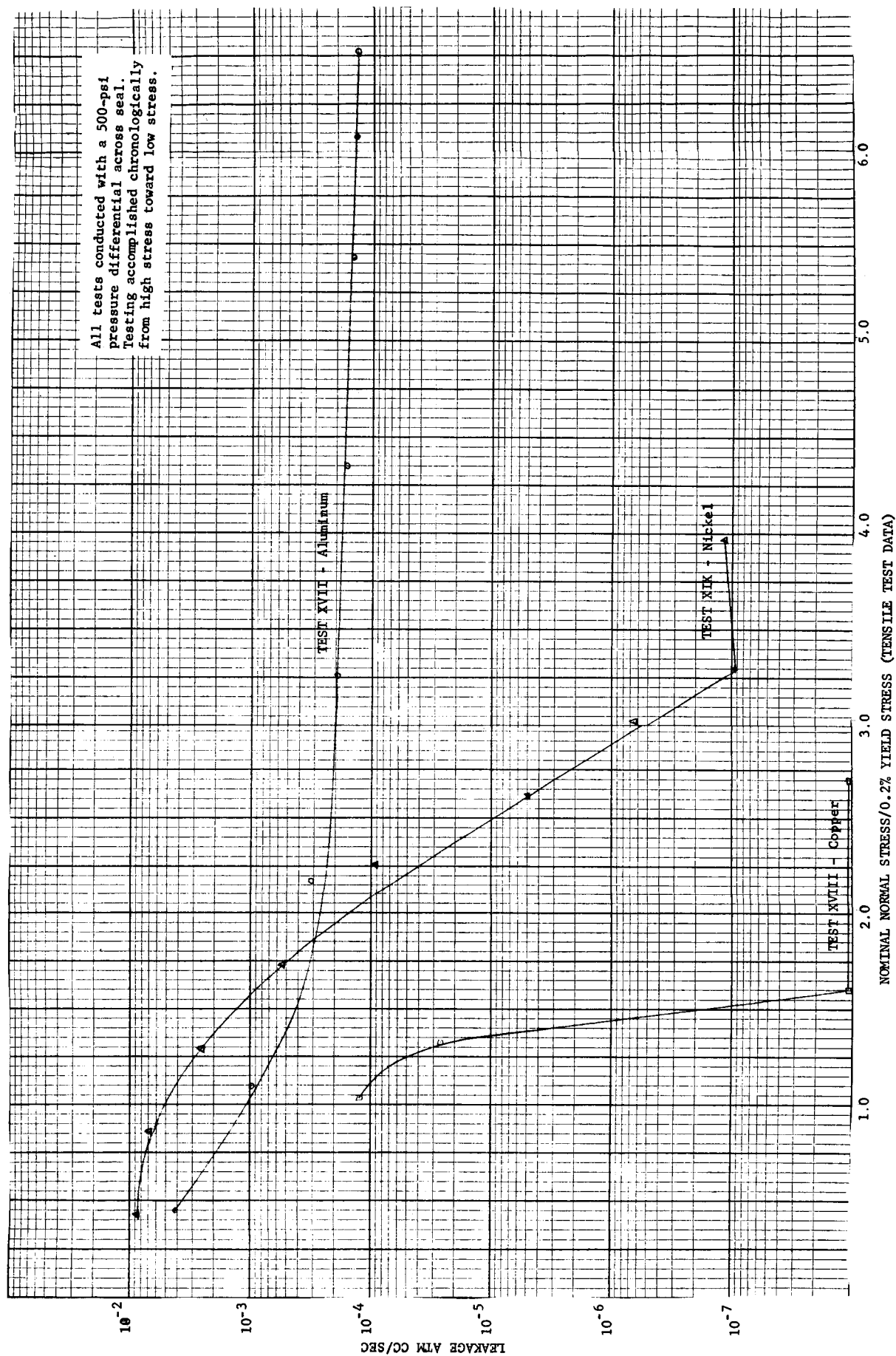


FIGURE 36.17 LEAKAGE RESULTS - PHASE III, COARSE CIRCUMFERENTIAL MACHINED SURFACE FINISH



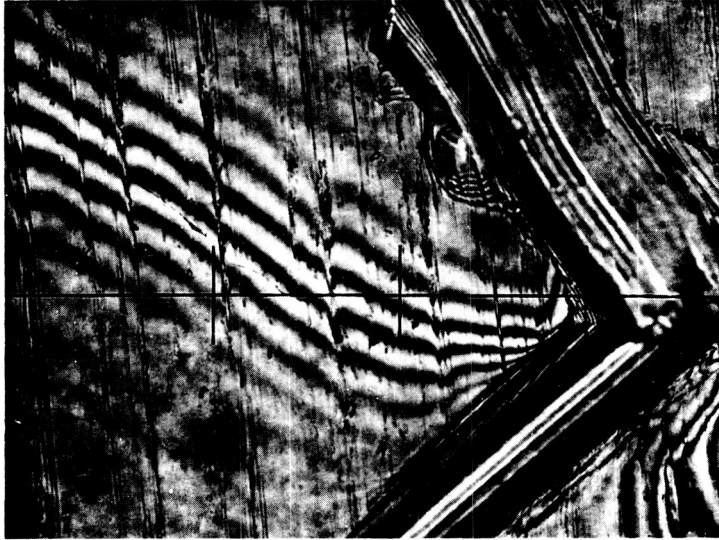


FIGURE 36.18 Diamond burnished stainless steel sealing surface used in Test IX with a lead gasket. Magnification: 0.00194 inch between scale marks. Interference lines 11.8 micro-inches apart.

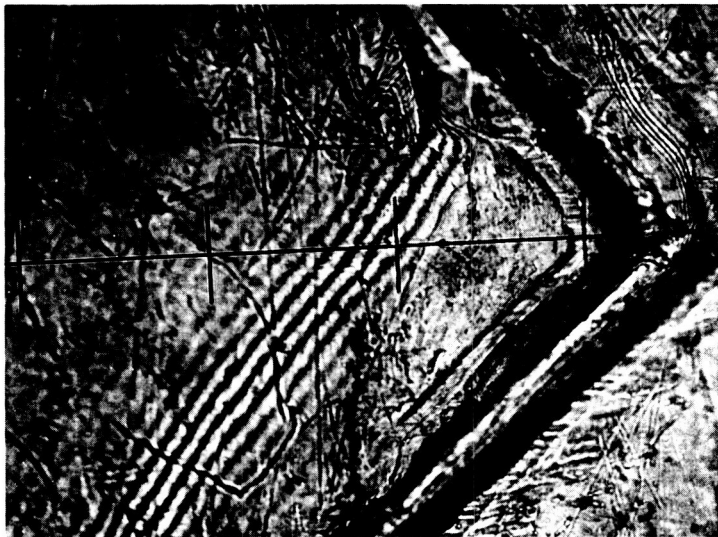


FIGURE 36.19 Lead gasket used in Test IX with diamond burnished stainless steel sealing surface (FIG. 18) Magnification: 0.00194 inch between scale marks. Interference lines 11.8 micro-inches apart. Maximum nominal normal gasket stress -  $1.42 \times 0.2\%$  YIELD STRENGTH (LEAK TEST DATA)

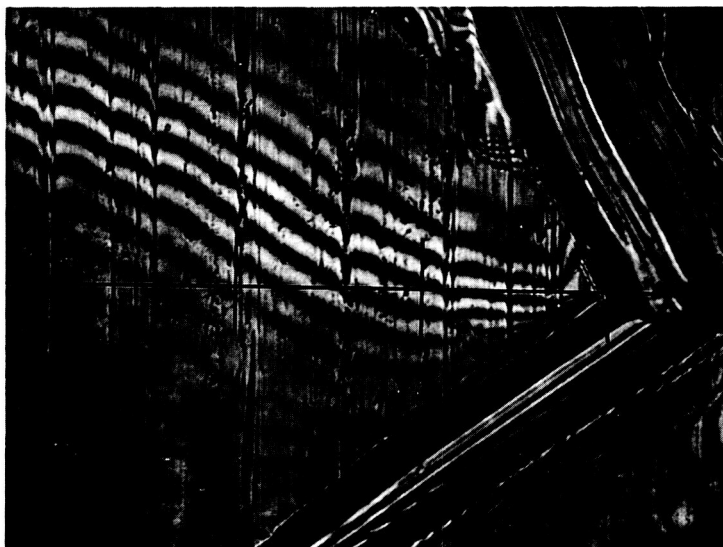


FIGURE 36.20 Diamond burnished stainless steel sealing surface used in Test X with a nickel gasket. Magnification: 0.00194 inch between scale marks. Interference lines 11.8 micro-inches apart. (Same surface as used with lead gasket in Test IX, FIG. 36.18)

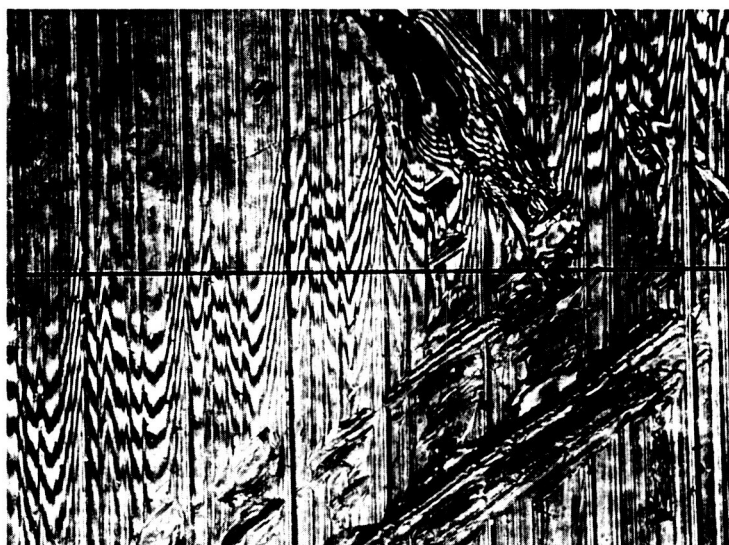


FIGURE 36.21 Nickel gasket used in Test X with diamond burnished stainless steel sealing surface. (FIG. 36.20) Magnification: 0.00194 inch between scale marks. Interference lines 11.8 micro-inches apart. Maximum nominal normal gasket stress -  $1.27 \times 0.2\%$  yield strength (LEAK TEST DATA)

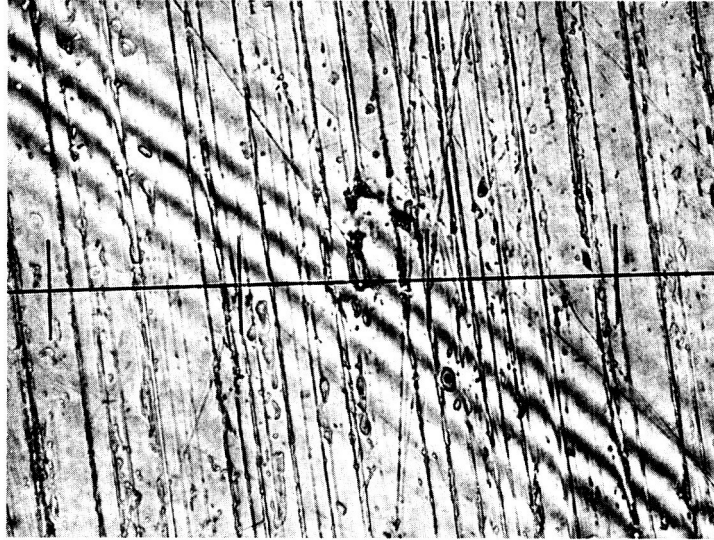


FIGURE 36.22 Diamond burnished aluminum sealing surface used in Test XIII with aluminum gasket. Magnification: 0.00194 inch between scale marks. Interference lines 11.8 micro-inches apart.

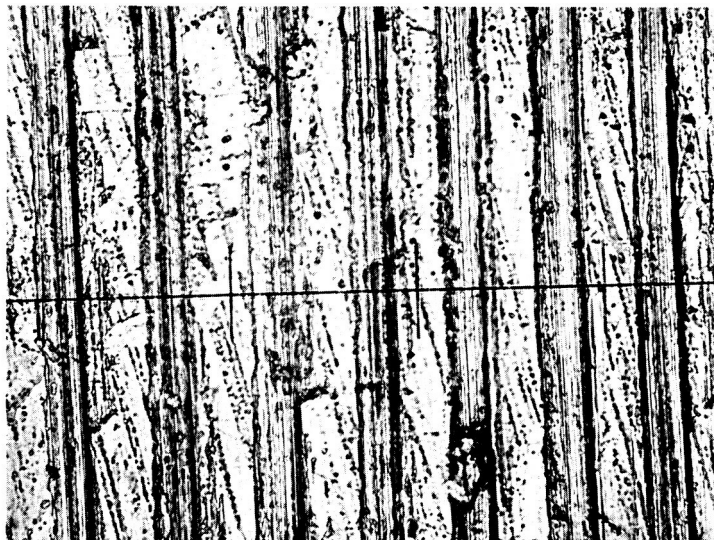


FIGURE 36-23 Aluminum gasket used in Test XIII with diamond burnished sealing surface (FIG. 36.22) Magnification: 0.00194 inch between scale marks. Maximum nominal normal gasket stress -  $1.27 \times 0.2\%$  YIELD STRENGTH (LEAK TEST DATA)



FIGURE 36.24 Diamond burnished aluminum sealing surface used in Test XV with copper gasket. Magnification = 0.00194 inch between scale marks.



FIGURE 36.25 Copper gasket used in Test XV with diamond burnished aluminum sealing surface. (FIG. 36.24) Magnification: 0.00194 inch between scale marks. Photo taken at outside edge of gasket. Maximum nominal normal gasket stress -  $2.05 \times 10^{-2}$ %. YIELD STRENGTH (LEAK TEST DATA)



FIGURE 36.26 Radially ground aluminum sealing surface used in Test VII with lead gasket. Magnification: 0.00482 inch between scale marks.

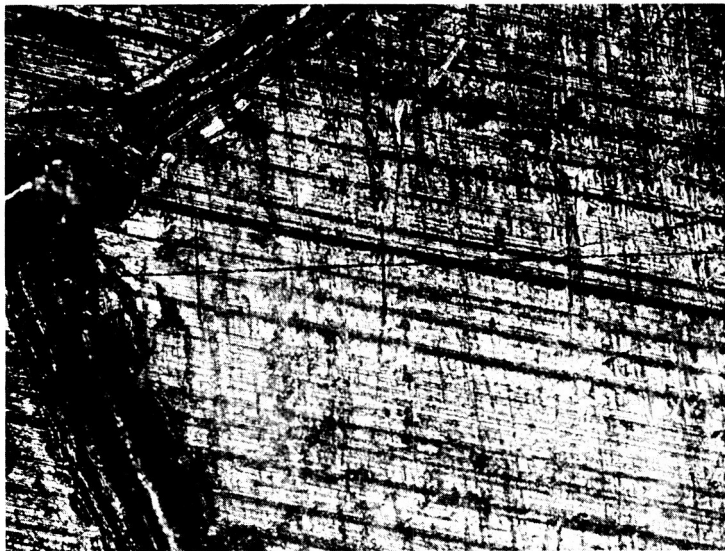


FIGURE 36.27 Lead gasket used in Test VII with radially ground aluminum sealing surface (FIG. 36.26). Magnification: 0.00482 inch between scale marks. Maximum nominal normal gasket stress -  $1.27 \times 0.2\%$  YIELD STRENGTH (LEAK TEST DATA)



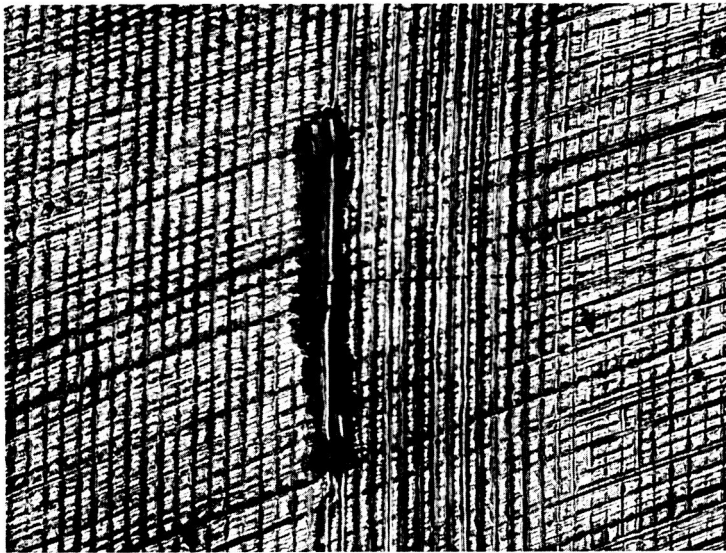


FIGURE 36.28 Photomicrograph of aluminum gasket after leakage test with radially ground 347 stainless steel sealing surface; - Test XVI. Photo near center of gasket width.  
Magnification: 0.0125 inch between scale marks  
Maximum nominal normal gasket stress -  $2.52 \times 0.2\%$   
YIELD STRENGTH (LEAK TEST DATA)

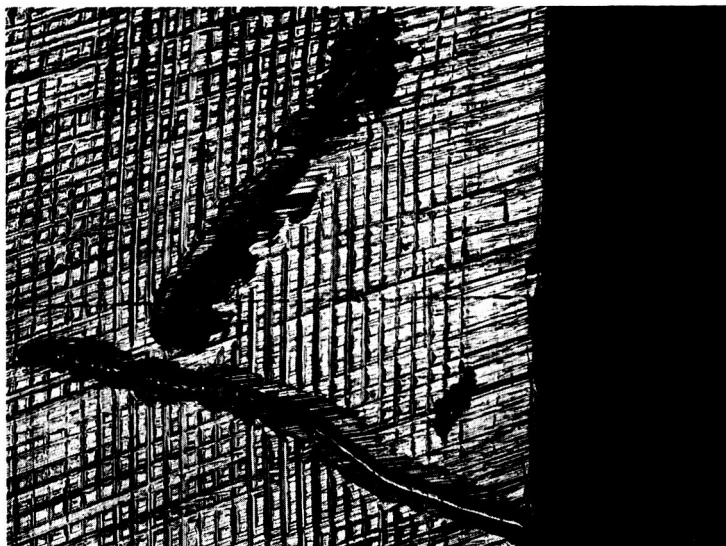


FIGURE 36.29 Photomicrograph of aluminum gasket after leakage test with radially ground 347 stainless steel sealing surface; - Test XVI. Photo near edge of gasket.  
Magnification: 0.0125 inch between scale marks.  
Maximum nominal normal gasket stress -  $2.52 \times 0.2\%$   
YIELD STRENGTH (LEAK TEST DATA)



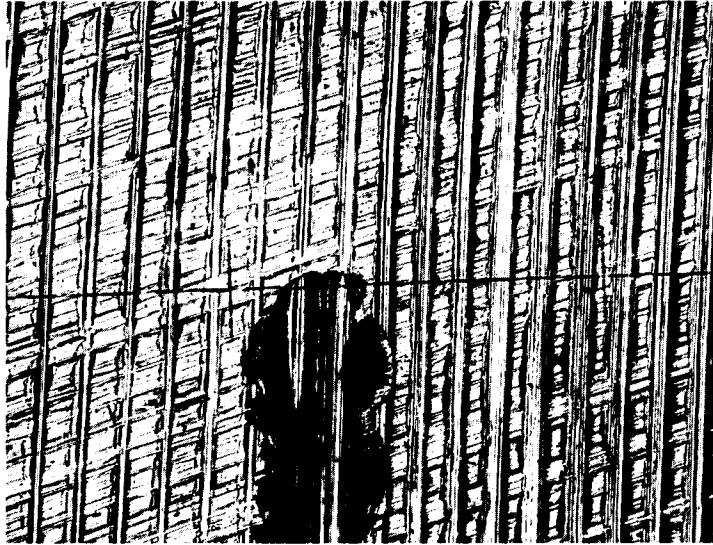


FIGURE 36.30 Photomicrograph of aluminum gasket after leakage test with radially ground 347 stainless steel sealing surface; - Test XVI. Photo near center of gasket width. Magnification: 0.00482 inch between scale marks. Maximum nominal normal gasket stress -  $2.52 \times 0.2\%$  YIELD STRENGTH (LEAK TEST DATA)

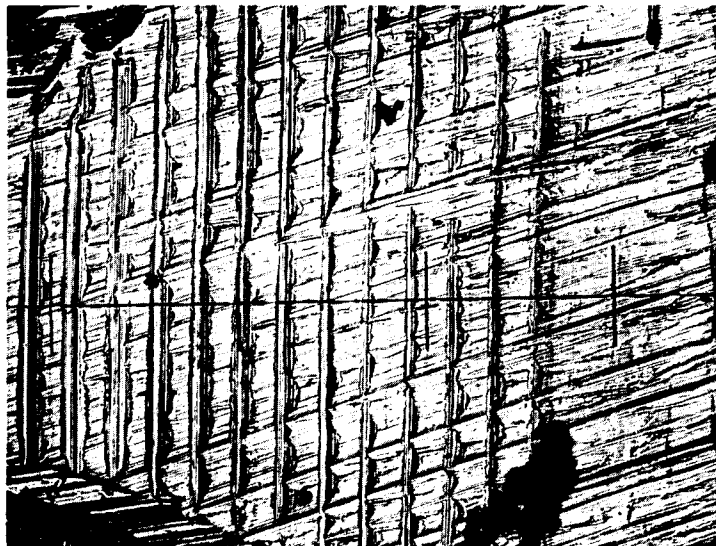


FIGURE 36.31 Photomicrograph of aluminum gasket after leakage test with radially ground 347 stainless steel sealing surface; - Test XVI. Photo near edge of gasket. Magnification: 0.00482 inch between scale marks. Maximum nominal normal gasket stress -  $2.52 \times 0.2\%$  YIELD STRENGTH (LEAK TEST DATA)



FIGURE 36.32 Photomicrograph of aluminum gasket after leakage test with radially ground 347 stainless steel sealing surface; - Test XVI. Photo near center of gasket width. Magnification: 0.00192 inch between scale marks. Maximum nominal normal gasket stress -  $2.52 \times 0.2\%$  YIELD STRENGTH (LEAK TEST DATA)

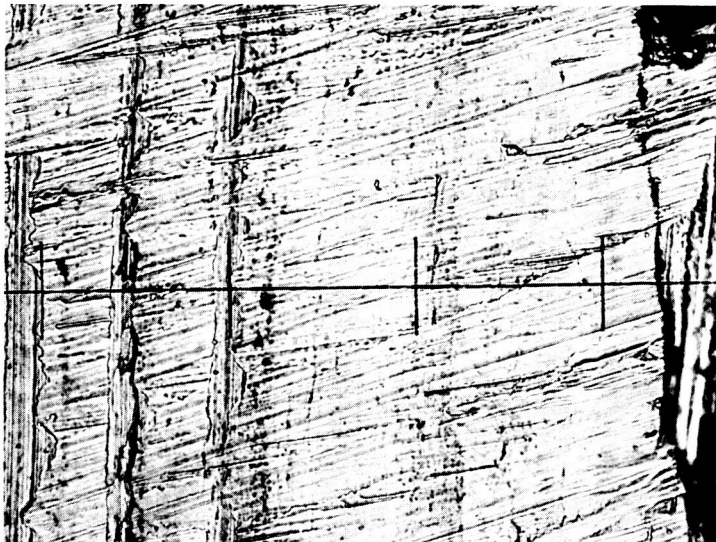


FIGURE 36.33 Photomicrograph of aluminum gasket after leakage test with radially ground 347 stainless steel sealing surface; - Test XVI. Photo near edge of gasket. Magnification: 0.00192 inch between scale marks. Maximum nominal normal gasket stress -  $2.52 \times 0.2\%$  YIELD STRENGTH (LEAK TEST DATA)

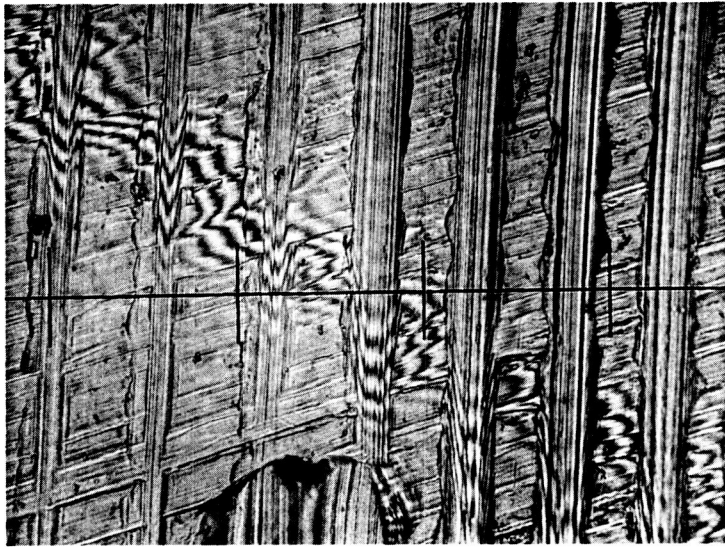


FIGURE 36.34a Interference photomicrograph of aluminum gasket after leakage test with radially ground 347 stainless steel sealing surface; - Test XVI. Photo near center of gasket width. Magnification: 0.00192 inch between scale marks. Interference lines 11.8 microinches apart. Maximum nominal normal gasket stress -  $2.52 \times 0.2\%$  YIELD STRENGTH (LEAK TEST DATA)

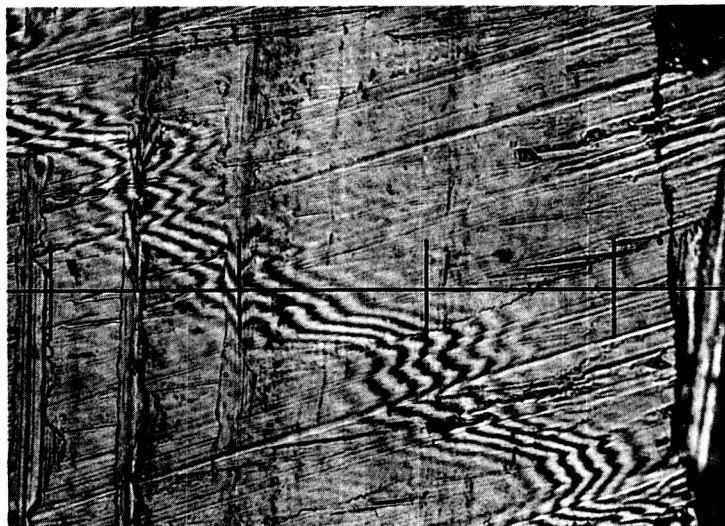


FIGURE 36.34b Interference photomicrograph of aluminum gasket after leakage test with radially ground 347 stainless steel sealing surface; - Test XVI. Photo near edge of gasket. Magnification: 0.00192 inch between scale marks. Interference lines 11.8 microinches apart. Maximum normal nominal gasket stress -  $2.52 \times 0.2\%$  YIELD STRENGTH (LEAK TEST DATA)

## 36.2 Experimental Results - Plastic Gaskets

The experimental results for plastic gaskets are organized in terms of the gasket-flange configuration for sealing surface mating and test conditions used to investigate the various gasket phenomena.

### 36.2.1 Sealing Surfaces

The plastic gasket materials were mated with 347 stainless steel and 2024(24S)T4 aluminum sealing surfaces. The yield stress of the flange materials is several times that of the plastic gaskets so that mating will occur through compliance of the plastic material to the surface of the flange material. Therefore, the only test configuration variables affecting mating at the interface are the flange surface finish and the plastic gasket material. The three different surface finishes on the flange material used on the plastic gasket tests are described below.

- (a) The first surface will be defined as a medium-roughness circumferentially machined finish. The roughness is called medium in reference to the fine and coarse roughness finishes used in the metal gasket tests. The concentric grooves were machined with no lead and with a pitch of .002 inch. The result is an approximately wedge-shaped profile with a 150 micro-inch r.m.s. roughness. A typical profile trace of this surface finish made by the Taylor-Hobson "Talysurf" is shown in Figure 36.35.
- (b) A diamond burnish finish was made by a circumferential rubbing with a diamond tool. This process produces a very smooth surface with approximately a 5 micro-inch r.m.s. roughness. Typical "Talysurf" profiles at high magnification are shown in Figures 36.37 and 36.38.
- (c) A radially ground surface finish was produced by a tool cutting on a 2-inch radius to produce approximately straight-line grooves in the radial direction. These grooves had a .003 inch pitch and approximately a 40 micro-inch r.m.s. roughness. A typical "Talysurf" profile taken in the tangential direction is shown in Figure 36.36.

The three surface finishes were on different flange materials, but this is not a factor in the sealing process, since both flange materials appear as rigid bodies to the soft plastic materials. Inspection of the flange surface finish after each test showed that the finish was not damaged. This observation allowed the different plastics and later the various rubber-like materials to be tested on the same finish for each of the three types of surfaces discussed.

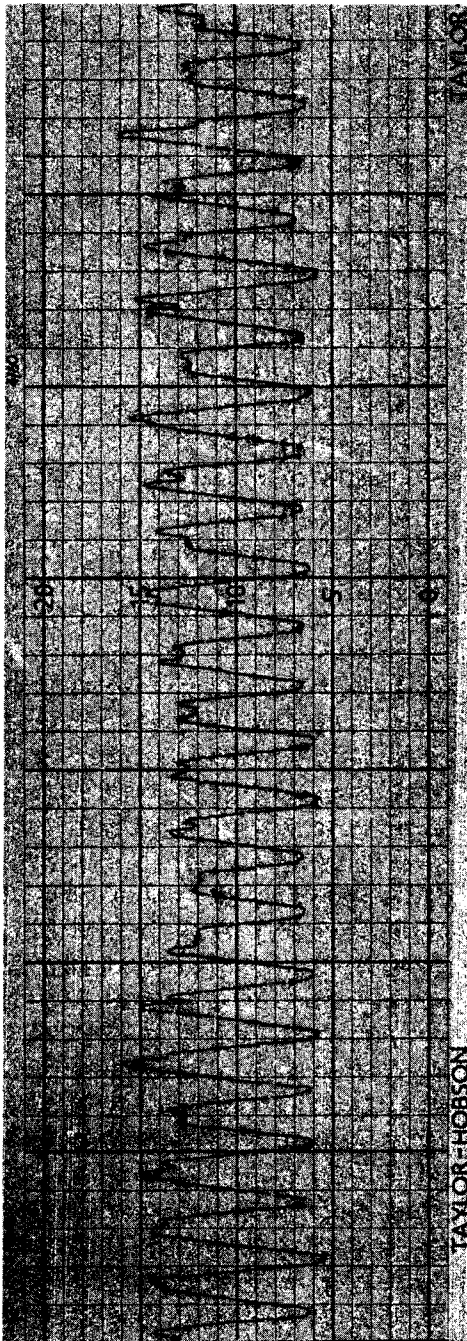


FIGURE 36.35  
circumferential machined surface  
Typical "Talysurf" radial profile  
Vertical Scale: 50 micro-inches  
between light lines  
Horizontal Scale: .01 inch  
between heavy lines

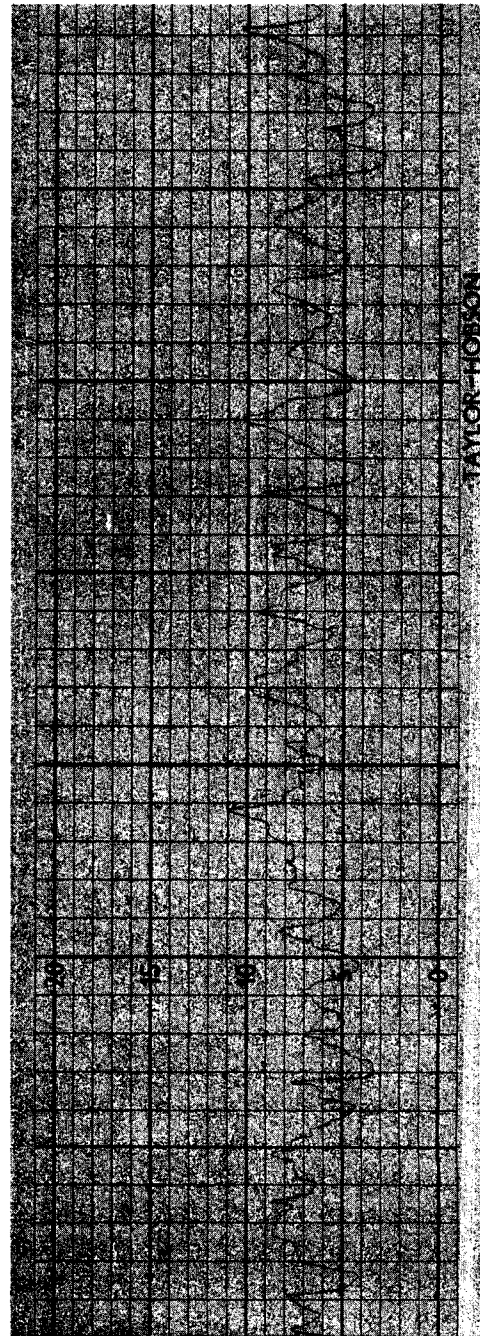


FIGURE 36.36  
radially machined surface  
Typical "Talysurf" circumferential  
profile  
Vertical Scale: 20 micro-inches  
between light lines  
Horizontal Scale: .01 inch  
between heavy lines



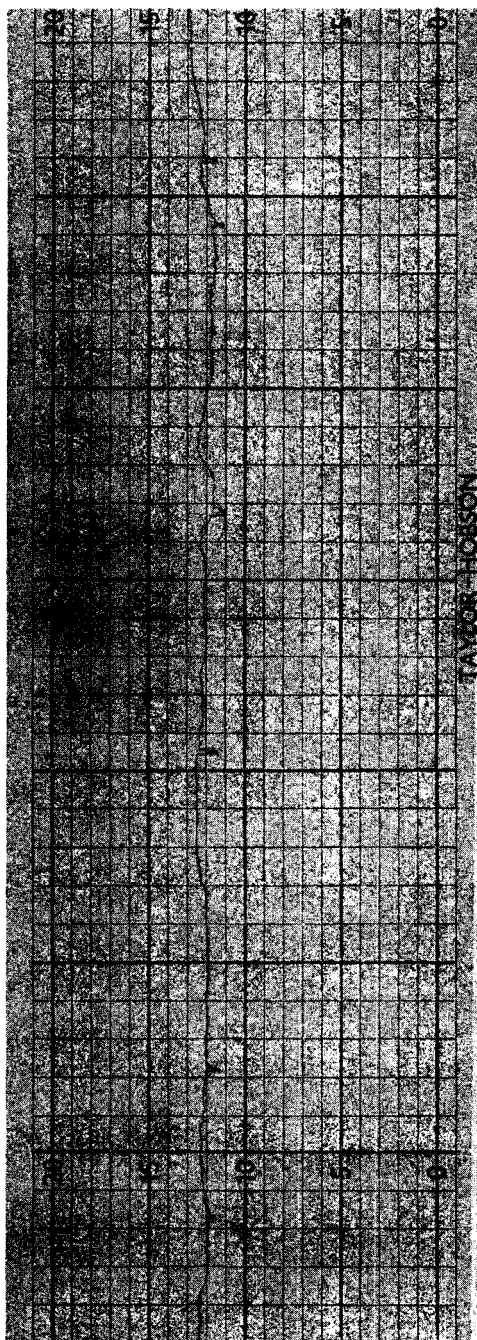


FIGURE 36.37  
diamond burnished finish

Typical "Talysurf" radial profile

Vertical Scale: 10 micro-inches  
between light lines

Horizontal Scale: .01 inch  
between heavy lines

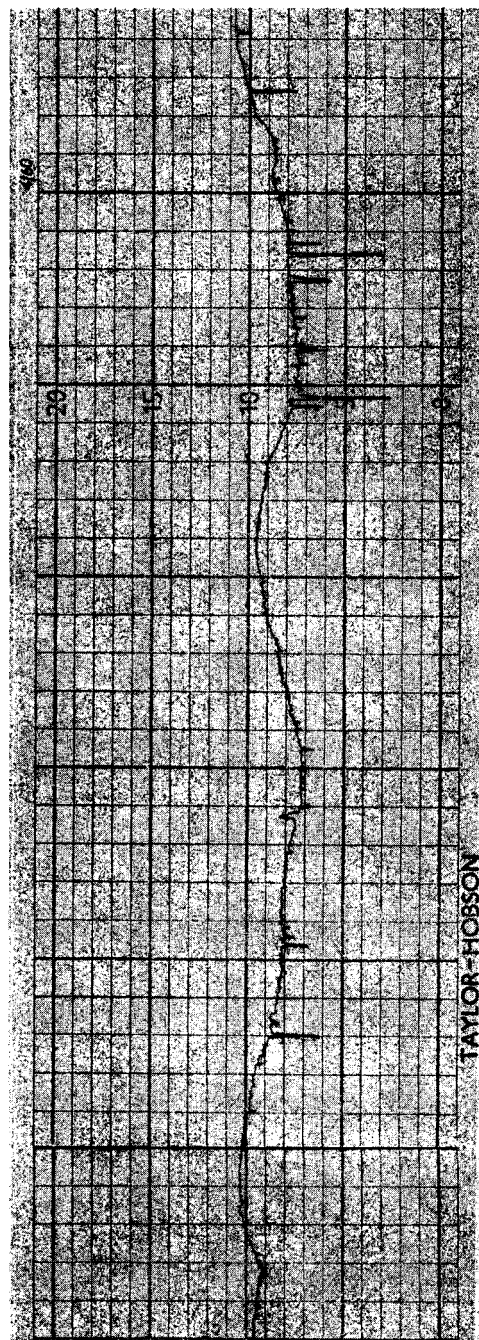


FIGURE 36.38  
diamond burnished finish

Typical "Talysurf" radial profile

Vertical Scale: 5 micro-inches  
between light lines

Horizontal Scale: .01 inch  
between heavy lines

Listed in Table 36.2 is the schedule of tests conducted with reference to sealing surface finish and plastic gasket material.

TABLE 36.2 PLASTIC TEST SCHEDULE

Gasket Material	Sealing	Surface	Finish
	Circumferential Machining	Diamond Burnished	Radially Ground
KEL-F81	P-1	P-6	P-10
Saran	P-2	P-7	P-11
Teflon-FEP	P-4	P-8	P-12
Teflon-TFE	P-5	P-9	P-13
Duroid-5600	P-3		

### 36.2.2 Experimental Leakage Rates

The experimental procedure used for the plastic gasket materials is outlined in section 35.3.3 of this report. The results are reported quantitatively in the form of leakage values as a function of the test variables and qualitatively in the form of surface profile observations which show the degree of mating at the interface. The experiments were conducted in three phases, each investigating important gasket phenomena.

The results of Phase I show the leakage as a function of the gasket stress with a one-atmosphere pressure difference maintained across the seal. The stress parameter has been normalized by dividing the actual stress by the .2% compressive yield stress obtained from the data of each test. The Phase I results for each gasket material with various surface finishes grouped together are presented in Figures 36.39 through 36.42. These graphs show the general stress level needed to seal each gasket and the effect of the sealing surface finish. The Phase I results for the circumferential machined surface finish with all the gasket materials grouped together are presented in Figure 36.43. This graph compares the relative sealing ability of each gasket.

The results of Phase II show the leakage as a function of the pressure differential across the seal with the normal gasket stress held constant. Figure 36.44 shows the sensitivity to pressure for the seal obtained in Phase I as a function of gasket materials on the circumferential machined surface finish. The insensitivity here is also characteristic of the other surface finishes.

The results of Phase III show the sensitivity of leakage to the removal of load with the pressure difference across the seal maintained constant. Figures 36.45 through 36.47 show the sensitivity to removal of load

for the various plastic materials grouped on the same surface finish.

The qualitative results are presented in Figures 36.48 through 36.53 as a set of "Talysurf" profilometer traces showing the gasket material before and after test.



FIGURE 36.39 LEAKAGE RESULTS - PHASE I  
 KEL-F81 Gasket Mated With Various Surfaces  
 All Tests With 1 ATM Pressure of Helium Across Seal

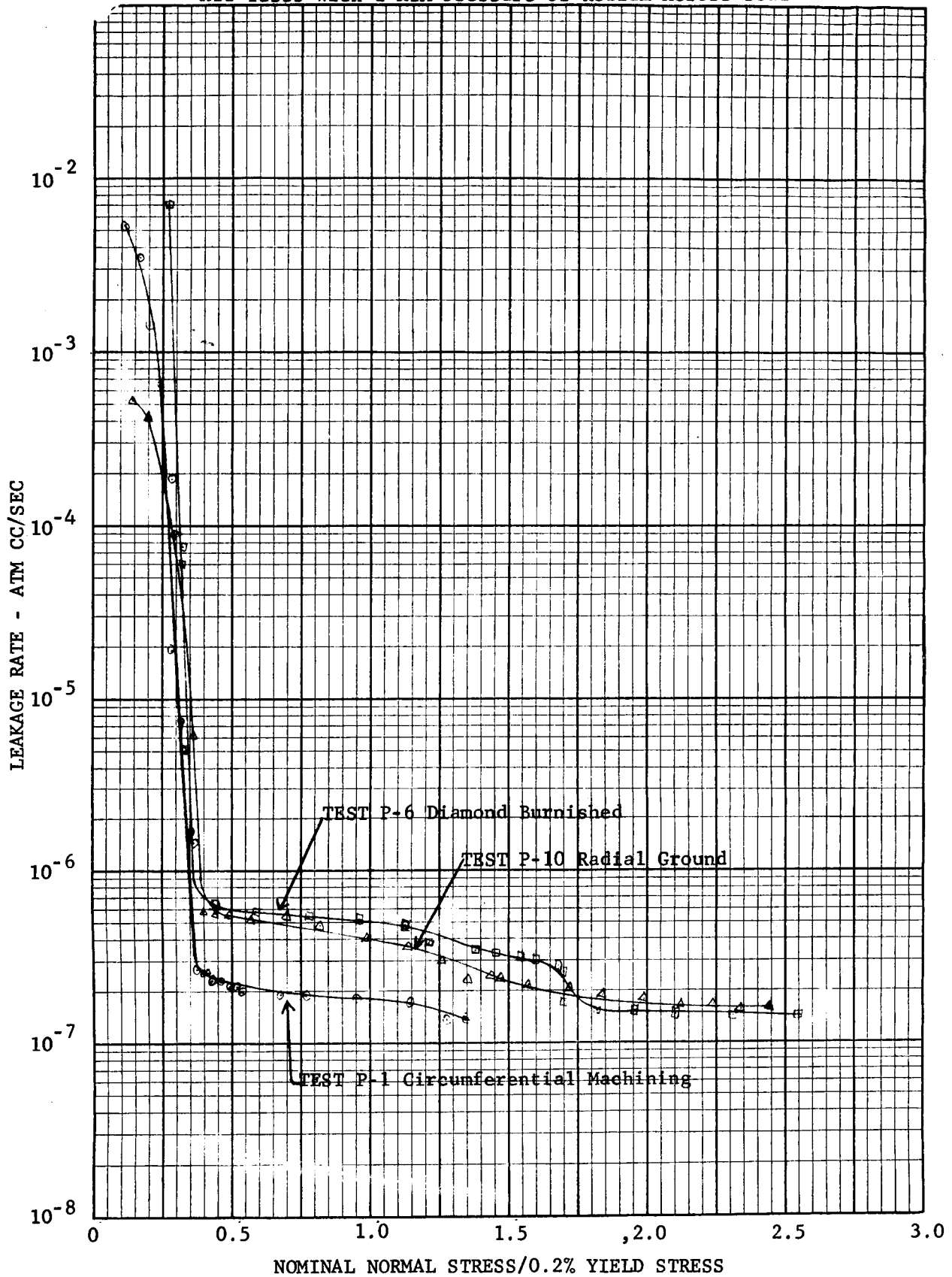


FIGURE 36.40 LEAKAGE RESULTS - PHASE I  
 Saran Gasket Mated With Various Surfaces  
 All Tests With 1 ATM Pressure of Helium Across Seal

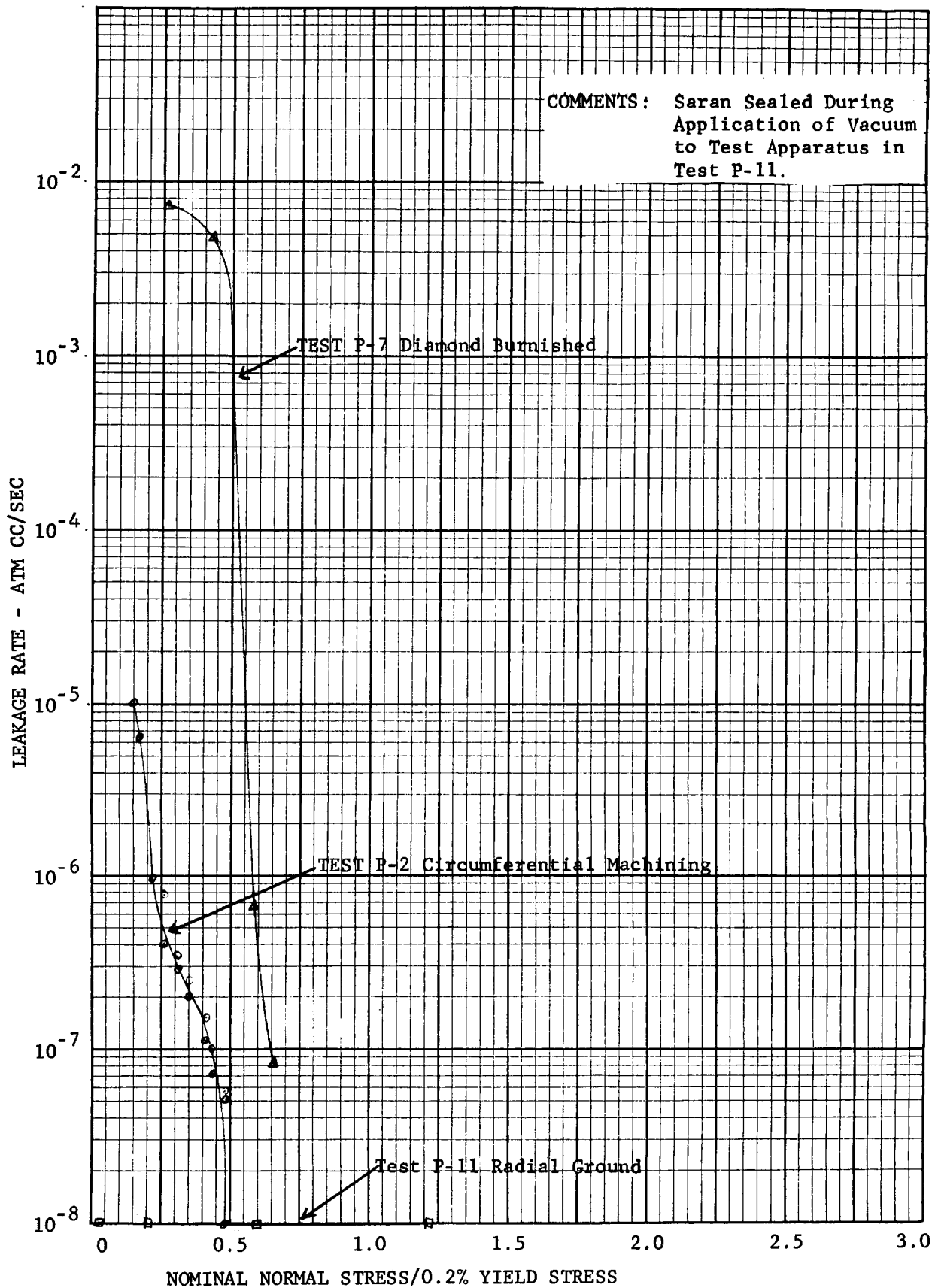


FIGURE 36.41 LEAKAGE RESULTS - PHASE I  
 Teflon - FEP Gasket Mated With Various Surfaces  
 All Tests With 1 ATM Pressure of Helium Across Seal

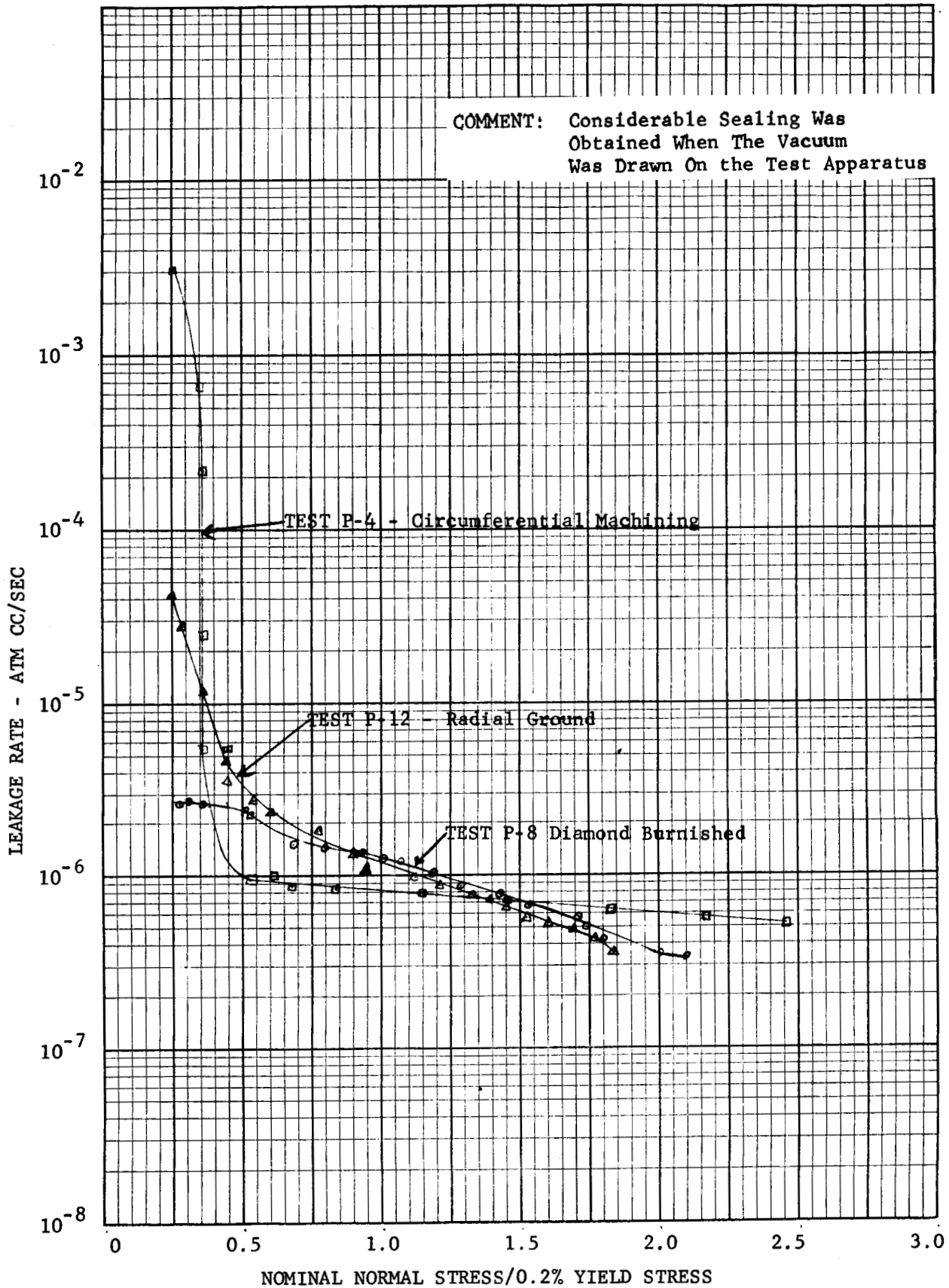


FIGURE 36.42 LEAKAGE RESULTS - PHASE I  
Teflon-TFE Gasket Mated With Various Surfaces  
All Tests With 1 ATM Pressure of Helium Across Seal

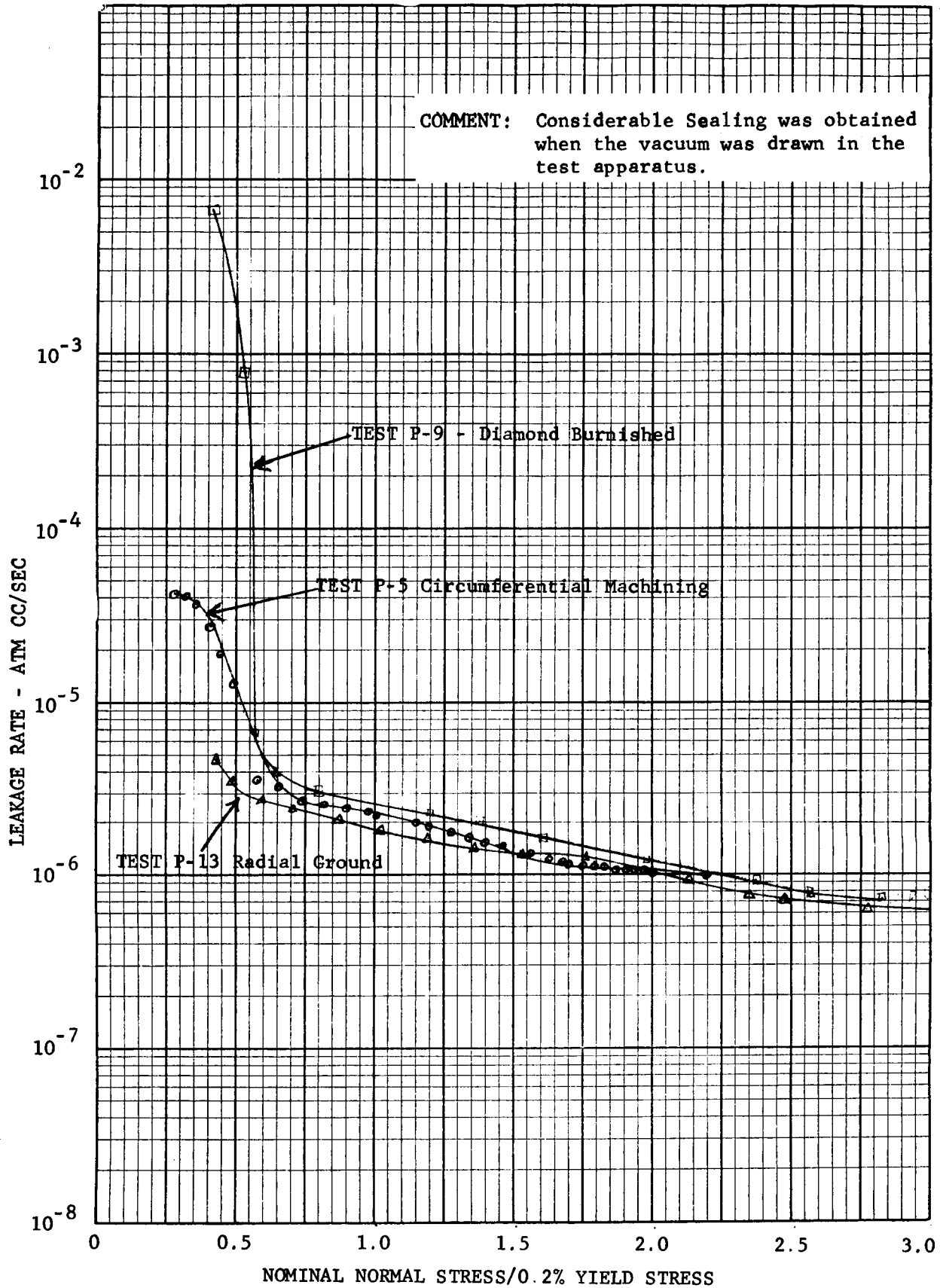


FIGURE 36.43 LEAKAGE RESULTS - PHASE I  
Various Gaskets Mated With Circumferentially Machined Surface  
All Tests with 1 ATM Pressure of Helium Across Seal

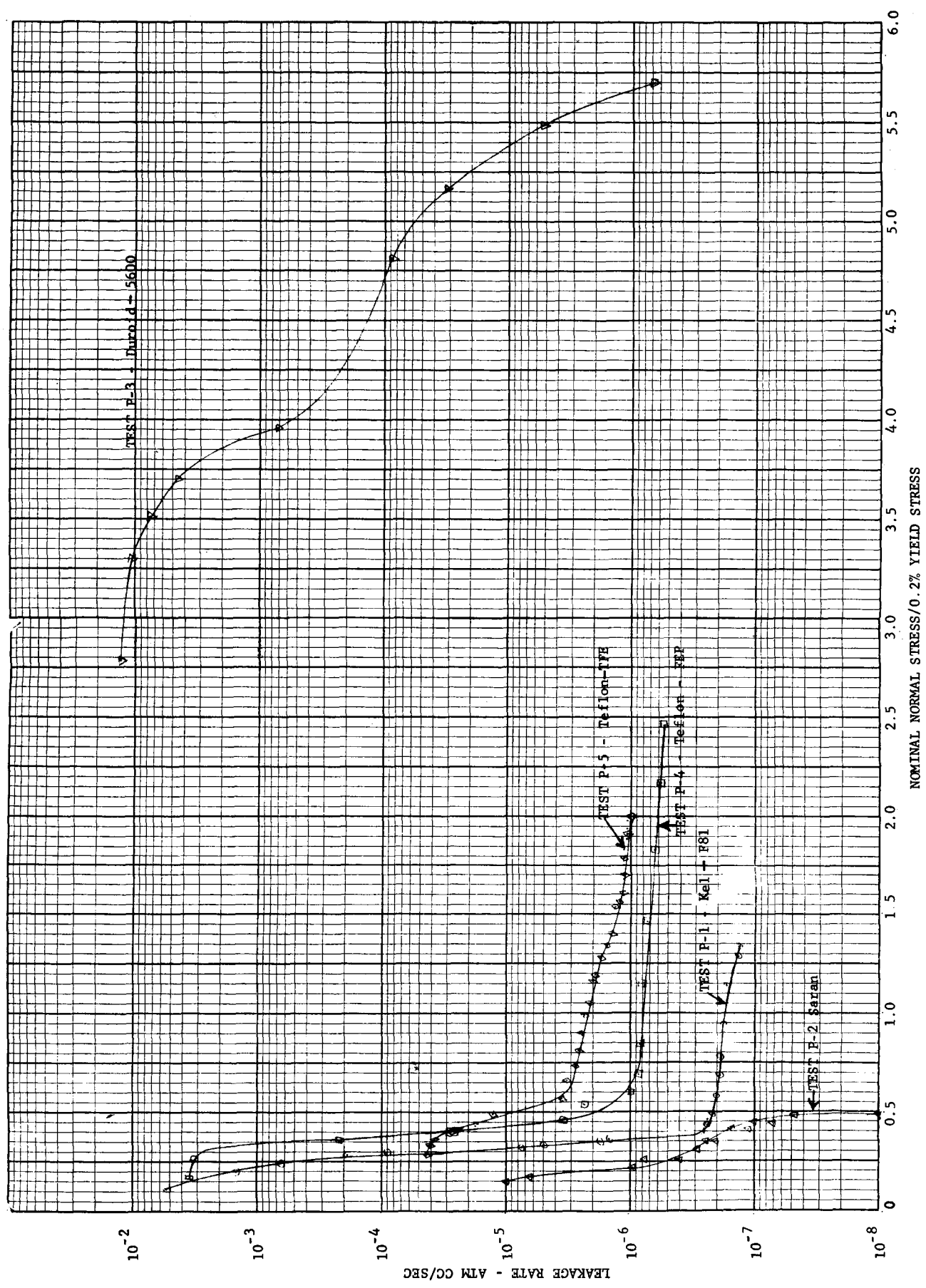


FIGURE 36.44 LEAKAGE RESULTS - PHASE II  
 Various Gaskets Mated With Circumferential Machined Surface  
 Pressure Gradually Increased to Maximum

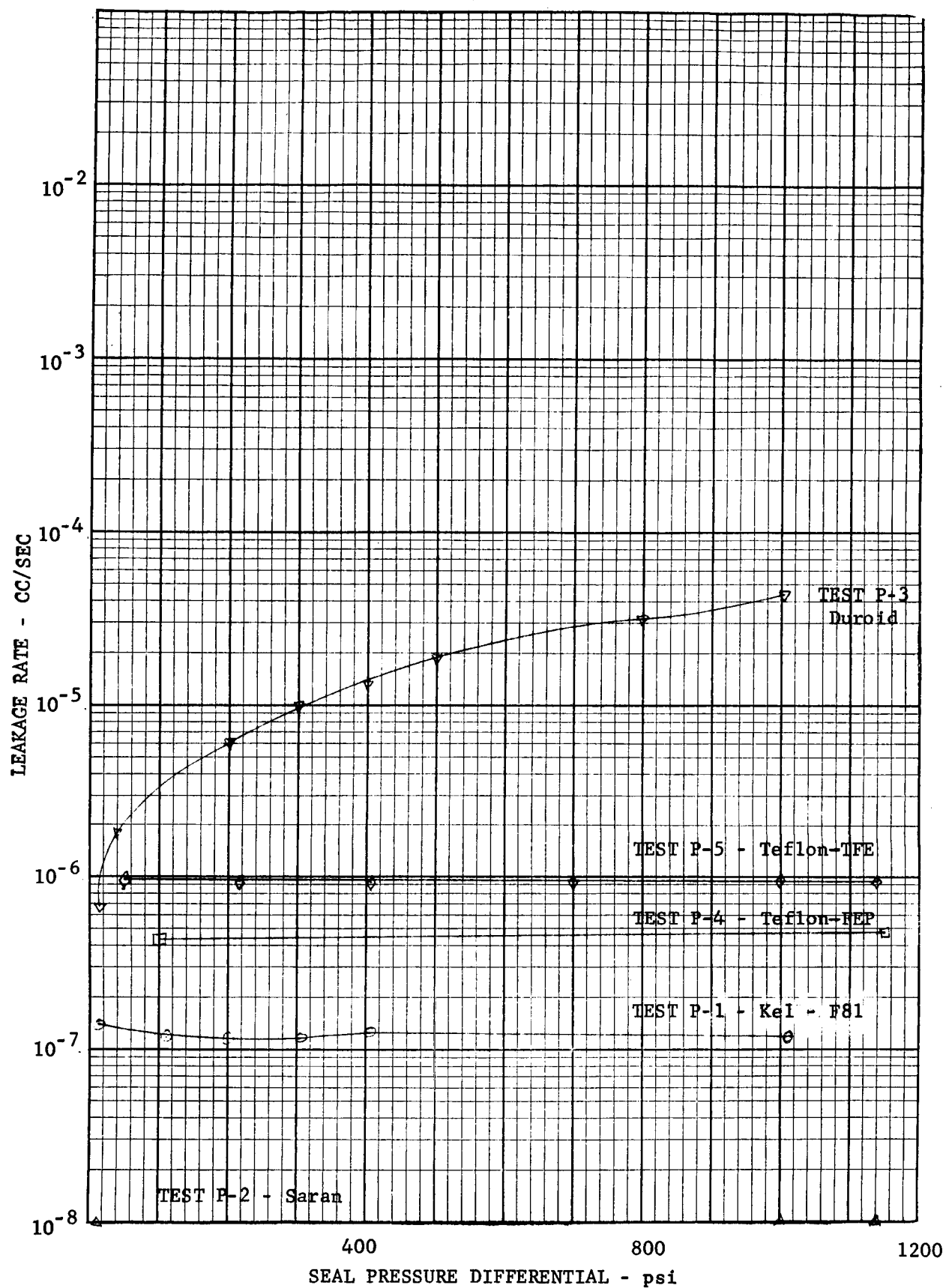


FIGURE 36.45 LEAKAGE RESULTS - PHASE III  
Various Gaskets Mated With Circumferential Machined Surface  
All Tests With 500 psi Pressure of Helium Across Seal

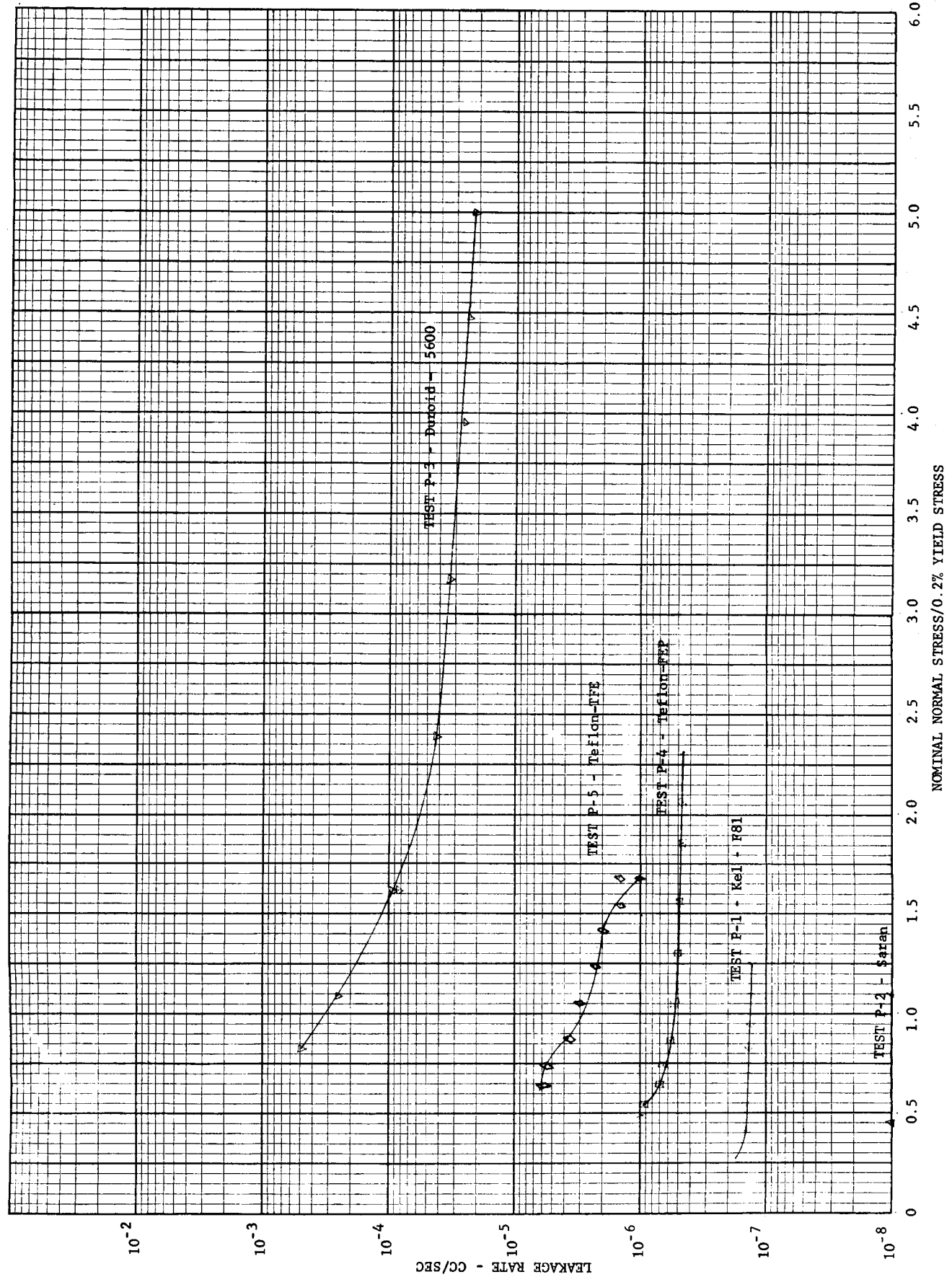


FIGURE 36.46 LEAKAGE RESULTS - PHASE III  
 Various Plastics Mated With Diamond Burnished Finish  
 All Tests With Approximately 1000 psi Pressure Across Seal

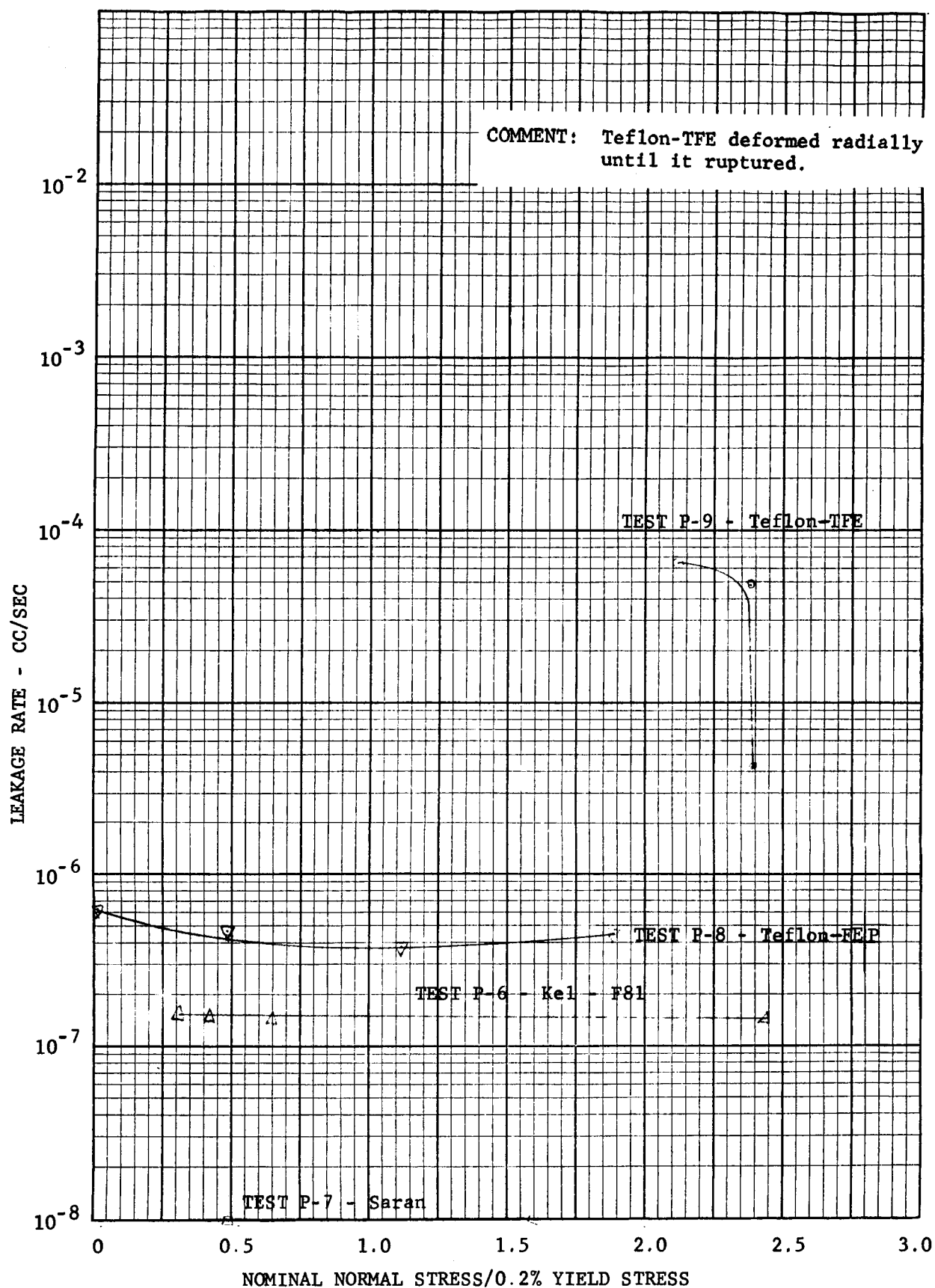
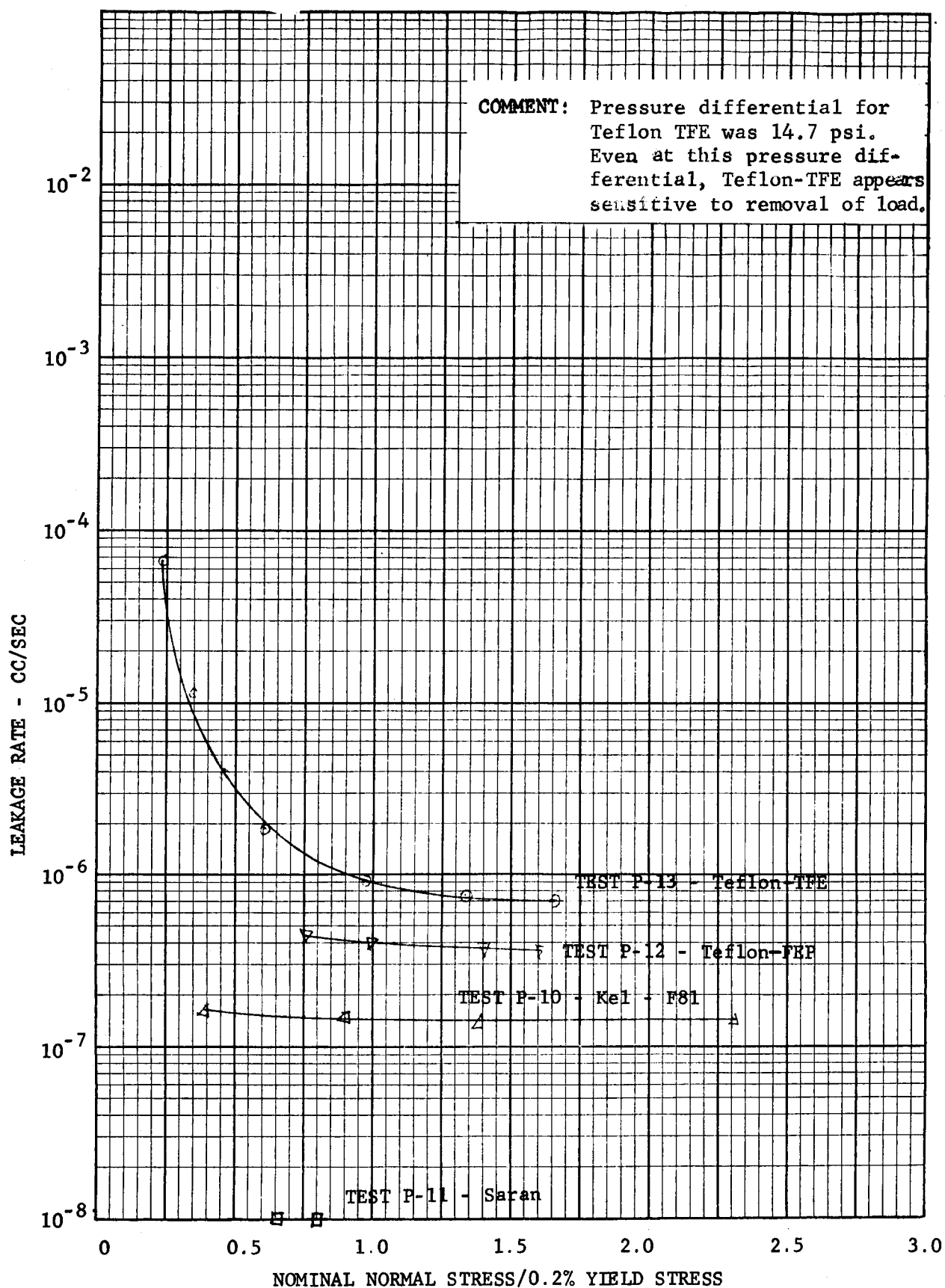




FIGURE 36.47 LEAKAGE RESULTS - PHASE III

Various Gaskets Mated With Radially Ground Finish

All Tests (Except Teflon-TFE) With 1100 psi Pressure Across Seal



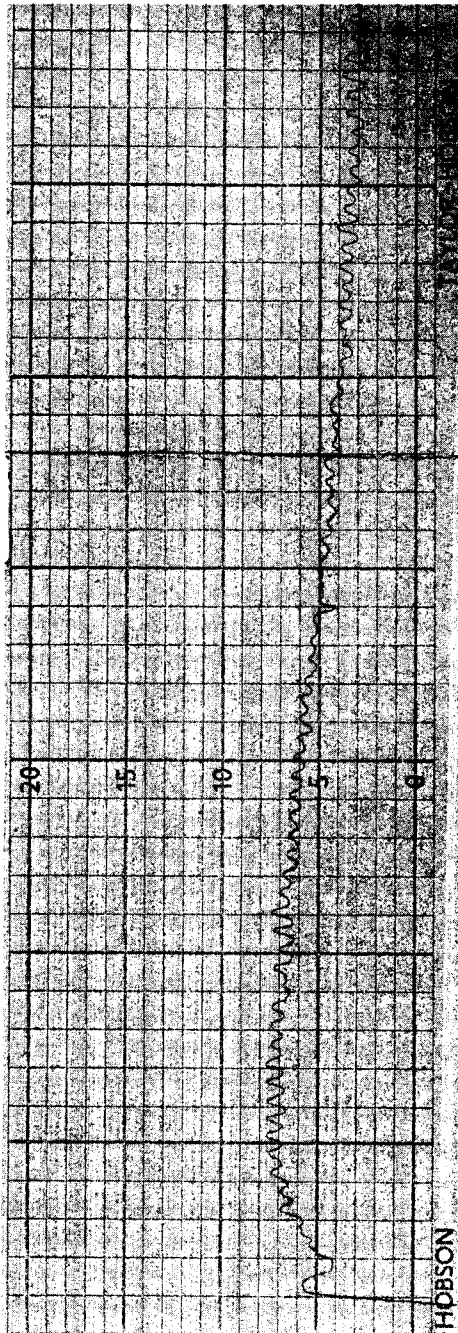


FIGURE 36.48  
 KEL-F81 gasket before test  
 Typical "Talysurf" radial profile  
 Vertical Scale: 50 micro-inches  
 between light lines  
 Horizontal Scale: .01 inch  
 between heavy lines

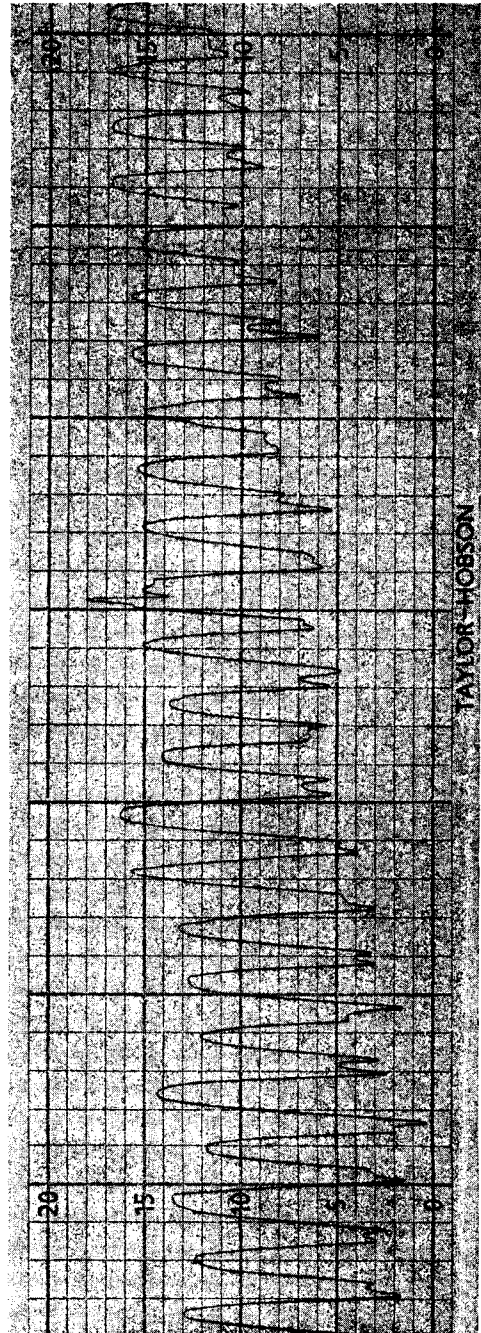


FIGURE 36.49  
 KEL-F81 gasket after test  
 mating with circumferential  
 machined surface  
 Typical "Talysurf" radial profile  
 Vertical Scale: 50 micro-inches  
 between light lines  
 Horizontal Scale: .01 inch  
 between heavy lines

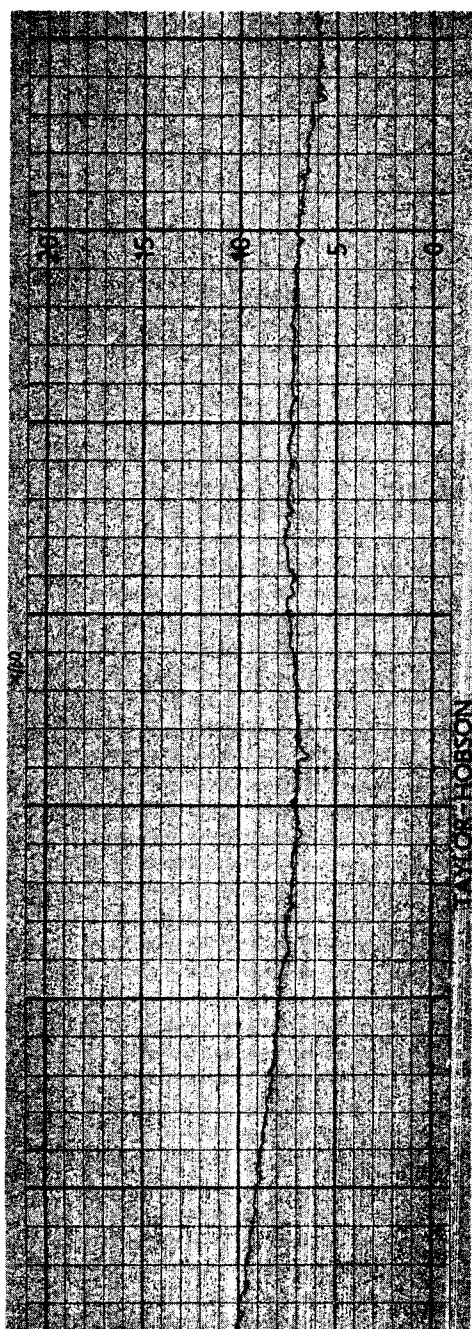


FIGURE 36.50  
 KEL-F81 Gasket after test  
 mating with diamond burnished finish  
 Typical "Talysurf" radial profile  
 Vertical Scale: 50 micro-inches  
 between light lines  
 Horizontal Scale: .01 inch  
 between heavy lines

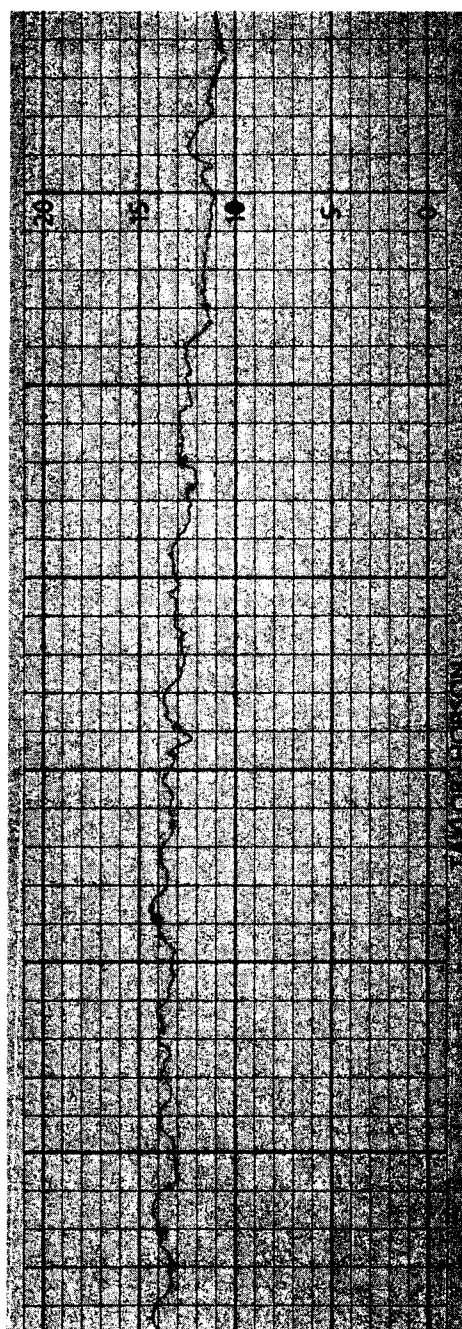


FIGURE 36.51  
 KEL-F81 gasket after test  
 mating with radially ground finish  
 Typical "Talysurf" circumferential  
 profile  
 Vertical Scale: 50 micro-inches  
 between light lines  
 Horizontal Scale: .01 inch  
 between heavy lines

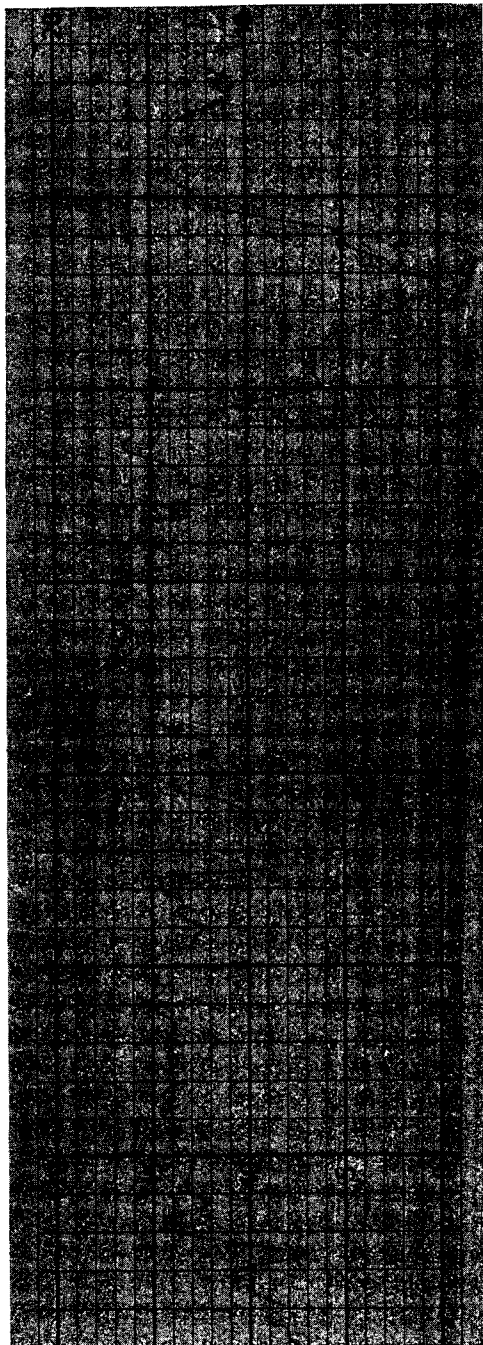


FIGURE 36.52

Duroid-5600 Gasket before test

Typical "Talysurf" radial profile

Vertical Scale: 100 micro-inches  
between light lines

Horizontal Scale: .01 inch  
between heavy lines

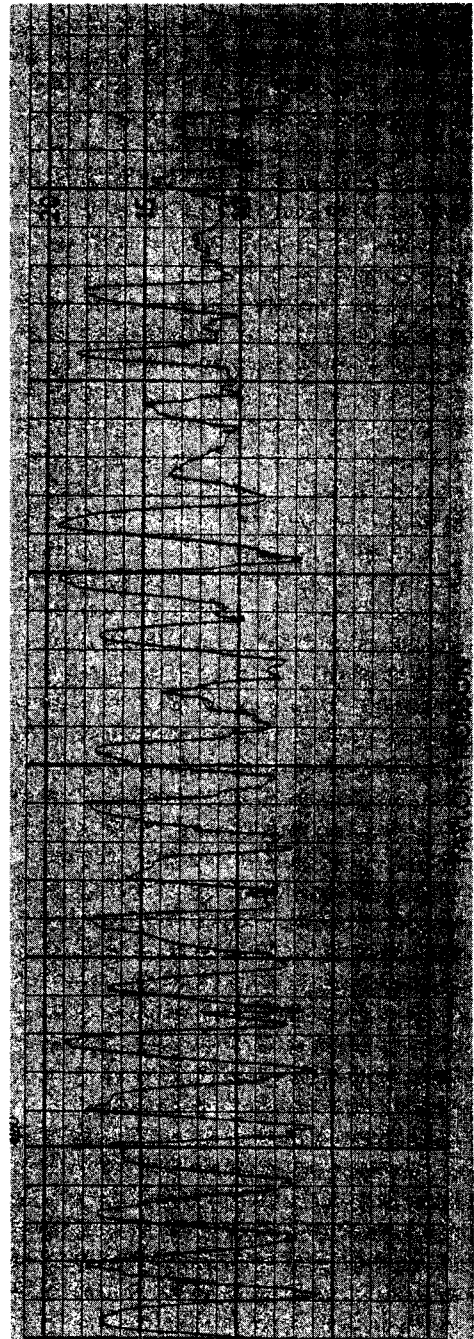


FIGURE 36.53

Duroid-5600 Gasket after test mating  
with circumferentially machined surface

Typical "Talysurf" radial profile

Vertical Scale: 50 micro-inches  
between light lines

Horizontal Scale: .01 inch  
between heavy lines

### 36.3 Experimental Results - Rubber Gaskets

The experimental results for rubber-like materials are discussed in relation to the sealing surfaces used and the normal stress and internal pressure loading on the gasket.

#### 36.3.1 Sealing Surfaces

The discussion of section 36.2.1 similarly applies to the rubber gasket tests since a soft gasket was forced to comply with the same sealing surface finishes.

Listed in Table 36.3 is the schedule of tests conducted for rubber gaskets with reference to surface finish.

TABLE 36.3 ELASTOMER TEST SCHEDULE

Gasket Material	Sealing	Surface	Finish
	Circumferential Machining	Diamond Burnished	Radially Ground
Viton-A	E-1	E-5	
Neoprene	E-2		E-6
Hypalon	E-3		
Silicone	E-4	E-7	E-8

#### 36.3.3 Experimental Leakage Rates

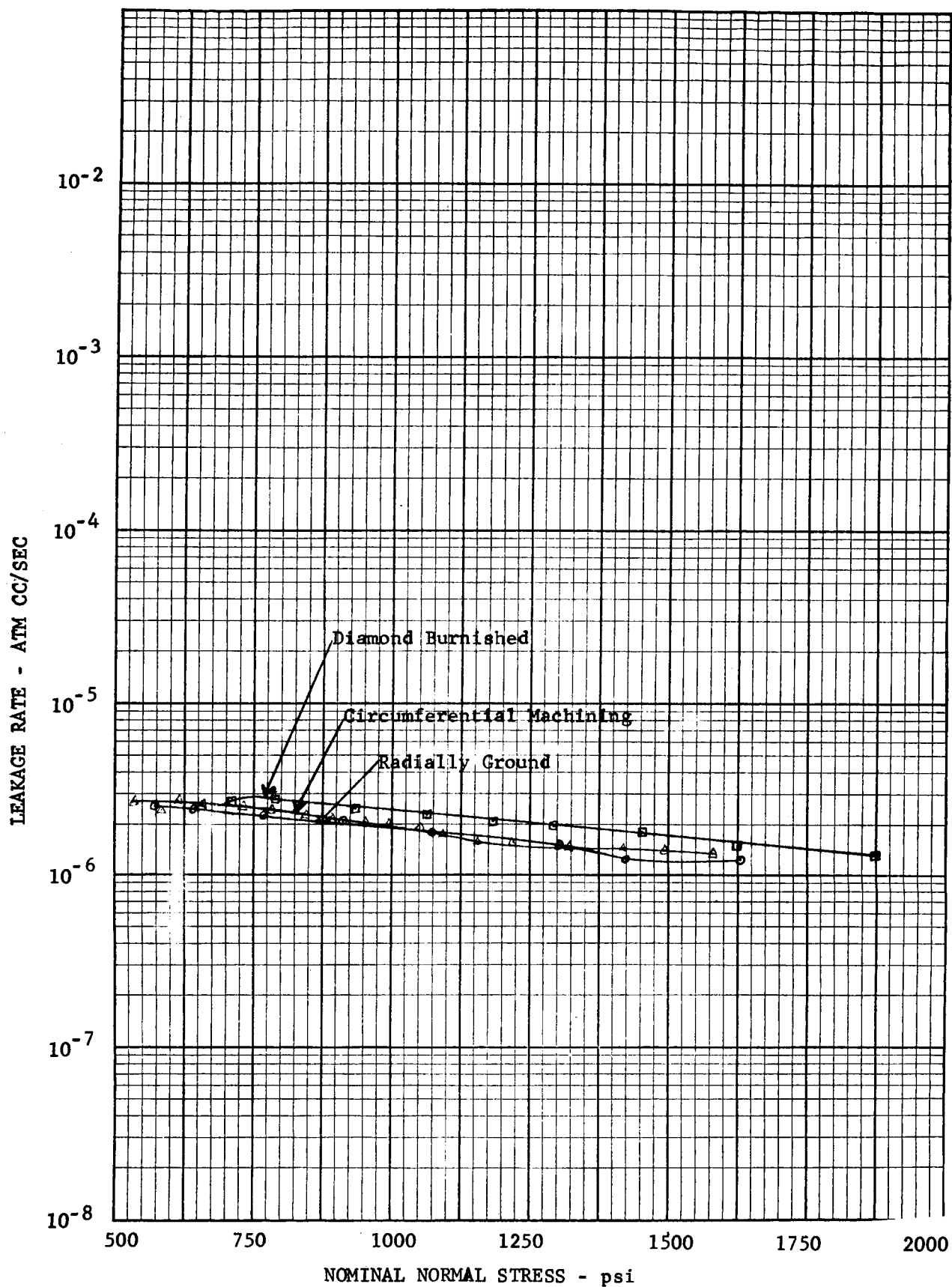
The experimental procedure previously outlined for metals and plastics had to be modified for the rubber gasket tests. The rubber-like materials are so soft that sufficient deformation occurred to cause mating at the interface when a small initial load was placed on the gasket. This initial load was necessary to obtain the vacuum around the apparatus needed for mass spectrometer leakage readings. The Viton - A, neoprene and hypalon gaskets sealed before leakage measurements could be made. The internal pressure was then increased in an effort to break the seal. The seal would break catastrophically when the internal pressure of the gasket approached the normal stress on the gasket. There was no measurable leak through the interface of Viton - A, neoprene and hypalon for normal test loads and pressures. ~~Silicone~~ rubber gaskets, however, showed a low value of leak which was independent of surface finish and normal stress as shown in Figure 36.34. This leakage is believed to be diffusion of the helium

through the gasket and was proportional to the internal pressure. The response of the leakage to a sudden change in internal pressure was very slow, on the order of one hour. This time lag is indicative of a diffusion type process as compared to leakage through holes at the interface.

Since the test results of tests E-1, E-2, E-3, E-5 and E-6 all showed that these materials sealed (when the initial vacuum load was placed on the gasket) independent of surface finish, no further tests with these combinations were run.

FIGURE 36.54 LEAKAGE RATES - RUBBER GASKETS

Silicone Rubber on various surface finishes  
One atmosphere pressure difference across seal





## 37. EXPERIMENTAL OBSERVATIONS AND CONCLUSIONS

by

Forrest O. Rathbun, Jr. & George W. Sarney

### 37.0 Summary

In this section, the interpretations of the results of all experimental observations are presented. References to the data found in Section 36 are made. The conclusions with regard to each type gasket material are grouped in separate subsections.

The important conclusions and recommendations are also summarized in Section 31.2.



### 37.1 Experimental Observations for Metal Gaskets

#### 37.1.1 Experimental Gasket Deformations

Post-leak-test measurements of the nominal dimensions of the gaskets show that the material deforms inwardly and outwardly to about the same extent. The radial deformations inward and outward were identical in all cases involving the stronger gasket materials (aluminum, copper, nickel); in these cases, the deformation was slight, however.

In the case of indium and lead where the deformations were great, the changes inside radius and outside radius were not identical but quite close. Change in outside radius was slightly larger than the change in inside radius. In these cases the ratio between normal gasket stress and internal pressure was not as great as in the former cases. Hence, the internal pressure had some effect on the gasket deformation.

It can be concluded, however, that in the metal gasket tests the deformation was nearly a plane-strain phenomenon (as far as gross deformation are concerned), and that curvature and internal pressure played very small roles in determining the geometry of gasket deformation.

#### 37.1.2 Gasket Material Flow Along Interfaces

Tests with gasket materials which underwent large plastic deformations (indium, lead) show that the surfaces initially in contact tend to remain in contact and that the material flow radially tends to emanate from the internal portion of the gasket. This tendency was noted visually in early tests where the gasket surfaces were not thoroughly cleaned. The final area of contact showed the original "dirty" inner region and a bright outer ring. It can be seen then that the bulk flow occurred as shown in Figure 37.1.

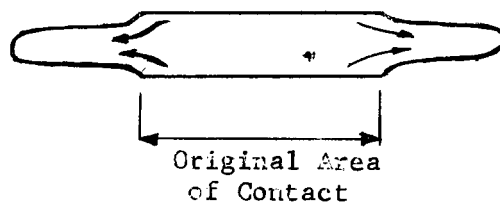


FIGURE 37.1 Description of Large Bulk Gasket Flow  
(For Normal Stress  $\gg$  Yield Stress)

From this observation, it is concluded that the friction along the interface between gasket and sealing surface plays a major role in the actual mode of deformation of the gasket. The problem of the gasket bulk flow then becomes very similar to the Prandtl problem bulk flow of a purely plastic material between two rigid flat plates. The analogy is quite good in the case of the soft metals and generally descriptive in any case where the gasket yield strength is much lower than the sealing surface material yield strength.

Thus, the phenomenon of sealing - the closing of the space between the two surfaces - becomes affected by the friction, at least that portion of the mating accomplished during gross gasket deformation.

### 37.1.3 Variation in Plastic Deformation Across Gasket Width

If the gasket - sealing surface compression phenomenon is nearly the same as the Prandtl problem phenomenon, then the normal stress distribution on the gasket surfaces will be of the form shown in Figure 37.2. (Ref. 1,2).

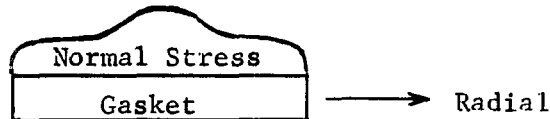


FIGURE 37.2 Normal Stress Distribution on Gasket

The nominal normal stress is, of course, the average value of such a distribution, and is known from the applied load. The distribution shown is predicated on the gasket being purely plastic, the sealing surface being rigid, and the ends of the gasket being unrestrained.

No controlled measurements on the normal stress distribution were made during the investigation. However, some observations show that the distribution is probably correct. During test XII, where a nickel gasket was used in conjunction with a radially ground sealing surface, great difficulty was experienced in attaining a low leakage rate. Thus the gasket stress was increased to a maximum value of 79,150 psi, which is 2.02 times the 0.2% yield strength of the stainless steel. Hence, gross plastic deformation occurred in the head and body of the apparatus. An annular shaped depression was formed under the gasket. Its profile was as shown in Figure 37.3.

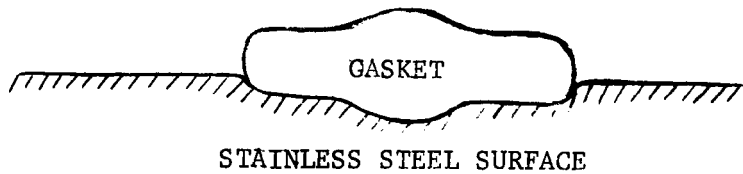


FIGURE 37.3 Deformation of Stainless Steel Sealing Surface

The similarity between the depression profile and the probable stress distribution on the gasket surface (and therefore the steel) can be noted. Thus, even in the case of nickel, the strongest of the gasket materials used, the stress distribution shown in Figure 37.2 seems descriptive.

Concomitant with the depression in the stainless steel in test XII, a retention of the original surface finish was noted. While the stainless steel had deformed grossly, the surface geometry (asperity distribution) had not. Pre-test and post-test profilometer traces showed that the surface had changed very slightly. Only the tips of the asperities had been rounded somewhat. The rms and CLA values of the surface had not changed appreciably.

Such a phenomenon can be predicted from previous experimental and analytical (Ref.1) work on rigid dies and plastic half spaces. Slip line theory predicts that the plastic flow will initially occur at a distance beneath the area of contact and to the sides as shown in Fig. 37.4.

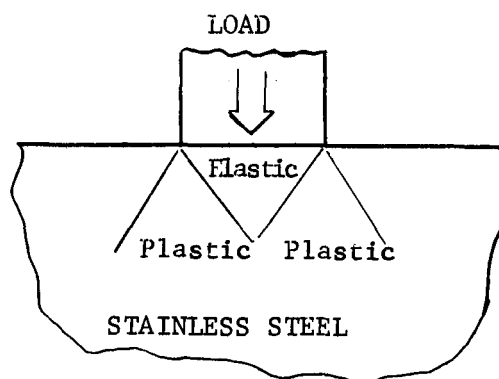


FIGURE 37.4 Probable Plastic - Elastic Regions in Stainless Steel

Such a phenomenon has some practical ramifications regarding the fluid-connector problem. First, the stronger of the two metals will retain to a great extent its surface profile. Since the weaker material (usually the gasket) will deform plastically and fill the spaces between asperities on the stronger material, those asperities are "protected" during further deformation of the system. Re-use of the sealing surface (the stronger material) is thus possible, even in cases where the applied stress has exceeded its yield stress. (In cases where the substructure has been grossly deformed, this is certainly not true).

Secondly, it is illustrated that no matter how high the normal stress, the surface deformation is not severe on the stronger material. Hence, it must be concluded that the sealing must be completely accomplished by deformation of the weaker material. It can be shown that even with higher normal stresses, further deformation will occur at other than the area of contact (beneath the surface of the stronger material).

The important question arising from the above observations is, "What effect does increasing normal stress have on the weaker material?" That is, can the weaker material completely mate across the area of contact?

Results of several tests show that the degree of mating, even under extremely high stress, is not uniform. Figures 36.28 through 36.34 illustrate clearly the non-uniformity of mating. The test results shown apply to an aluminum gasket and a radially ground stainless-steel sealing-surface material. The phenomenon was not limited to this particular test; however, this test illustrates both the non-uniformity (and distribution) of mating and other important phenomena occurring in Figure 36.28 through 36.34, the asperities running roughly horizontally constitute the pattern of asperities on the stainless steel. These asperities were not originally on the aluminum shown. The vertical lines are the asperities machined onto the gasket, and constituted the original gasket profile. The gouge marks shown in the photos are the stylus marks originally made on the stainless steel and not originally appearing on the gasket material. The original directions of asperities are as shown in Figure 37.5.

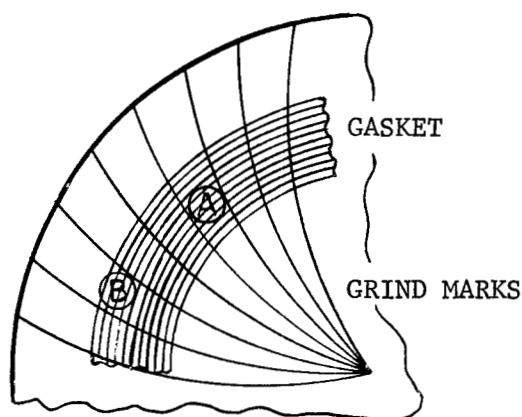


FIGURE 37.5 Surface Profile Directions, Test XII

Upon completion of the leakage test, the gasket was removed from the fixture and the photos taken at locations A and B (Figure 37.5).

In Figure 36.28, the central area A is shown; and it is obvious that the degree of mating is very poor. The vertical lines dominate. Figure 36.29 shows location B; and it can be seen here that the horizontal lines not only dominate, but are the only pattern visible at the edge. From Figs. 36.30 and 36.31, it can be estimated that, at the center, mating occurred over about 40% of the area and near the edge, from about 65% up to 100% at the very edge. The interference lines in Figures 36.34a and 36.34b show that where mating did occur, at the edge or near the center, the mating was the same. (The variation in interference lines is the same magnitude). Inspection of the stainless steel surface at the same points showed identical features. Two important phenomena are seen here - each very important in connector design.

First, it can be seen that the best mating (sealing) does not occur at the point of maximum normal stress; it occurs at the edge, where normal stress was minimal. It does occur where the greatest amount of gross gasket translation took place. It can be seen that, no matter how hard the gasket is pushed vertically onto the sealing surface, if the gasket material is contained (as it is at the center) the gross deformation is not large. This, theoretically, is due to a large hydrostatic condition of stress, but a small stress deviator, (the plastic deformation being proportional to the stress deviator). At the edge, where no constraint is available, the deformation is large, and the mating better. Here the stress levels are less; however, the stress deviator is large, and the hydrostatic stress is small.

The phenomenon can also be explained by viewing the mating as a function of shear deformation. Where no shear deformation at surface was allowed, the mating was poor. Where the surfaces "slid", one with respect to the other the mating was good.

Hence, we conclude that mating of surfaces is best performed not by brute-force compression, but by the shear deformation of the softer material. Hence, geometrical configurations which utilize shear deformation as the means of sealing (such as knife-edge seals) have excellent prospects of success.

Secondly, test XII (along with other tests) illustrates that, even though the stronger material in a flat annular gasket geometry connector has asperities running in the direction of potential leakage flow, the prospects of obtaining a successful seal are good. In this test (and others) very low leakages were attained. This is true because the "hills and valleys" of the stronger material not only are paths for fluid flow, but are excellent paths for plastic flow of the gasket material. As the gasket flows outward, little geometric resistance to plastic flow at the interface exists. Hence, the mating is quite good. An important corollary of this is that surface-finish requirements on flanges need not be so severe in

certain cases if the phenomenon occurring is understood and offers the type of mating described above.

#### 37.1.4 Phase II Results Compared to Analytical Predictions

Experimental leakage rate results can be compared with analytical leakage rates for given pressure differentials in order to estimate an average leakage path height for the experimental case. (Section 22) Relationships between internal pressure, height of passage, and leakage rate have been plotted for an annular passage. The analysis on which the plots are based considers the possibility of both viscous and molecular flow. No deviations from a uniform path geometry are considered, however; whereas in the annular gasket experiments, the flow paths are nonuniform. Hence, only the gross dimensions can be compared. However, such an analysis is extremely useful for a cross-check with experimental results. Also, the comparison between experimental results and these particular analytical predictions will be useful in evaluating the possibility of disregarding the details of the actual flow paths in establishing useful design criteria.

In the leakage experiments, height of gap is not a measured quantity; leakage rate and pressure differential are known quantities. At the terminal state of gasket deformation (maintained during Phase II), the internal pressure is varied, and the leakage recorded. Hence, assuming that the gap height (whatever its geometry) is constant during this phase, we can superpose the experimental Phase II data for a given test on a predicted plot. In accomplishing this, the experimental leakage rate and internal pressure will be plotted. The resultant equivalent height (and the variation thereof) will be noted. If the analytical graph were to agree with the test results completely, then this plot would be a vertical line.

When a value of  $h$ , now an equivalent gap height, is found by the above means, an evaluation of the reasonableness of such a figure can be gained by inspection of the interference photomicrographs taken of the gasket after the completion of the tests.

Since the experimental results encompass leaks through two identical passages (above and below the gasket), the total experimental leakage rate must be divided by two. The graphs incorporate this correction.

In this section, comparisons of analytically predicted leakages and experimentally gained leakages are made for each type surface finish. Extensions of leakage prediction graphs from Section 22 for extremely low values of  $h$  are reproduced; the traces have been corrected for the experimental nominal gasket dimensions and for a zero value of external pressure. All Phase II data which followed continuous curves have been plotted.

Observing the shape and direction of the experimental lines on the analytical predictions, one sees that the lines nearest to the vertical are those for diamond burnished surfaces, Fig. 37.6. The lines for the

fine circumferential machined surface tests (Fig. 37.8) and the radially ground surface (Fig. 37.7) tests deviate from the vertical by a large amount. The coarse circumferential machined surface test (Fig. 37.9) yields near-vertical lines, and another means has to be used to estimate their validity.

The value of  $h$  (gap between surfaces) for the diamond burnished cases range from about 0.03 micro-inch to 0.3 micro-inch. In order to establish whether these are reasonable values of an equivalent gap height, one can inspect photos of the mated surfaces used during these tests.

The matching surfaces of both tests X and XV are shown in Figs. 36.20, 36.21, 36.24, and 36.25. From the interference line pattern in Fig. 36.20 (stainless steel surface, Test X) it can be seen that the grooves in the surface are about 8 micro-inches deep at most. From Figure 36.21 (the nickel gasket, Test X), it can be seen that the mating is local along the peaks of the asperities existing originally on the gasket. It is also seen from the uniformity of interference lines on the deformed peaks that the mating was excellent at those points. However, no evidence exists of the nickel deformation being such as to fill the grooves in the steel. Also noted is that, since the mating is local (along concentric rings), the concept of a path length being equal to the gasket width does not hold true. At best, the comparison between experiment and theory in this case holds true locally, but not across the gasket width. For such local areas of contact, another path-length parameter equal to the sum of the widths of each line of contact could be used; however, this would be of limited use in prediction of leaks since, unless the equivalent width could be measured in advance, no meaningful results could be attained. Figures 36.24 and 36.25 (Test XV, copper gasket - aluminum sealing surface) yield more meaningful data, in that the mating occurred over more of the total area - again in concentric rings. Also, even the most minor grooves and pits existing on the sealing surface (Fig. 36.24) show up on the mated portions of the copper (Figure 36.25). Here, where the value of path length can be evaluated as being not more than 50% in error (one half of total area mated), the analytical predictions offer a more accurate model. It is noted that the value of an equivalent  $h$  of less than one micro-inch is at least reasonable (from the photos) over the mated area. Thus, for the combination of smooth sealing surfaces and soft gaskets, the analytical predictions are quite good. If a value of  $h$  can be predicted for a strong smooth flange and soft metal gasket under a given load, then the leakage can be predicted well by the analysis of section 22.

For the coarse machined surface finish, the mating was accomplished only locally and in non-uniform patterns; hence, the analytical model does not apply.

FIGURE 37.6 LEAKAGE RATE FOR HELIUM AT 20°C FOR AN ANNULAR PASSAGE EQUAL TO EXPERIMENTAL NOMINAL DIMENSIONS, WITH 0 PSI EXTERNAL PRESSURE. COMPARISON WITH DIAMOND BURNISHED EXPERIMENTAL SURFACE FINISH RESULTS.

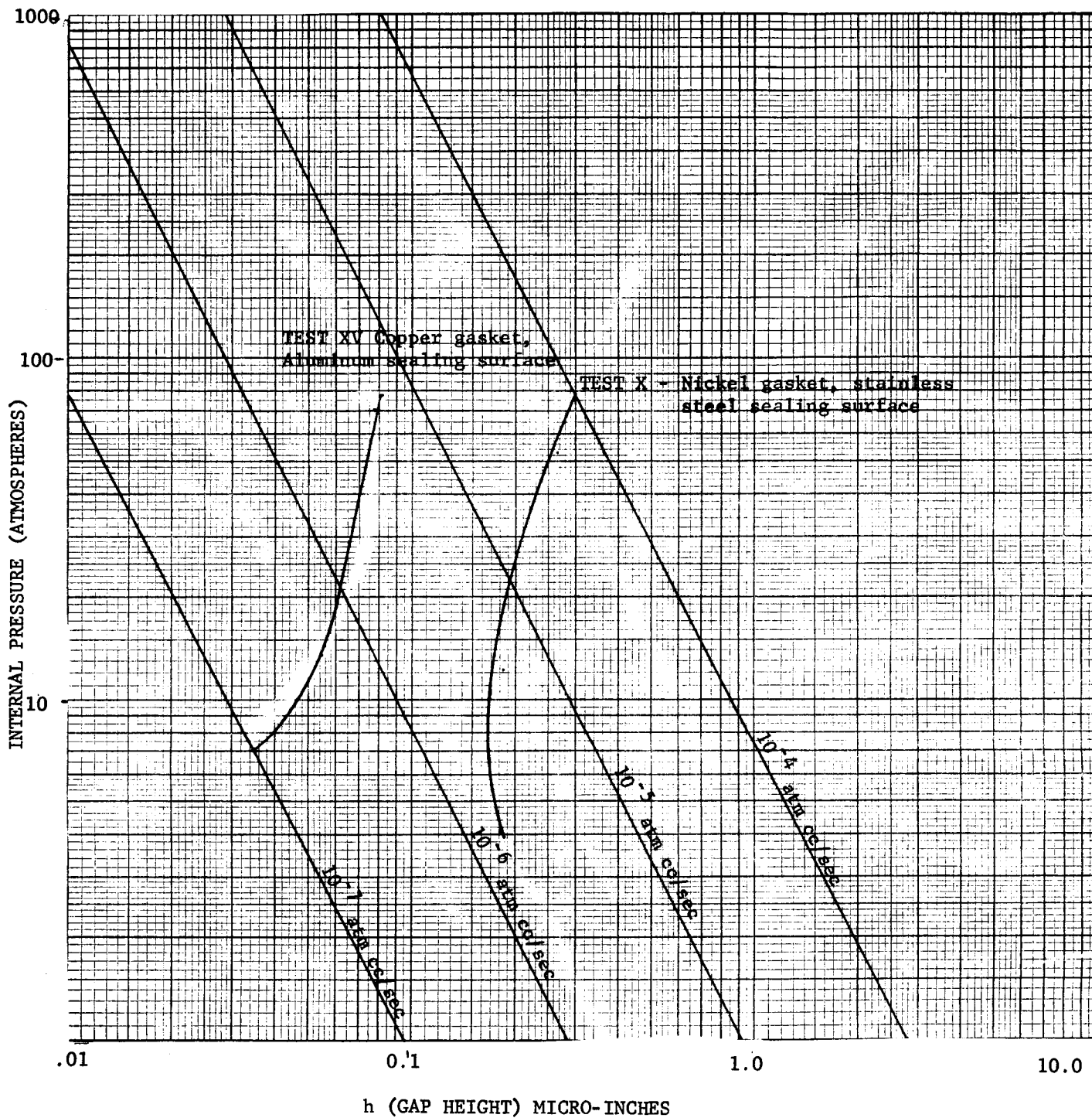




FIGURE 37.7 LEAKAGE RATE FOR HELIUM AT 20°C FOR AN ANNULAR PASSAGE EQUAL TO EXPERIMENTAL NOMINAL DIMENSIONS, WITH 0 PSI EXTERNAL PRESSURE. COMPARISON WITH RADIALLY GROUND EXPERIMENTAL SURFACE FINISH RESULTS

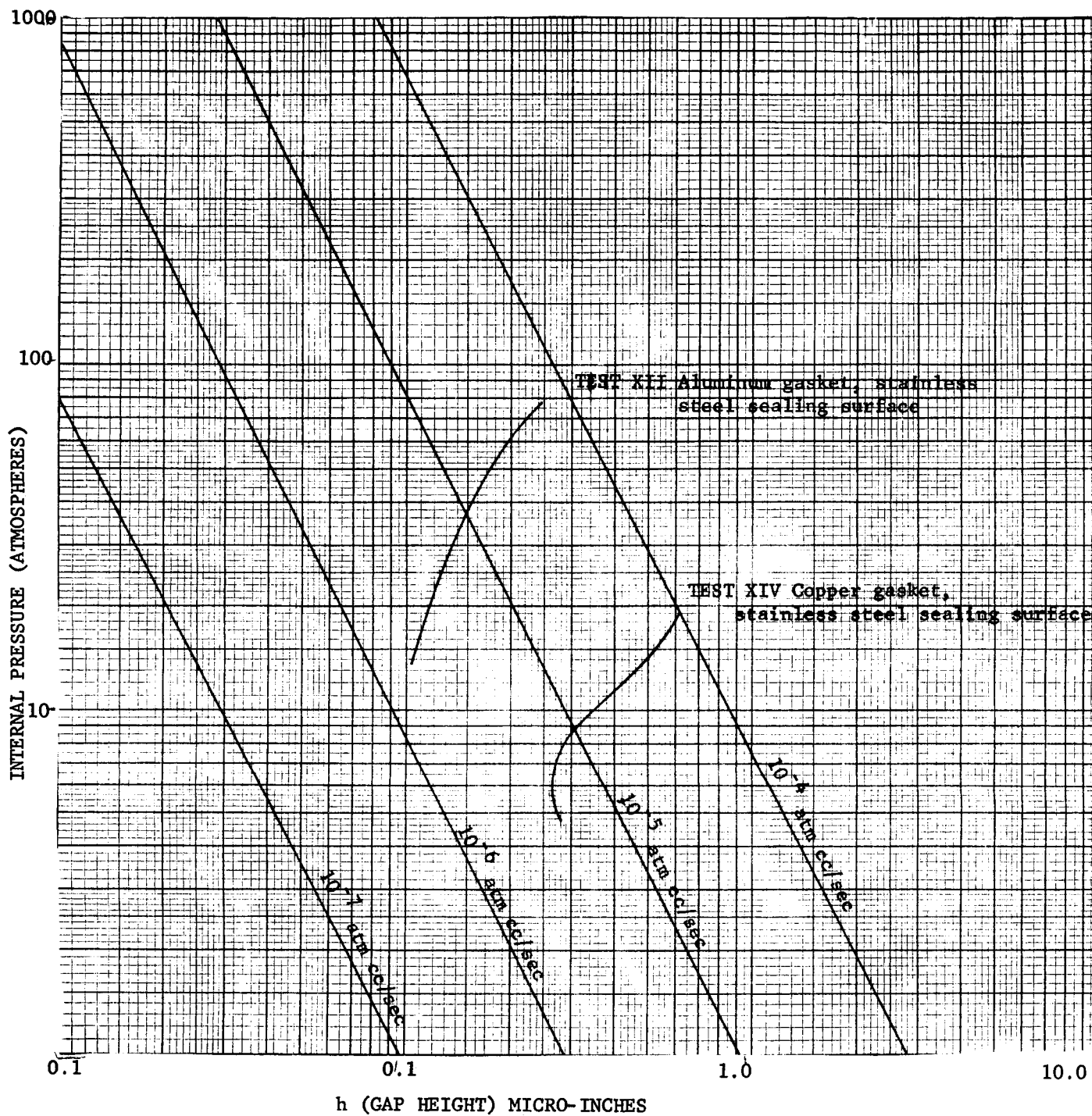


FIGURE 37.8 LEAKAGE RATE FOR HELIUM AT 20°C FOR AN ANNULAR PASSAGE EQUAL TO EXPERIMENTAL NOMINAL DIMENSIONS, WITH 0 PSI EXTERNAL PRESSURE. COMPARISON WITH FINE CIRCUMFERENTIAL MACHINED EXPERIMENTAL SURFACE FINISH RESULTS

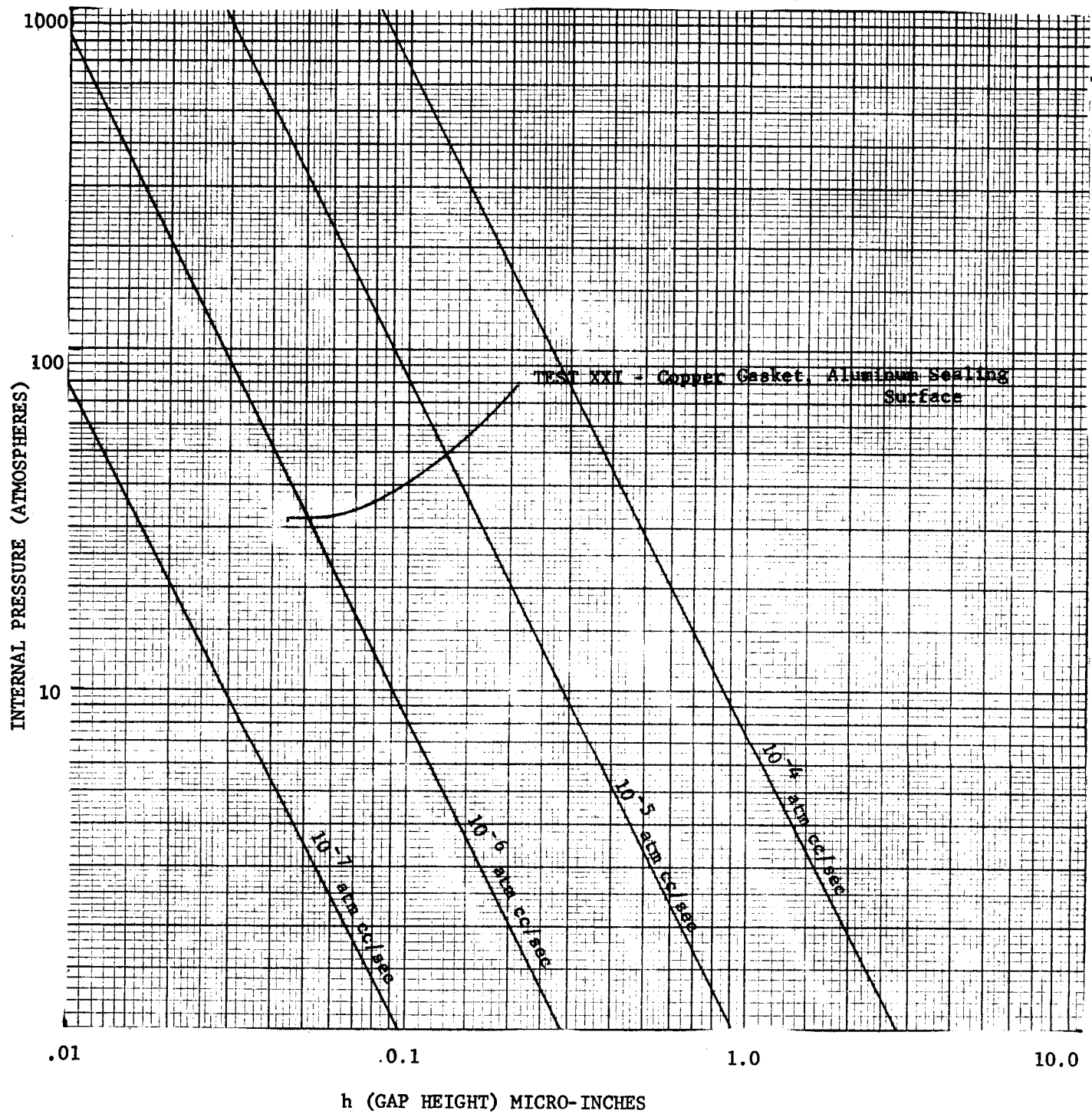
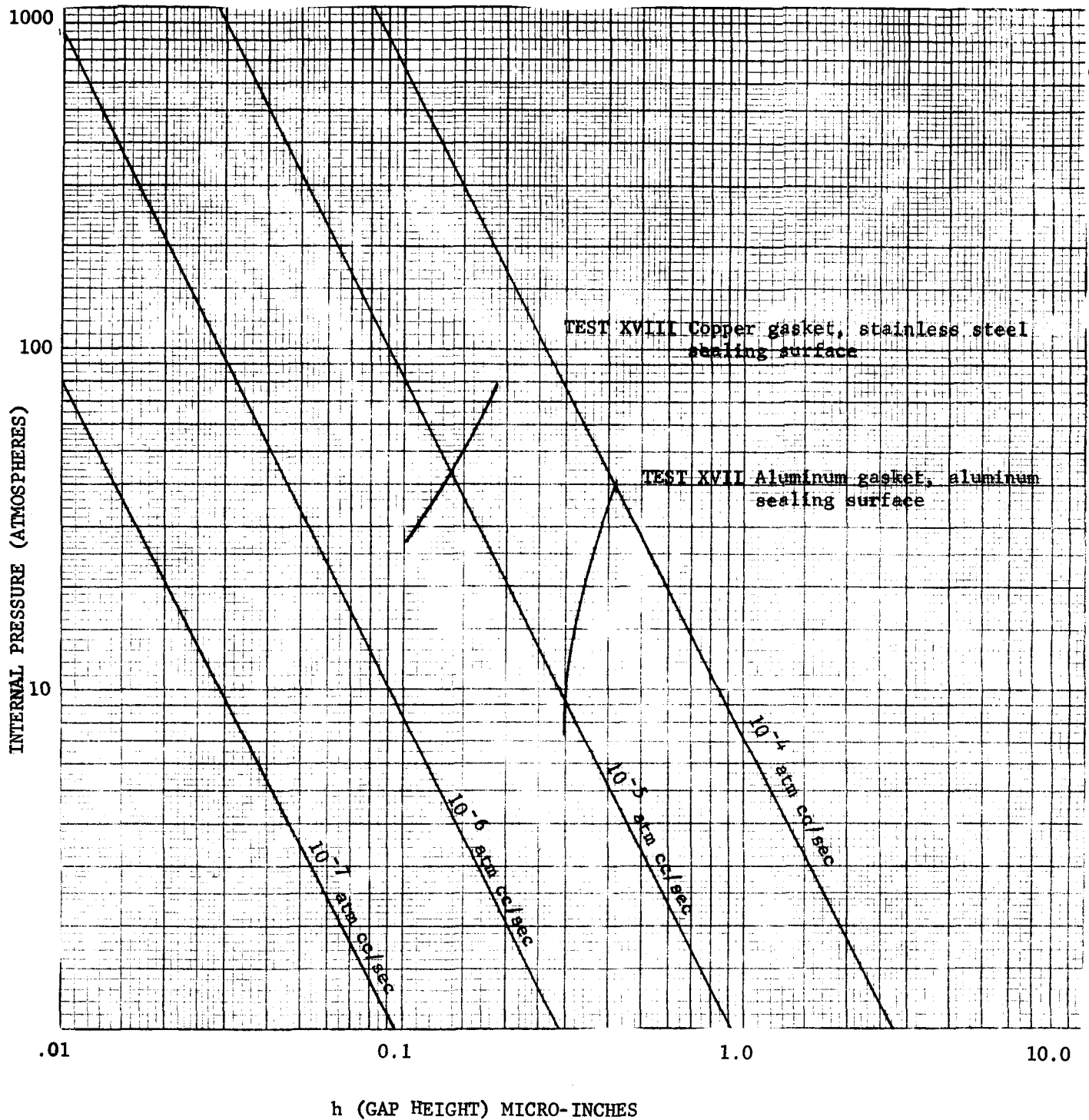


FIGURE 37.9 LEAKAGE RATE FOR HELIUM AT 20°C FOR AN ANNULAR PASSAGE EQUAL TO EXPERIMENTAL NOMINAL DIMENSIONS, WITH 0 PSI EXTERNAL PRESSURE. COMPARISON WITH COARSE CIRCUMFERENTIALLY MACHINED EXPERIMENTAL SURFACE FINISH RESULTS



### 37.1.5 Evaluation of Phase I Leakage (Figures 36.6-36.9)

During Phase I, the two parameters varied from test to test were surface finish and gasket material. In order that a comparison of materials could be made, the stress level at each stage was divided by the yield strength of the gasket material. Two such yield strengths were used; the first is that measured from a tensile test (and would constitute a pure material property known by the test), and the second is the stress level at which gross yielding occurred during the leakage experiment. This, of course, is also a function not only of the material properties but also of the geometry of the gasket and the friction at the interface between gasket and sealing surface.

Comparing curve shapes for all tests conducted, it becomes apparent that surface finish has a larger role than the deformation properties of the materials. It can be said, in general, that traces for a given surface finish are similar in shape regardless of the gasket material used.

Diamond burnished surface tests yield curves similar to those hypothesized in Section 32.2 for the five regimes of flow. During the very early stages, little reduction of leakage is noted. As the asperities begin to deform plastically, the leakage decreases rapidly. As bulk flow begins and hinders further deformation at the interface, the leakage decreases at a slower rate. Finally, in most cases, the leakage decreases more rapidly as the bulk flow of gasket material causes a good seal at the gasket edge. The radially ground surface tests showed a sudden and transient increase in leakage rate during the test as is explained in Section 37.1.8. The fine machined surfaces show an exponential decay in leakage during this phase. The coarse machined tests displayed no consistent pattern. Post-test inspection of the mated surfaces showed that in the coarse machined cases, the mating was very localized along asperity peaks with only a small amount of the total area mated. This was true to a lesser extent for the fine machined case.

When the yield-strength data from tensile tests were used as a normalizing factor, the spread in curves for a given surface finish was great. However, when the compressive yield stress as determined during the leak tests was used, the curves become much closer in all cases, and the following statements can be made:

- (1) For the diamond burnished surface tests the leakage rate reached  $10^{-6}$  atm cc/sec by the time 1.6 times the yield stress was reached for all cases. The steepest slope of the leakage stress curve occurred at stress levels of about .25 times the yield stress.
- (2) For the radially ground case, the sudden increase in leakage rate occurred between 1.25 and 1.5 times the yield strength. Sealing to the degree of  $10^{-6}$  atm cc/sec was attained in all cases by a stress level of 2.1 times the yield strength.

- (3) For the fine machined surface, the sealing occurred at about the yield stress in two cases, and at 1.30 times the yield stress in another.
- (4) Again, the coarse machining surface tests yielded wide scatter, two tests sealing at about 1.7 times the yield stress and one at about 5 times the yield stress.

Thus, in all cases except for one coarse machined surface case, sealing to  $10^{-6}$  atm cc/sec was attained by the time the stress level was equal to 2.1 times the yield stress. Thus twice the yield stress (where the yield stress is identified as the point of initiation of bulk yielding of the gasket) appears to be a reasonable minimum value of stress for general flat annular gasket use.

#### 37.1.6 Evaluation of Phase II Leakage (Figures 36.10-36.13)

The meaningful information found in Phase II is the sensitivity of the leakage to internal pressure. Can data gained at a one-atmosphere pressure differential be used when the pressure is increased?

Results show that the lead and indium (soft metals) are very insensitive to pressure, regardless of surfaces used. The most sensitive is the radially ground surface. Whether the leak was molecular or viscous cannot be determined from the tests concluded. One important fact shown in Phase II is that the curves are generally smooth, indicating that a solid mating has been attained, and no "blowout" occurred during the test. The conclusion gained from this phase is that insensitivity to pressure can only be assured when very soft gaskets are utilized.

Loads found from Phase I for small leakages must be increased to insure sealing at higher internal pressures. However, it was noted on several tests that the increase of load at the close of Phase II to cause the leak to drop was not too great, never an increment more than 0.25 times the yield stress.

#### 37.1.7 Evaluation of Phase III Leakage (Figures 36.14-36.17)

A very important consideration in any connector is what happens when the initial sealing stress decreases. Will the seal open? Phase III results largely answer this question. From the graphs showing leakage as a result of decreasing load, it can be concluded that

- (1) If a very soft gasket is used, and mating is nearly completed over the apparent area (large plastic deformations), the connector will be almost completely insensitive to reduction of stress.
- (2) As the gasket material becomes stronger, and the deformation

is, to a great degree, elastic, the seal will be very sensitive to loss of stress.

- (3) The coarse surface finish tests, where sealing occurred only at points, show that the seal is extremely sensitive.
- (4) For smooth surfaces, the sensitivity is less.

The most important factor is the amount of plastic flow in the system at the time. If the plastic flow is the factor governing leakage, then the seal will be generally insensitive. The plastic flow can be caused by the disparity in material strengths or by surface geometry.

#### 37.1.8 Comparison Between Experimental Results and Analytical Passage Height Predictions

In the experiments, no length measurements on the passage height existing between mated surfaces were made directly. However, if an equivalent passage is an adequate parameter to help define the flow through whatever interface gap exists between gasket and sealing surface, then the flow through the passage will be proportional to the cube of the equivalent height if the flow is viscous or proportional to the square of the equivalent height if the flow is molecular (Section 22). Hence, if the rate of leakage flow through a passage were known accurately, then with a knowledge of pressure differential, path length, and path width, one could calculate the passage height. Moreover, if the leakage rate were monitored for various stresses applied to the gasket while other parameters remained fixed, then the equivalent passage height could be determined as a function of stress. Phase I of the leakage experiments accomplishes such a measurement. If an equivalent passage height is an adequate parameter to describe the phenomenon, then the curve of leakage vs. normal stress should be of the same shape as a curve defining  $h^2$  or  $h^3$  as a function of normal stress, depending on whether the flow is molecular or viscous (Sec. 33.3).

The analysis of Section 33, using a statistical model of the surface profiles of the mated materials, leads to a prediction of an equivalent passage height as a function of normal stress for various material strain-hardening characteristics. The prediction is illustrated graphically in Fig. 33.9. The ordinate of the graph,  $(h_e/h_r)^3$ , is, as outlined in Section 33, the cube of equivalent height ( $h_e$ ) divided by a height  $h_r$ , descriptive of the original surface finishes of both mated surfaces. As noted in Section 33.3, these curves apply only for viscous flow; for molecular flow, the ordinates of the curves would differ, though their general shapes would remain the same.

Comparison between Fig. 33.9 and the experimental leakage curves, Figs. 36.6 through 36.9, shows that the shapes of most of the experimental curves are in general agreement with the calculated curve for zero strain hardening. However, the experimental curves show that the stress required for complete sealing is less than the three times the yield stress predicted

by the calculations. This discrepancy appears to be due to a combination of two factors:

1. The compressive yield stress,  $S$ , as determined during the leak test (Section 32) is higher than the initial compressive yield stress  $Y_0$  (Sec. 33.4). The stress  $S$  includes the effect of lateral containment, and by measuring  $S$  as the 0.2% compressive yield stress, some strain-hardening effect may be included.
2. The mutual interaction of asperities and the nonuniformity of sealing over the seal surface evidently cause complete sealing at a lower stress level than that predicted by the analysis which neglects these effects.

This comparison suggests that for most of the tests, the mutual interaction of asperities, which is beneficial for sealing, more than offsets the adverse effect of strain hardening. While the experimental curves were for flow in the molecular range, whereas the analytical curve was calculated for flows in the viscous range, this difference does not change the basic conclusions. A few of the experimental curves - for example, those for diamond-burnished copper (Fig. 36.6) and coarse machined aluminum (Fig. 36.9) - appear to show some strain-hardening effect.

For the calculated curve with zero strain hardening (Fig. 33.9), the inflection point comes when the stress is half of the stress needed for complete sealing (i.e., when the stress is 1.5 times the initial yield point) and when  $h_e$  is slightly smaller than  $h_r$ . (For pure molecular flow, it can be shown that  $h_e$  would be exactly equal to  $h_r$  at this point.) Inflection points were discernible in the experimental tests for some of the diamond-burnished surfaces (Fig. 36.6) and some of the radially ground surfaces (Fig. 36.7). For the circumferentially machined surfaces (Figs. 36.8 and 36.9), the inflection points were less well defined. The leakage value at the inflection point, when converted to an equivalent passage height (Figs. 37.6 through 37.9), give an indication of the rms passage height taken perpendicular to the direction of flow. To see whether these predictions may be reasonable, Table 37.1 has been compiled.

TABLE 37.1 Comparison of Passage Height Values  
Gasket materials: high-purity aluminum, copper, nickel  
Sealing surfaces: stainless steel, aluminum

Type of finish on sealing surface	Experimentally measured $h_r$		$h_r$ estimated from inflection points of flow vs stress curves (across direction of flow)
	Along direction of flow micro-inches	Across direction of flow micro-inches	
Diamond burnished	30	—	1 to 3
Radially ground	30	50	1.5 to 2
Fine machined	104	—	3 to 10
Coarse machined	310	—	10

For the circumferentially machined gaskets mating with diamond burnished and circumferentially machined sealing surfaces, it seems plausible that the rms surface finish along the asperities could be 3% to 10% of the rms surface finish across the asperities, so the concept of an equivalent passage height seems reasonable. For the circumferentially machined gaskets mating with radially ground sealing surfaces, the mating action is evidently localized, as shown by the photomicrographs of Figs. 36.28 to 36.34, and the concept of an equivalent passage height does not apply.

That the radially ground case does not compare favorably is not surprising. The phenomenon involved differs somewhat from the other sealing mechanisms. Since observations in all cases show that the best sealing occurs at the edges of the gaskets, it is noted immediately that for low stress levels, the only sealing in radially ground surfaces occurs at the edges (due to the natural fluid flow paths in the surface profile). As the stress level rises initially, the sealing improves; however, at the stress level at which gross gasket flow is initiated, the gasket material at the edge moves "suddenly" with respect to the sealing surface; thus breaking temporarily the seal which existed. As the material flows further, the added plastic deformation causes the system to reseal. The phenomenon of breaking the seal and resealing shows clearly in three cases, and is evident upon close inspection in two other cases (Fig. 36.7).



## 37.2 Experimental Observations for Plastic Gaskets

### 37.2.1 Experimental Gasket Deformations

Post-leak-test observations of the deformed gaskets show that the material deforms inwardly and outwardly by the same amount. This is true because the pressure difference across the seal was held to one atmosphere during the initial gasket loading phase of the test. The flange materials have a much higher yield stress than the gasket materials and appear as rigid bodies during the test. Therefore, the deformation of the plastic gaskets was a plane strain phenomenon.

Accurate knowledge of the gasket surface area is necessary to predict the gasket stress at any load during test. This was accomplished by assuming a constant volume compression of the gasket and monitoring the thickness during the test. The initial and final measurements of the gasket volume indicated that a constant volume compression was the case. The Duroid-5600 gasket was the only material to exhibit a lower final volume which was due to the large number of voids evident in this material.

All the plastic gaskets exhibited some cold flow. This was noted to be a minimum for KEL-F81 and very pronounced for Teflon-TFE and FEP. This effect was not investigated quantitatively as it had no measurable effect on the interface sealing. An increase in gasket load would be followed by a slow settling process of varying degrees for each material. The leakage would respond about as fast as the load application. There would be some small change in leakage after this initial change due primarily to the increased interface area as the gasket settled. The leakage and gasket deflection measurements for each load would be taken after a sufficient delay so that no more measurable deflection of the gasket occurred.

### 37.2.2 Gasket Interface Phenomenon

In all tests the plastic gaskets were subject to large plastic deformations. As in the case of metal gaskets the surfaces initially in contact remained in contact and bulk flow occurred radially in and out from the center thickness of the gasket. These gaskets deformed in the flow mode illustrated in Figure 37.1. The one notable exception to this mode of deformation was Teflon-TFE in test P-9 when mated with a diamond burnished finish. Teflon has a very low coefficient of friction ( $\mu = .04$ ) and was mated with a very smooth surface so that there was relatively little resistance to sliding at the gasket interface. During the test with the gasket subject to internal pressure the leakage was noted to increase very slowly at a constant gasket load until suddenly the gasket ruptured, as illustrated in Figure 36.46. The slow change in leakage was indicative of cold flow of the Teflon in the radial direction. The gasket literally expanded and ruptured like a balloon. In cases where there is inadequate friction to prevent sliding at the gasket interface some other form of constrain must be used to prevent blow-out. This is especially true for gasket materials such as Teflon-TFE which exhibit cold flow.

A measure of the friction effect at the interface can be obtained for the various surface finishes used in these tests by comparing the yield-stress values for each gasket material as a function of the mating surface. As expected,

the rougher surface constrains the gasket more and increases its yield stress.

### 37.2.3 Surface Replication

Examination of the plastic gaskets after test indicates that extremely good replication of the mating flange surface was obtained. Figures 36.48 through 36.51 show KEL-F81 before and after tests on each mating surface. Figure 36.51 should be compared with the radially machined surface profile in Figure 36.36; however, they are at different magnifications on the vertical scale. Figure 36.50 should be compared with the diamond burnished surface finish of Figure 36.37 which is at the same magnification. The high degree of mating shown in these profile traces is typical of the other gasket materials tested.

Duroid 5600 is the one material which did not show good mating; this is probably due to its ceramic fiber inserts. Figure 36.52 at low magnification shows the very rough surface before test. Figure 36.53 showing Duroid after mating with the circumferential machined surface should be compared with Figure 36.36. This comparison shows that the asperities on the Duroid are not as uniform as those on the machined flange surface so that mating was not complete. During this test the nominal gasket stress was raised to approximately six times the yield stress (which is actually the yield stress of the teflon filler) and the leakage was reduced only to  $2 \times 10^{-5}$  atm cc/sec. The seal was sensitive to internal pressure and removal of load, giving further indications that mating was not complete and that voids were present.

The degree of mating appears to be independent of location on the gasket. In general the interface sealing necessary to stop leakage was obtained at a very low value of nominal stress. These two observations indicate that the mechanism by which plastics conform to the mating surface differs greatly from that discussed for metal gaskets. Plastics are visco-elastic substances so that flow of the gasket material into the spaces between the asperities is obtained without exceeding the yield stress of the elastic state. Profile tracings have been recorded after the test of the plastic gaskets in which the yield stress of the material was not exceeded and hence there were no gasket bulk deformations. These profile tracings again showed a high degree of mating.

There seems to be a state of plastic deformation retained at the mated surface due to the viscous nature of the plastic material rather than to plastic deformation of the elastic state.

### 37.2.4 Evaluation of Phase I Leakage (Figures 36.39 - 36.43)

During Phase I, the two parameters varied from test to test were surface finish and gasket material. In order that a comparison could be made between materials, the nominal gasket stress was divided by the 0.2% compressive yield stress of each material. The yield stress used was the value obtained from each leak test and represents gross deformations during the leakage experiment. This value includes the test geometry, interface friction and material property effects.

The Phase I results shown in Figures 36.39 to 36.42 compare the three surface finishes for the same gasket material. These figures all indicate that interface sealing is independent of surface finish. Figure 36.43 shows that all gasket materials except Duroid-5600 on the same surface finish seal to about  $10^{-6}$  atm cc/sec at 0.3 to 0.5 normalized yield stress. The Duroid-5600 leaked at a stress level of about 6 times the yield stress of the teflon filler material. This is due to a combination of poor interface sealing caused by the hard ceramic fiber inserts and permeation through the material due to its large void content. Examination of its surface after the test showed that the interface mating was poor. (Figure 36.53)

The KEL-F81, Saran, Teflon-FEP and Teflon-TFE all sealed to a measurable low leak ( $10^{-6}$  atm cc/sec) independent of material and surface finish. Sealing was obtained without bulk deformation of the gasket as it occurred very much below the yield stress of each material. The normalized stress level necessary to induce viscous flow into the areas between the sealing surface asperities is the same for all materials and surface finishes. It must be noted that the absolute stress level needed for sealing is not independent of surface finish since the yield stress used in normalizing varies for each surface finish with the same material (See Table 34.7). This does indicate that the yield stress for each gasket configuration is an excellent parameter for normalizing leakage data.

The Phase I leakage values appeared to level off and become almost independent of gasket stress after the initial leakage decay. The value of this terminal leakage differs for each material (Figure 36.43) but is independent of surface finish. The sensitive mass spectrometer at this point is measuring permeation flow of helium through the gasket material. The permeation rates for each material as presented in Table 34.6 will be used to compare the terminal leakage measured with that expected by permeation for the gasket geometry, pressure level and gas-material combination. The values of permeation rate presented in Table 34.6 are for various listed gases at room temperature. The values presented in this section include a factor which relates the flow of helium through the material to the listed gas, and is based on private conversations with Dr. F.J. Norton\*. These approximations are necessary due to the sparsity of data on permeation and will suffice to get an order of magnitude check on the leakage. The leakage due to permeation is evaluated as follows and the results are presented in Table 37.1.

$$\text{Leakage } Q = PA \frac{\Delta p}{L} (\text{cc/sec})$$

$$\text{where: } P = \text{permeation rate, } \frac{\text{cm}^3 - \text{mm}}{\text{sec cm}^2 - \text{atm}}$$

$$A = \text{normal flow area, cm}^2$$

$$L = \text{length of flow path, mm}$$

$$\Delta p = \text{pressure causing leakage, atm}$$

---

\* Dr. F.J. Norton - General Electric Research Laboratory (See also Sec. 23)

Gasket: 0.06" thick, 0.125" wide  
 1.187" nominal diameter  
 Pressure: 1 atm pressure difference  
 across gasket

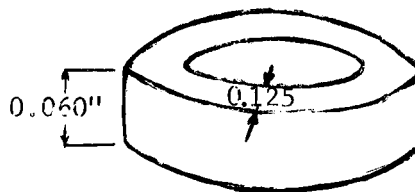


FIGURE 37.10 Gasket Configuration

For the gasket geometry and pressure level in these tests we get

$$Q = .282 P$$

The value of the leak for each gasket material is tabulated below.

TABLE 37.1 Permeation Leakage Comparison

<u>Material</u>	<u>Permeation Rate for Helium</u>	<u>Calculated Leakage</u> atm cc/sec	<u>Measured Leakage</u> atm cc/sec
KEL-F81	$2 \times 10^{-6}$	$5.6 \times 10^{-6}$	$1.5 \times 10^{-7}$
Saran	$1 \times 10^{-8}$	$2.8 \times 10^{-8}$	$1.0 \times 10^{-8}$
Teflon-FFP	$2 \times 10^{-7}$	$5.6 \times 10^{-7}$	$5.3 \times 10^{-7}$
Teflon-TFE			$1.0 \times 10^{-6}$
Duroid	not available		

The order of magnitude of the measured terminal leak is the same as that expected by permeation. The permeation rate for KEL-F81 appears high especially in view of information in Reference 4 of this Section. A qualitative discussion of permeation through plastics is presented there, listing in order of increasing permeation rate: Saran, KEL-F81 and Teflon. This is the trend noted in the leakage results of these tests.

It is concluded that during Phase I all plastic gaskets seal at the interface at about 0.4 normalized stress independent of surface finish. The leakage remaining is independent of further gasket loading and is a measure of permeation through the gasket material. Although the level of the permeation leak here is low, it may become significant for gaskets with a larger flow-area-to-flow-path-length ratio or for higher internal pressures.

### 37.2.5 Evaluation of Phase II Leakage (Figure 36.44)

During Phase II the internal pressure on the gasket was gradually increased to record the sensitivity of the seal to internal pressure. The plot of Figure 36.44 is truly representative of the results obtained for all gaskets (except Duroid-5600) on all surface finishes. The insensitivity to internal pressure is another good indication of excellent mating at the interface. Duroid-5600 was very sensitive to pressure, which is again due to poor mating at the interface.

As the pressure was gradually increased, the leakage remained at the permeation level recorded at the end of Phase I. Permeation did not increase with internal pressure because this phase of the test was run in a relatively short time compared to the time response of the diffusion process. A long-time test run on silicone rubber gasket material indicated that the time constant for permeation with a fast change in internal pressure is approximately one hour. The response time of leakage through holes at the seal interface is very fast, so that the results of Phase II indicate the insensitivity of the interface seal to internal pressure.

#### 37.2.6 Evaluation of Phase III Results (Figures 36.45 - 36.47)

Phase III results show the insensitivity of most of the plastic gaskets to removal of normal stress. Duroid-5600 is again sensitive due to the poor mating at the interface. Teflon-TFE shows sensitivity to removal of stress, probably due to its marked tendency to cold flow. In particular, test P-9 with Teflon-TFE on a diamond burnish finish, the gasket showed cold flow in the radial direction due to internal pressure until the gasket ruptured.

Other plastic gaskets were insensitive to the removal of normal stress, indicating that good mating was obtained at the interface consisting of plastic rather than elastic deformations.

### 37.3 Elastomer Gaskets

#### 37.3.1 Experimental Results - Phase I

As outlined in Section 36.3 the experimental procedure for elastomer gaskets was limited by the test apparatus. The Viton-A, Neoprene and Hypalon gaskets all sealed to  $10^{-8}$  cc/sec (the sensitivity of the mass spectrometer) with a nominal gasket stress of 575 psi. This was the value of stress caused by the initial load when a vacuum was drawn on the test apparatus. This sealing was the same for each material and surface finish tested.

Silicone rubber demonstrated a low value of leak which was independent of normal gasket stress and surface finish, as shown in Figure 36.54. Silicone rubber sealed at the interface, as did the other elastomers, during the application of the vacuum load. The leak recorded was permeation through the silicone material as verified by experimental observations and a calculation of expected permeation rate similar to that comparison for plastic gaskets. Sudden changes in internal gasket pressure caused only very slow changes in measured leakage rate, taking over one hour to reach a steady-state leakage at the new pressure. This response time is characteristic of a permeation process as compared to the very fast response time for flow through holes at an interface. The steady-state leakage rate was also a linear function of the internal gasket pressure, which is characteristic of a diffusion process. The calculation for the permeation leakage based on the permeation rates given in Table 34.10 with corrections for helium gas follows:

TABLE 37.2 Elastomer Permeation Rates  
(Based on Section 37.2.4)

Elastomer Material	Permeation Rate for Helium $\frac{\text{cm}^3}{\text{sec cm}^2 \text{ atm}}$	Calculated Leakage atm cc/sec	Measured Leakage atm cc/sec
Silicone	$4.0 \times 10^{-5}$	$1.13 \times 10^{-5}$	$1.3 \times 10^{-6}$
Neoprene	$.6 \times 10^{-7}$	$1.69 \times 10^{-8}$	$1.0 \times 10^{-8}$

The measured leakage is lower than the calculated leakage for silicon due to some extent to the stress level in the test gasket. Also the value of the permeation rate appears high in comparison with other data, especially since it is from the same source as the abnormally high leakage data for KEL-F81 (See Section 37.2.4). An order-of-magnitude verification that the measured leakage was permeated through the material is thus obtained.

### 37.3.2 Experimental Results - Phase II and Phase III

The procedure on tests exhibiting sealing during the application of the initial vacuum load was to increase the internal pressure on the gasket to try to break the seal. There was a limit on the internal pressure as it would produce a force to act against the testing-machine load which stressed the gasket. It was therefore possible to approach the case of zero normal stress on the gasket. When this was done, a catastrophic blow-out would occur at the surface of the gasket (the gasket would not rupture). There was no gradual increase in leakage as the pressure was increased. This indicated that a very good replication of the mating surface had been made by the elastomer gasket.

When the internal pressure was increased on the silicone gasket, the leakage would gradually increase with a response time of over one hour. The internal pressure and steady-state leakage were linearly related as evidenced by the following data from test E-7 at a constant gasket stress level of 1600 psi

<u>Gasket Pressure Difference</u> <u>psi</u>	<u>Leakage</u> <u>cc/sec</u>
14.7	$1.3 \times 10^{-6}$
250	$2.5 \times 10^{-5}$
500	$3.9 \times 10^{-5}$

These data show, that large values of leak might be obtained with a gasket with a wider permeation flow path or shorter flow-path length or with higher internal pressures.

### 37.3.3 Surface Mating

Qualitative examination of the surfaces of the rubber gaskets after test using a "Talysurf" profilometer indicated poor replication. However, the leakage results conclusively showed that excellent mating must have occurred. This mating was elastic in nature and hence the surface rebounded after removal of the test load and prevented monitoring of surface replication. The elastomer materials are so soft that large elastic deformations are possible with a very low stress level. The rubber gaskets with their great compliance sealed primarily by elastic, not plastic, deformation.

#### 37.4 References

1. J.F. Nye, "Experiments on the Plastic Compression of a Block Between Rough Plates," J.A.M. Sept. 1952, pp. 337-346.
2. R. Hill, E.H. Lee, S.J. Tupper, "A Method of Numerical Analysis of Plastic Flow in Plane Strain and Its Application to the Compression of a Ductile Material Between Rough Plates," J.A.M., March 1951, pp. 46-52.
3. R. Hill, The Mathematical Theory of Plasticity, Oxford University Press, 1956.
4. F.J. Norton, "Permeation of Gases through Solids," Journal of Applied Physics, Vol. 28, No. 1, January 1957, pp. 34-39.



DISTRIBUTION LIST FOR REPORTS ON CONTRACT NAS 8-4012

NASA Headquarters, Washington 25, D.C.

Mr. Henry Burlage, Jr.  
Chief, Liquid Propulsion Systems, RPL (3)

Mr. A.O. Tischler  
Assistant Director for Propulsion, MLP (1)

NASA, Marshall Space Flight Center, Huntsville, Alabama

Mr. Charles Wood (M-P&VE-PT), Technical Manager (24)  
Office of Technical Information, M-MS-IPC  
Contracting Officer, M-P&C-C  
Patent Office, M-PAT

NASA Other Locations

Technical & Scientific Information Facility  
Attention: NASA Representative, Code CRT  
P.O. Box 5700, Bethesda, Maryland (24)

Attention: Technical Librarian

Ames Research Center  
Moffett Field, California (2)

Goddard Space Flight Center  
Greenbelt, Maryland (2)

Jet Propulsion Laboratory  
California Institute of Technology  
4800 Oak Grove Drive  
Pasadena, California (2)

Langley Research Center  
Langley Field, Virginia (2)

Lewis Research Center  
21000 Brookpark Road  
Cleveland 35, Ohio (2)

Marshall Space Flight Center  
Huntsville, Alabama (2)

Manned Spacecraft Center  
Houston, Texas (2)

Advanced Research Projects Agency  
Pentagon, Room 3D154  
Washington 25, D.C.

Aeronautical Systems Division  
Air Force Systems Command  
Wright-Patterson Air Force Base, Ohio

Attention: Technical Librarian

Air Force Missile Development Center  
Holloman Air Force Base, New Mexico

Air Force Missile Test Center  
Patrick Air Force Base, Florida

Air Force Systems Command, Dyna-Soar  
Air Force Unit Post Office  
Los Angeles 45, California

Army Ordnance Missile Command  
Redstone Arsenal, Alabama

Armed Services Technical Information Agency  
Arlington Hall Station  
Arlington 12, Virginia

Arnold Engineering Development Center  
A.E.O.R.  
Tullahoma, Tennessee

Bureau of Naval Weapons  
Department of the Navy  
Washington 25, D.C.

Central Intelligence Agency  
2430 E. Street, N.W.  
Washington 25, D.C.

Headquarters, United States Air Force  
Washington 25, D.C.

Office of Naval Research  
Washington 25, D.C.

Attention: Technical Librarian

Picatinny Arsenal  
Dover, New Jersey

Rocket Research Laboratories  
Edwards Air Force Base, California

U.S. Naval Ordnance Test Station  
China Lake, California

U.S. Atomic Energy Commission  
Technical Information Services  
Box 62  
Oak Ridge, Tennessee

Liquid Propellant Information Agency  
Johns Hopkins University  
Applied Physics Laboratory  
8621 Georgia Avenue  
Silver Spring, Maryland

Aerojet-General Corporation  
P.O. Box 296  
Azusa, California

Aerojet-General Corporation  
P. O. Box 1947  
Sacramento 9, California

Aeronutronic  
A Division of Ford Motor Company  
Ford Road  
Newport Beach, California

Aerospace Corporation  
2400 East El Segundo Boulevard  
El Segundo, California

Arthur D. Little, Inc.  
Acorn Park  
Cambridge 40, Massachusetts

Astropower, Inc., Subsidiary of Douglas  
Aircraft Company, Inc.  
2968 Randolph Avenue  
Costa Mesa, California

Astrosystems, Inc.  
82 Naylor Avenue  
Livingston, New Jersey

Atlantic Research Corporation  
Edsall Road and Shirley Highway  
Alexandria, Virginia

Attention: Technical Librarian

Beech Aircraft Corporation  
Boulder Facility  
Box 631  
Boulder, Colorado

Bell Aerosystems Company  
P. O. Box 1  
Buffalo 5, New York

Bendix Systems Division  
Bendix Corporation  
Ann Arbor, Michigan

Boeing Company  
P. O. Box 3707  
Seattle 24, Washington

Convair (Astronautics)  
Division of General Dynamics Corporation  
P. O. Box 2672  
San Diego 12, California

Curtiss-Wright Corporation  
Wright Aeronautical Division  
Wood-ridge, New Jersey

Douglas Aircraft Company, Inc.  
Missile and Space Systems Division  
3000 Ocean Park Boulevard  
Santa Monica, California

Fairchild Stratos Corporation  
Aircraft Missiles Division  
Hagerstown, Maryland

General Electric Company  
Missile and Space Vehicle Department  
Box 8555  
Philadelphia, Pennsylvania

General Electric Company  
Rocket Propulsion Units  
Building 300  
Cincinnati 15, Ohio

Grumman Aircraft Engineering Corporation  
Bethpage, Long Island, New York

Kidde Aero-Space Division  
Walter Kidde and Company, Inc.  
675 Main Street  
Belleville 9, New Jersey

Attention: Technical Librarian

Lockheed Aircraft Corporation  
Missile and Space Division  
Sunnyvale, California

Lockheed Propulsion Company  
P.O. Box 111  
Redlands, California

Marquardt Corporation  
16555 Saticoy Street  
Box 2013 - South Annex  
Van Nuys, California

Martin Division  
Martin Marietta Corporation  
Baltimore 3, Maryland

Martin Denver Division  
Martin Marietta Corporation  
Denver, Colorado

McDonnell Aircraft Corporation  
P. O. Box 6101  
Lambert Field, Missouri

North American Aviation, Inc.  
Space & Information Systems Division  
Downey, California

Northrup Corporation  
1001 East Broadway  
Hawthorne, California

Pratt & Whitney Aircraft Corporation  
Florida Research & Development Center  
West Palm Beach, Florida

Radio Corporation of America  
Astro-Electronics Division  
Defense Electronic Products  
Princeton, New Jersey

Reaction Motors Division  
Thiokol Chemical Corporation  
Denville, New Jersey

Republic Aviation Corporation  
Farmingdale  
Long Island, New York

Attention: Technical Librarian

Rocketdyne (Library Dept. 586-306)  
Division of North American Aviation, Inc.  
6633 Canoga Avenue  
Canoga Park, California

Space General Corporation  
9200 Flair Avenue  
El Monte, California

Space Technology Laboratories  
P. O. Box 95001  
Airport Station  
Los Angeles 45, California

Stanford Research Institute  
333 Ravenswood Avenue  
Menlo Park, California

TAPCO Division  
Thompson-Ramo-Wooldridge, Inc.  
23555 Euclid Avenue  
Cleveland 17, Ohio

Thiokol Chemical Corporation  
Redstone Division  
Huntsville, Alabama

United Aircraft Corporation  
East Hartford Plant  
400 Main Street  
Hartford, Connecticut

United Technology Corporation  
587 Methilda Avenue  
Sunnyvale, California

Vought Astronautics  
Box 5907  
Dallas 22, Texas

Armour Research Foundation  
Illinois Institute of Technology  
10 West 35th Street  
Chicago 16, Illinois

Battelle Memorial Institute  
505 King Avenue  
Columbus 1, Ohio

National Bureau of Standards  
Cryogenic Engineering Laboratory  
Boulder, Colorado